PREDICTION OF CO$_2$ CORROSION WITH THE PRESENCE OF ACETIC ACID

A thesis submitted to The University of Manchester for the

degree of

Doctor of Philosophy

In the Faculty of Engineering and Physical Sciences

2005

MOKHTAR CHE ISMAIL

SCHOOL OF MATERIALS

Word count = 21,000 words.

ABSTRACT

The roles and effects of organic acid species in CO_2 corrosion have received relatively little attention and thus have not been included in the corrosion analysis of oil and gas systems. This is potentially detrimental as most of the predictive models used for materials selection do not incorporate considerations of the effects of such species. The scope of the study is to understand and predict the effect of organic acids, acetic acid specifically, on the CO_2 corrosion rate of carbon steel. The electrochemical studies consist of static test and rotating cylinder electrode (RCE) tests that focus on the effect of acetic acid species concentrations on the corrosion rate with the presence of CO_2 at fixed pH and different temperatures. These studies are based on linear polarisation resistance (LPR) and potentiodynamic polarisation methods of a three-electrode system. The results are compared with the performance predicted by three openly available predictive models; NORSOK, Cassandra and de Waard Milliams models. The results of static tests showed that the corrosion rate increases almost linearly with the concentration of acetic acid under non-scaling conditions and decreases to a low value after the formation of protective film. The RCE tests at pH 5.5 show similar results, with an increased corrosion rate that varies linearly with the acetic acid concentration. In addition, the presence of more than 400 ppm acetic acid at $22^{\circ}C$ and 800 ppm at $50^{\circ}C$ reduces the corrosion rate due to inhibition. The cathodic reaction in the presence of acetic acid is diffusion controlled but changes to mixed diffusion and charge–transfer control at high acetic acid concentration. There is no significant change in the anodic reaction mechanism with the presence of acetic acid. The overall corrosion process is mainly controlled by a charge transfer process. Based on the findings, it is concluded that acetic acid species increase the corrosion rate of carbon steel in CO_2 corrosion substantially from the additional cathodic reactions of acetic acid dissociation and direct reduction of acetic acid. Standard predictive models do not account for the presence of acetic acid in CO_2 corrosion. Thus, new equations are proposed to predict the CO_2 corrosion rate of carbon steel with the presence of acetic acid for stagnant/low-flow and turbulent flow conditions.

DECLARATION

I declare that no portion of the work referred to in the thesis has been submitted in support of an application for another degree or qualification of this or any other university or other institute of learning.

Mokhtar Che Ismail

DEDICATION

In memory of my mother (Norma Daud), who passed away on 29/12/04.

My appreciation to my family for their support; my wife(Hadijah Dolah) and six children (Rufaidah, Mujahid, Aqilah, Luqman, Syahidah and Najihah).

ACKNOWLEDGEMENT

THE AUTHOR

Graduated with B.E (Mechanical Engineering) in 1989 from the University of Newcastle Australia. I was certified by Board of Engineers Malaysia as Professional Engineer in 1996. I was also awarded the prestigious ASEAN Postgraduate Scholarship in 1997 and completed M.Sc. (Materials Science and Engineering) from the National University of Singapore in 1998.

My professional expertise has been developed from my experience as Materials Engineer at Intel and later as Inspection Engineer at the national Oil Company PETRONAS. Now I am lecturing at the newly established university, Universiti Teknologi Petronas, with the aim to contribute in the shaping of engineers through teaching and mentoring and to develop an expertise through research and consultancy. Having experienced both as practicing professional engineer and academician, I believe the PhD qualification is the beginning of a new endeavour.

1.0 INTRODUCTION

1.1 Overview

The prime objective in the corrosion design basis (CDB) memorandum of an oil and gas exploration and production (E&P) project is to ensure cost optimisation and structural integrity of the installation. This entails detailed evaluation of all possible corrosion risks that govern the basis of material selection in the design stage. The correct selection of materials and corrosion mitigation methods is critical in order to withstand the potential corrosivity of the hydrocarbon sources throughout the design life.

Corrosivity in oil and gas pipelines and associated equipments originates from the composition of the oil or gas sources. Primary constituents of the sources are carbon dioxide (CO_2), hydrogen sulphide (H_2S), dissolved oxygen, organic acids and other impurities that affect the thermodynamics and kinetics of the corrosion. Other factors that govern the corrosion are: operating pressure, operating temperature, flow rate, pH and material characteristics.

Many researchers [1-12] have conducted extensive studies of possible mechanisms of CO_2 corrosion with different variables and proposed possible anodic and cathodic mechanisms. Various CO_2 corrosion predictive models were then developed as tools in the design stage. Since these models are based on different philosophies and input parameters, the results of the predictions do not always tally. Depending on which predictive model is used, different material selection systems and mitigation methods could be suggested. Since carbon steel is widely used, the prime mitigation method of CO_2 corrosion of carbon steel relies on the effectiveness of the corrosion inhibitor and protectiveness of the corrosion film.

One of the other constituents of the hydrocarbon sources that is regarded as a key issue in CO_2 corrosion is organic acid, primarily acetic acid [13]. It is known to be corrosive but has not been extensively researched and thus not accurately represented in the currently

9

available predictive models [14]. The presence of this organic acid is revealed in typical analyses of formation water as in Table 1.1 below.

Table 1.1: Example of formation water chemistry [15]

Dissolved Solids	Concentration (ppm)
CATIONS	
Sodium	29910
Potassium	325
Magnesium	50
Barium	270
Strontium	600
Iron (total)	2.5
Dissolved Iron	<0.05
ANIONS	
Chloride	52110
Sulphate	10
Carbonate	0
Bicarbonate (include organic acids)	570
Hydroxide	0
Additional Elements	
Lithium	4
Silicon	21
Phosphorus	<0.15
Boron	71
Aluminium	<0.5
Volatile fatty Acids	
Acetate	455
Propionate	47
Butyrate	<10

The roles and effects of the acetic acid species present in the system are not clear and thus warrant further studies. Clear understanding of all possible influential elements in the CO_2 corrosion process could lead to more accurate corrosion prediction that is important in the design stage. This is not only relevant to safety, by avoiding under design, but also to cost through avoidance of over design.

Thus, the objective of the study is to establish the effects of acetic acid on the CO_2 corrosion of oil and gas pipelines. The effects are to be incorporated in a predictive model so that reliable prediction of CO_2 corrosion of the carbon steel pipeline with the presence of acetic acid can be achieved.

2.0 BACKGROUND THEORY AND LITERATURE REVIEW

2.1 Corrosion Design Basis (CDB)

In any oil and gas exploration and production (E&P) project, detailed evaluation of all possible corrosion risks is done which then forms a corrosion design basis memorandum of the project. This eventually forms the basis of material selection in the design stage and then provides inputs for maintenance and inspection strategies in the operation stage. Typically, this is done in conceptual and detailed design stages as described in the following sections.

2.1.1 Corrosivity Evaluations

In the corrosion design basis, the corrosivity evaluations of hydrocarbon systems should consider all important parameters in a particular field. Typical parameters that could form the basis for material selection of the project can be broken down into several groups as shown in Figure 2.1.
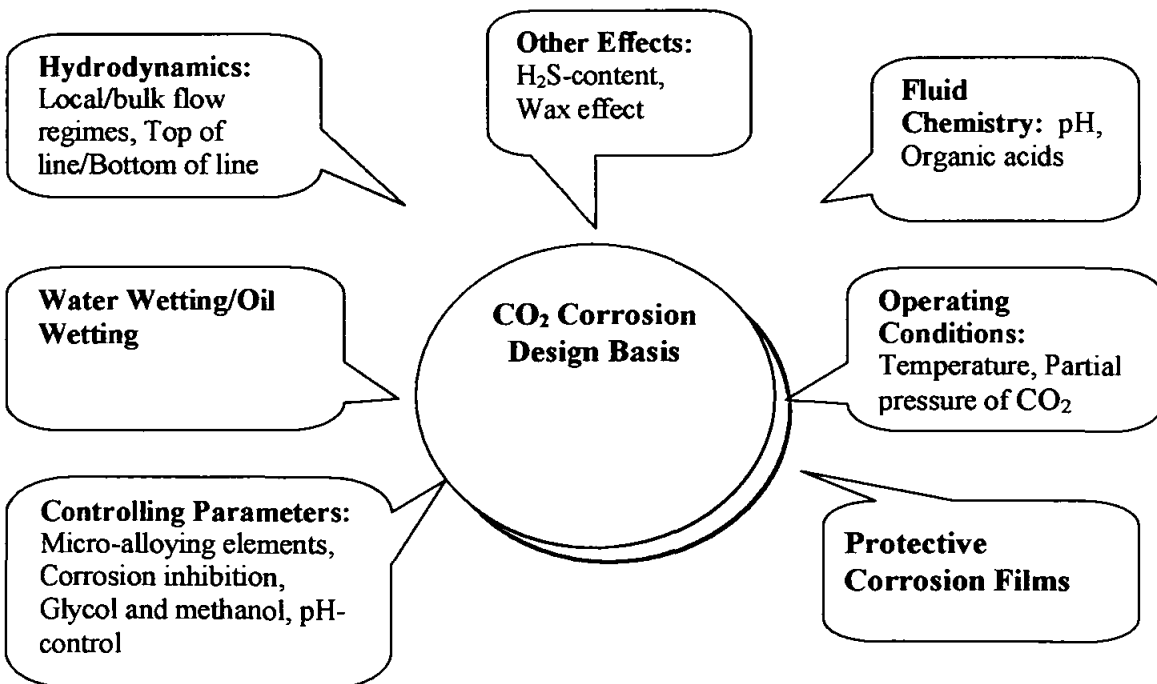
Figure 2.1: Parameters affecting CO_2 corrosion design.[16]

These factors influence the chemistry of both the formation and dissolution of the corrosion products, the rates of chemical reactions, and the rates of transport of species involved in the corrosion. The importance some of these parameters in CO_2 corrosion prediction models is summarised as follows:

- Effect of pH.

  Determination of a realistic estimate of the actual pH in the water phase, either the condensed water or formation water, is important in corrosion evaluation of oil and gas wells and pipelines. This includes the effect of bicarbonate produced by corrosion on the pH of condensed water and bicarbonate and organic acids on the pH of the formation water. It is known that the reported pH in a water analysis, usually measured at atmospheric conditions after depressurisation, is most often totally useless for a corrosion prediction [17]. The actual pH in the system must be calculated from the CO_2 partial pressure, temperature, bicarbonate content in the water, ionic strength and organic acid content. Another factor for consideration is the possibility of misinterpretation of acetic acid and other organic acids as bicarbonate that leads to a higher calculated pH. This misinterpretation has been cited by the early work of Crolet [18] and later by Hedges [14].

- Effect of protective corrosion films

  Formation of protective iron carbonate films especially at high temperature or high pH can affect the corrosion rate substantially. Protective films will not form at low temperature, as the iron carbonate solubility is high and the precipitation rate is slow. However, protective iron carbonate films can form at high temperature, as the iron carbonate solubility is lower and the precipitation rate much faster. This can lower the corrosion rate from several mm/yr for carbon steel without any corrosion films to less than 0.1 mm/yr when protective films are present.

13

- Effect of oil wetting

  Corrosion takes place only when water is present at the surface and no corrosion if oil wets the surface. If the water is transported as a water-in-oil emulsion or dispersion, corrosion can be substantially reduced.

- Temperature

  The corrosion rate increases with temperature when no protective corrosion products are formed.

- Partial pressure

  The corrosion rate increases with increasing CO_2 partial pressure. This is due to lower pH, which increases the solubility of the corrosion products.

- Velocity

  Increasing the fluid velocity may increase the rate of transport of species important to the corrosion process in gas/water systems. However, increasing the velocity may slow corrosion in oil systems, due to the entrainment of water in oil and thereby causing the steel to be wetted with oil rather than water. The velocity may also influence how corrosion inhibitors are transported or function.

2.1.2 Material Selection

The overall objectives of the material selection are to determine which material or material system offers the optimum solution for the project. In most cases, the design of CO_2 corrosion involves an evaluation of the suitability of using carbon steel or low-alloy steel which offer the following advantages:[19]:

- Satisfactory performance predictions
- Life cycle costs
- Ease of fabrication/installation.

14

The methodology applied to optimise the material selection is based on the predicted corrosion rates with a typical approach as follows:

- Calculate the expected corrosion rates of carbon steel using the predictive model.
- Determine whether or not corrosion inhibitor can reduce the corrosion rates to an acceptable level.
- Evaluate the applicability of different Corrosion Resistant Alloys (CRA).

One good example of a detailed life cycle analysis is given by Rippon [20].

The default material is always carbon steel for low to medium corrosion rates with the option to include corrosion allowances and to deploy corrosion inhibitor. For more aggressive conditions, CRA is technically justified. Since carbon and low alloy steels are extensively used in offshore and onshore oil and gas installations, accurate predictions of the corrosion rates of these materials in CO_2 environments are required. Thus, clear understanding of corrosion process of carbon steel in the environment, including the effect of inter-related parameters, is required.

2.2 CO_2 Corrosion

2.2.1 Overview

The corrosion problem in the oil and gas exploration and production sector is mainly due to the presence of a substantial carbon dioxide (CO_2) content in reservoir. Carbon dioxide dissolves in formation or condensed water resulting in a weak acid. The corrosion process of this so-called 'sweet corrosion' is complex as many parameters are involved in the mechanism of anodic and cathodic reactions. The effects of CO_2 partial pressure and temperature on the corrosion rates are shown in Figure 2.2 below.
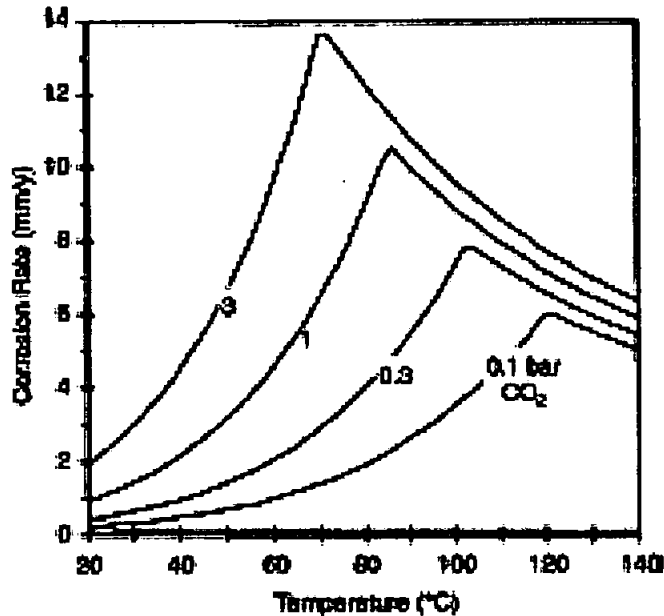
Figure 2.2: Effect of temperature on corrosion rate at different CO_2 pressure. [10]

Another important feature of CO_2 corrosion is the formation of a protective film that is a function of many parameters such as pH and temperature. The film, however, may be damaged and thus result in localised corrosion in the form of "ringworm and mesa".
With those considerations, the common approach to characterize CO_2 corrosion is to scrutinize the mechanisms and model them to predict the corrosion rate.

2.2.2 Mechanism

Corrosion of carbon steel with the presence of dissolved CO_2 and other related species, such as H_2CO_3, HCO_3^- and Fe^{2+}, involves a number of chemical, electrochemical and transport processes that occur simultaneously. Turgoose, Cottis and Lawson [21] emphasised that these electrochemical reactions are affected by solution composition and hydrodynamics and are indeed complex as many species interact in the boundary layer. Various mechanisms have been proposed in different studies. Nesic et al. [22] presented good overviews of these possible reactions. Nonetheless, these were done without considering the effect of acetic acid species in the system.

16

Thus, in order to study the effect of acetic acid in CO_2 corrosion, compilation of the possible anodic and cathodic reactions is done with the inclusion of the possible reactions of acetic acid species.

The possible reactions involved in this system can be derived from consideration of the chemical reactions of CO_2 and water systems, the cathodic mechanisms, the anodic mechanisms and influences of possible corrosion layers.

2.2.2.1 Chemical reactions of CO_2-water system

CO_2 contained in crude oil or gas flowing through the tubes and pipes reacts with formation or condensed water present in the system. Turgoose, Cottis and Lawson [21] presented the chemical reactions of the CO_2-water system at ambient temperature, and atmospheric pressure, including as a function of solution pH, based on the previous work by Kern [23]. The summary of chemical reactions in the CO_2-water system is shown in Table 2.1 below.

Table 2.1: Summary of chemical reactions of the CO_2-water system.

Possible Chemical Reactions	Equilibrium Constants	Remarks
1. Dissolution of carbon dioxide: $CO_{2(g)} = CO_{2(aq)}$	Dissolution constant K_d, $$K_d = \frac{[CO_{2(aq)}]}{P_{CO_{2(g)}}}$$	$[CO_{2(aq)}]$ = molar concentration of dissolved carbon dioxide $P_{CO_{2(g)}}$ = partial pressure of CO_2 gas.
2. Hydration of the dissolved gas to form carbonic acid, H_2CO_3:	Forward rate constant k_1 (= 0.0375 s^{-1}); Backward constant k_{-1} (=13.7 s^{-1})	The K_{hyd} value is almost independent of temperature but reduces to 2.31×10^{-3} at 300°C. [24]

$CO_{2(aq)} + H_2O \Leftrightarrow H_2CO_3$	Hydration constant $K_{hyd} = \dfrac{k_1}{k_{-1}} = 0.00258$ $k_1 = 8500 \text{ s}^{-1}$ and $k_{-1} = 1.9 \times 10^{-4} \text{ s}^{-1}$.	The small values of k_1 and k_{-1} mean that the CO_2 hydration reaction can be considered as a slow process and is therefore the rate determining step for subsequent reactions.
Another possible CO_2 hydration reaction for pH greater than 10 is: $CO_{2(aq)} + OH^- \Leftrightarrow HCO_3^-$		
3. Dissociation of the carbonic acid first to bicarbonate and then to carbonate. $H_2CO_3 \Leftrightarrow H^+ + HCO_3^-$	The dissociation constant for the first stage of this reaction is: $K_{a_1} = \dfrac{[H^+][HCO_3^-]}{[H_2CO_3]}$ $pK_{a_1} = 3.77$	The actual pK_{a_1} used here is lower than that normally reported ($pK_{a_1}' = 6.3$), since this latter value is based on carbonic acid plus dissolved CO_2 not just on carbonic acid as shown below; $K_{a_1}' = \dfrac{[H^+][HCO_3^-]}{[H_2CO_3] + [CO_{2(aq)}]}$ With the lower value, this means the CO_2 solutions are less well buffered than expected over short time periods. [21]

18

| 4. Further dissociation of bicarbonate producing carbonate ions: $$HCO_3^- \Leftrightarrow H^+ + CO_3^{-2}$$ | The dissociation constant K_{a_2} is $$K_{a_2} = \frac{[H^+][CO_3^{2-}]}{[HCO_3^-]}$$ $K_{a_2} = 4.8 \times 10^{-11} \ mol/dm^3$ $pK_{a_2} = 10.3$ | |

Based on the equilibrium constants above, the amount of each species as a function of the solution pH at 25°C and a CO_2 partial pressure of 1 bar, is shown in Figure 2.3. We observe from the figure that the dissolution of CO_2 gas and the hydration reactions are pH independent.
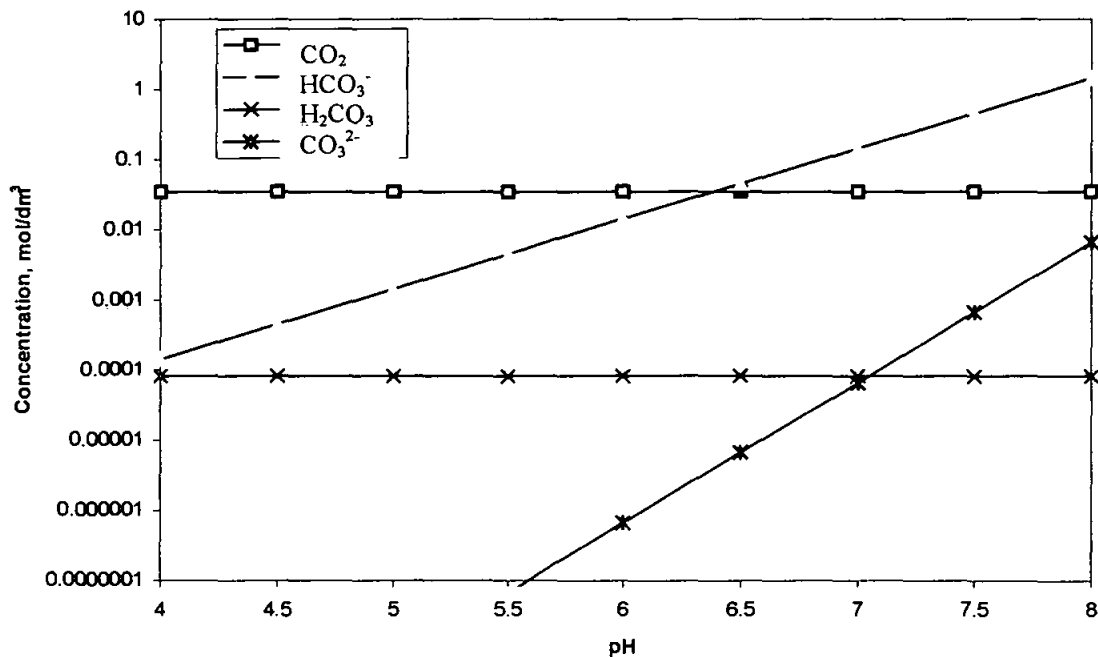
Figure 2.3: Concentration of carbonic species in water as a function of pH calculated at 1 bar CO_2 and 25°C.

Furthermore, we observe that at pH less than 5.5, the predominant carbonic species is the bicarbonate ion (HCO_3^-). As the solution pH increases the carbonate ion, CO_3^{2-}, becomes important in the solution.

In practical CO_2 corrosion environments, many other species are present and reacting in the water solutions, such as organic acid. In the case of carbon steel exposed to aqueous solution containing CO_2, the corrosion mechanism is further considered in the following sections.

2.2.2.2 Mechanism of Cathodic Reaction

The increase of corrosion rate with the presence of CO_2 is primarily due to the increases in the hydrogen evolution reaction. This supplements the usual pH-dependent proton discharge, as in strong acids (pH< 4), which is given by:

$$2H^+ + 2e \rightarrow H_2$$
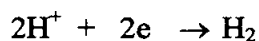
The rate-determining step is due to the diffusion rate of H^+ ions from bulk solution.[8]

In mildly acidic conditions, $4 < pH < 6$, which is typical of CO_2 solutions, direct reduction of carbonic acid becomes the dominant cathodic process as proposed by many authors such as de Waard – Milliams [1] and Gray et al [8].

$$2\ H_2CO_3 + 2e \rightarrow H_2 + 2HCO_3^-$$
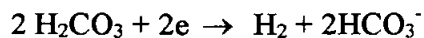
The dissociation of H_2CO_3 also contributes to the addition of H^+, which however, the effect is small [25].

It has also been suggested [9] that in CO_2 solution of pH 5, the direct reduction of bicarbonate ion becomes significant.

$$2HCO_3^- + 2e \rightarrow H_2 + 2CO_3^{2-}$$
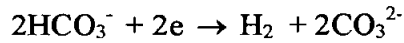
The summary of the possible mechanisms and the rate-determining step (RDS) in the reactions of the dissolved CO_2 with steel surfaces is compiled in Table 2.2 below.

Table 2.2: Compilation of the possible mechanisms and the rate-determining step (RDS) in CO_2 corrosion.

Reduction Mechanisms	Authors/Year	Remarks
Rate-determining reduction of carbonic acid with subsequent heterogeneous reformation from the bicarbonate and protons. $$H_2CO_{3_{(ads)}} + e^- \overset{rds}{\Rightarrow} H_{(ad)} + HCO_{3_{(ads)}}^-$$ $$HCO_{3_{(ads)}}^- + H_{(bulk)}^+ \Rightarrow H_2CO_3$$	de Waard-Milliams [1]/(1975)	Does not explain the subsequent experimental data of Schmitt and Rothman.
The cathodic limiting current density is the result of superimposition of processes influenced by diffusion and by a charge-transfer reaction, according to: $$i_{lim} = i_{diff} + i_R = C\omega^{1/2} + i_R$$ where i_{diff} is the diffusion component associated with the mass-transfer of reducible species from the bulk, consisting of: 1) $$H_{(bulk)}^+ \overset{rds}{\Rightarrow} H_{(ads)}^+$$ $$H_{(ads)}^+ + e^- \Rightarrow H_{(ads)}$$	Schmitt and Rothman [26,27]/(1977&1978)	Experimental data based on RDE which limits applicability to laminar flow conditions.

2) $H_2CO_{3(bulk)} \overset{rds}{\Rightarrow} H_2CO_{3(ads)}$ $H_2CO_{3(ads)} + e^- \Rightarrow H_{(ads)} + HCO_{3(ads)}^-$ and i_R is the limiting current due to a chemical reaction, (i_R), which is attributed to the slow hydration of CO_2 adsorbed on the electrode surface. $CO_{2(bulk)} \Rightarrow CO_{2(ads)}$ $CO_{2(ads)} + H_2O \overset{rds}{\Rightarrow} H_2CO_{3(ads)}$ $H_2CO_3 + e^- \Rightarrow HCO_3^- + H$		
An electrochemical-chemical reaction where the reduction of carbonic acid or bicarbonate yields bicarbonate or carbonate, respectively, which subsequently react with water to regenerate the reactant and produce hydroxide. • An electrochemical step: $H_2CO_3 + e^- \Rightarrow HCO_3^- + H$ or $HCO_3^- + e^- \Rightarrow CO_3^{2-} + H$ • Followed by a chemical step: $HCO_3^- + H_2O \Rightarrow H_2CO_3 + OH^-$ or $CO_3^{2-} + H_2O \Rightarrow HCO_3^- + OH^-$	Wieckowski et al. [33]/ (1983)	Supported the idea of a possible direct reduction of carbonic acid on the surface of the electrode as proposed by de Waard and Milliams.

22

Proposed a chemical-electrochemical mechanism; the rate determining is the result of the direct reduction of carbonic acid which is produced by the homogeneous CO_2 hydration reaction.	Eriksrud and Sontvedt [4]/(1984)	This mechanism is also known as CE and widely accepted by subsequent researchers.
Proposed that bicarbonate contributes towards reduction resulting in the formation of carbonate ions. $$2HCO_3^- + 2e^- \Rightarrow H_2 + 2CO_3^{2-}$$	Ogundele and White [5]/ (1986)	Covers only a small pH range (4.95 - 5.31), does not explain the results from rotating disc electrodes.
Proposed that the reduction rate of H_2CO_3 is controlled by the rate of a preceding chemical reaction identified as the carbon dioxide hydration reaction. They also suggested that from pH 6 to 10 the dissolution of carbon steel increased by the charge-transfer controlled reduction of HCO_3^-: $$HCO_{3(ads)}^- + e^- \Rightarrow H_{(ads)} + CO_3^{2-}$$	Gray et al. [8,9]/ (1989&1990)	
Proposed the cathodic mechanism that includes a chemical homogeneous reaction followed by an electrochemical process (CE mechanism) was a good approximation in the	Turgoose et al. [21]/ (1990)	In agreement with Eriksud [4] on homogeneous

pH range 4-5. However, it was indicated that above pH 6 the cathodic rate is controlled by the production of carbonic acid from the high concentration of bicarbonate at the surface of the electrode according to: $$HCO_3^- + H_2O \Rightarrow H_2CO_3 + OH^-$$		formation of carbonic acid.

Most of the earlier work was done using static fluid or laminar flows, which then limits the results to stagnant and low flow conditions.

The study of turbulent flow using the rotating cylinder electrode, (RCE), was done by Mendoza and Turgoose [28] on the cathodic kinetics of the CO_2 corrosion. They concluded that similar to the rotating disc electrode, there is a limiting current over a wide range of potentials, for pH 4. This limiting current was the result of flow dependent and flow independent components given by:

$$i_{lim} = C' + D' \omega^{0.7}$$

where C' and D' are constants.

Nesic et al. [29] also employing a RCE, supported the proposals of previous investigators [4,30] for a cathodic mechanism that includes a chemical reaction followed by an electrochemical reaction. They considered the cathodic reactions for an electrochemical model of CO_2 corrosion consisting of; H^+ reduction and direct reduction of H_2CO_3 and H_2O molecules. The cathodic current (i_c) was given by:

$$\frac{1}{i_c} = \frac{1}{i_{ct}} + \frac{1}{i_{lim}}$$

24

where the first term is the charge-transfer controlled current:

$$i_{ct} = i_0\, 10^{-\frac{\eta}{b_c}}$$

while the second term is the limiting current. In the case of H^+ reduction, the limiting current comes from the mass-transfer limitation for H^+ reduction:

$$i_{lim_{(H^+)}} = k_{H^+}\, F\, [H^+]_b$$

In the case of H_2CO_3 reduction, the limiting current is a consequence of the slow homogeneous CO_2 hydration and can be calculated as: [31]

$$i_{lim_{(H_2CO_3)}} = F\, C_{b_{H_2CO_3}}\, \sqrt{(D_{H_2CO_3} k_{-1})}$$

where F is the Faraday constant, $C_{b_{H_2CO_3}}$ and $D_{H_2CO_3}$ are the bulk concentration and diffusion coefficient for carbonic acid respectively and k_{-1} is the backwards dehydration constant for the hydration reaction of CO_2. It is stated that this equation derived by Vetter [31] and it is strictly valid only for stagnant solutions. As a first approximation, it was suggested [29] that this equation is correct at temperatures higher than 20°C and low velocities, ($\leq$ 1 m/s), when the mass-transfer layer is much thicker than the reaction layer.

On further experimentation, Nesic et al. [32] proposed a theoretical multiplier f which is significantly different from unity only when the thickness of the mass-transfer boundary is of the same order of magnitude as the reaction layer for H_2CO_3 hydration,

$$f = \coth(\zeta)$$

25

which takes into account the effect of flow on the chemical reaction limiting current. Parameter ζ was defined as the ratio of the mass transfer (δ_m) to the chemical reaction (δ_r) layer thickness:

$$\zeta = \frac{\delta_m}{\delta_r} = \frac{\dfrac{D_{H_2CO_3}}{k_{H_2CO_3}}}{\sqrt{\dfrac{D_{H_2CO_3}}{k_{-1}}}}$$

where $k_{H_2CO_3}$ is the mass-transfer coefficient for carbonic acid and k_{-1} is the backwards rate constant for the hydration reaction of CO_2. The limiting current due to H_2CO_3 reduction is now given by:

$$i_{lim_{(H_2CO_3)}} = F\, C_{b_{H_2CO_3}}\, \sqrt{(D_{H_2CO_3} k_{-1})}\, \coth(\zeta)$$

and for stagnant solutions $f = 1$, (i.e. Vetter's equation).

Nesic and co-workers [32] also proposed that the superposition of the limiting currents due to diffusion and reaction of H_2CO_3 molecules, could be expressed in terms of a pure limiting current, corrected for the presence of a rate limiting chemical reaction. In this way, the cathodic limiting current due to carbonic acid reduction measured in solutions containing dissolved CO_2 will be given by:

$$i_{lim_{H_2CO_3}} = F\, k_{H_2CO_3}\, C_{b_{H_2CO_3}}\, \zeta \coth(\zeta)$$

On further research, performed by Mendoza [33] using the RCE apparatus in the temperature range of 20°C to 80°C and P_{CO_2} of 0.1 and 1 bar, the findings of other scientists [4,29,30] were verified. The measured limiting current was found to depend on CO_2 partial pressure and flow. He suggested that as the solution pH increases the i_{lim} region tends to become less well defined, due to the higher contribution of the direct

26

reduction of carbonic acid to the overall cathodic mechanism, at 20°C and P_{CO_2} 1 bar. Subsequently the flow dependence of the limiting current becomes less pronounced. As the temperature of the solution increases the limiting current also increases. However, at low rotation speeds, the limiting region is less well defined than at room temperature. The flow independent limiting current was found to increase with CO_2 partial pressure and temperature, as measured indirectly from the intercept on the i_{lim} versus $u^{0.7}$ plots. The limiting current at pH 3.8 was found to be larger than the corrosion rate, at P_{CO_2} of 1 bar, indicating that under those conditions the system is under activation or charge-transfer control. However as the solution temperature increases, the corrosion rate becomes flow dependent and i_{corr} values are of the same magnitude as i_{lim}, especially at 80°C.

The corrosion rate at room temperature, P_{CO_2} 1 bar and saturation pH was found to be flow independent, in contrast to the observations by Nesic et al. [29]. On the other hand, it appears that increasing solution pH results in a slight increase in the i_{corr} values. At the natural saturation pH, the temperature has an even more detrimental effect on the corrosion rate, with the additional effect of flow sensitivity. In addition, reduction of the CO_2 partial pressure to 0.1 bar resulted in a flow dependent corrosion rate at the natural-saturation pH, whilst increasing the solution pH reduces the i_{corr} values and the flow sensitivity of the system. However, it has to be pointed out that all measurements performed a short time after immersion and thus the time factor was not incorporated into the results.

2.2.2.3 Mechanism of Anodic Reaction

The anodic reaction consists of several steps as proposed by Bockris et.al. [34] which can be simplified by

$$Fe \rightarrow Fe^{2+} + 2e$$

The mechanism proposed by Bockris et al. [34] has frequently been assumed to apply in CO_2 solutions. The assumption is not accurate as the pH dependency falls rapidly at pH higher than 4. [27]

Thus, in a recent study, Nesic et al. [29,101] proposed that mechanisms are different from that obtained in strong acids. They proposed that the anodic dissolution of iron is affected by the presence of CO_2.

Videm [35] suggested that dissolution of steel has a pH-dependent and pH-independent region where in the pH–dependent region the rate of charge transfer increases proportionally with the OH^- concentration. Above a certain pH, about 4.2, the dissolution is suggested to be pH-independent.

2.2.2.4 Chemistry of Acetic Acid

The dissociation of acetic acid in water is given by

$$CH_3COOH + H_2O \leftrightarrow CH_3COO^- + H_3O^+$$
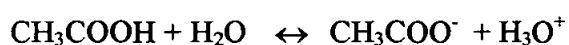
with $Ka = 1.74 \times 10^{-5}\ s^{-1}$ and $pKa = 4.76$.

This is a weak acid with the major species present in solution at equilibrium are CH_3COOH molecules.

In reaction with bicarbonate ion, acetate ion (Ac) and carbonic acid are produced as shown below.

$$CH_3COOH + HCO_3^- \leftrightarrow CH_3COO^- + H_2CO_3$$
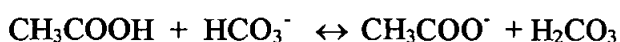
Since acetic acid is a stronger acid ($pKa=4.76$) than carbonic acid ($pKa=6.36$), the position of the equilibrium lies to the right .

Acetic acid (HAc) dissociates, and is then followed by electron transfer, as below:

$$HAc \leftrightarrow H^+ + Ac \quad \text{and}$$

$$H^+ + e^- \rightarrow 1/2H_2$$
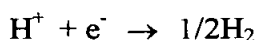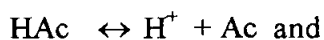
The dissociation reaction is very fast with a rate constant of about 10^6 s^{-1}; so the cathode reaction may be considered to be as follows [37]:

$$HAc + e^- \rightarrow 1/2\ H_2 + Ac$$
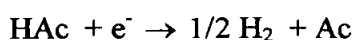
In consequence, it is not possible to distinguish the reductions of acetic acid and free protons [22].

The overall corrosion reaction for alloy steel in CO_2 containing environment with the presence of acetic acid is:

$$Fe + H_2CO_3 \rightarrow FeCO_3 + H_2$$
$$Fe + 2HAc \rightarrow Fe(Ac)_2 + H_2$$
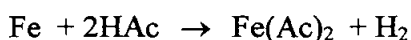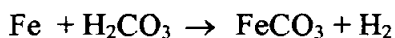
The corrosion product, iron carbonate, may form a protective film or semi-protective film that controls the corrosion. Iron acetate, which is much more soluble than iron carbonate, interacts with the iron carbonate formation leading to an increase in corrosion rate. This interaction between iron acetate and iron carbonate film is, however, not widely studied.

2.2.3 Film Formation

The electrochemical reactions are often accompanied by the formation of films of $FeCO_3$ (and/or Fe_3O_4) which can be protective or non-protective depending on the conditions under which they are formed [22]. The precipitation of $FeCO_3$ is favoured with increase

in pH, temperature and all measures that can reduce the transport of reactants and corrosion products from the steel surface [38].

Videm et al.[36] stated that, above 80°C, reliable scales are often found where as below this temperature, a pH value of at least 6 is required.

Ikeda et al[39] proposed two film formation models for high and low temperatures:

1) At high temperature bulk formation occurs, where film precipitation is controlled by the concentration of Fe^{2+} ions, $FeCO_3$ solubility and bicarbonate concentration.

2) At lower temperature, where the films are thin and relatively less protective, a surface formation model proceeds. Local pH increases favour $FeCO_3$ formation at surface anodic sites. The factors that control the formation are:
   - solubility product;
   - ferric ion concentration; and
   - carbonate/bicarbonate concentrations.

It is also noted that damage of protective films can occur due to fluid erosion effects or other local turbulence from fitting and joining protrusions. However, Schmitt et al. [40] argued that the damage of protective film is primarily due to the effect of intrinsic stresses not the extrinsic stress, such as wall shear stresses. He argued that the normal wall shear stress in flow systems is in the order of 10^{-5} to 10^{-4} N/mm^2, or even 10^{-2} to 10^{-5} N/mm^2 in turbulent flow conditions, which is much lower than scale adhesion strength of magnitude $1 - 30$ N/mm^2. Thus, it was stated that the requirements for prediction of protective film formation should encompass the followings[41]:
   - Formation of protective corrosion product layers;
   - Stability of these layers;
   - Adherence to the steel surface; and
   - Repair of damaged scales at temperature above 80°C. At lower temperatures, a pH value of at least 6 is required.

On the other hand, with the presence of acetic acid species in the bulk solution, which diffuse to the surface and corrosion films, a different phenomenon occurs. Crolet [42]

highlighted that any replacement of bicarbonate by an equivalent amount of acetate will decrease the protectiveness of the corrosion layer due to the increase the local solubility of iron and elimination of alkalinity. In addition, the internal acidification which provides a local acetate-rich environment would trigger localised corrosion of the steel.

Furthermore, Crolet [43] likened the role of acetic acid with respect to the iron carbonate layer to that of a fluxing or complexing agent.

2.2.4 Flow Effects in CO_2 Corrosion

The effects of flow on CO_2 corrosion, as discussed above, can be due to cavitation, erosion corrosion and flow-accelerated corrosion. In flow-accelerated corrosion, fluid flow increases the mass transfer of the chemical species to or from the metal surface.

In situations where a reaction is controlled by diffusion of reacting species, the corrosion rate is related to the concentration driving force (C) and the mass transfer coefficient (k). The mass transfer coefficient, k, is defined by

$$ilim = nFkCb$$

where *ilim* is the limiting current density for cathodic reaction and Cb is the bulk concentration of cathodic reactant. With the knowledge of the mass transfer coefficient (k), we can predict the corrosion rate due to a mass transport- controlled reaction.

There are many different empirical expressions relating mass transfer coefficients to flow rate, fluid flow properties, species properties and system geometry. These empirical relationships are conveniently expressed by dimensionless numbers. The common dimensionless numbers are listed in Table 2.3.

Table 2.3: The common dimensionless numbers.

Dimensionless Numbers	Descriptions
The Reynolds number $$Re = \frac{u\,l}{\nu}$$ where u is the mean velocity and ν is the kinematic viscosity of the fluid. The kinematic viscosity is given by the ratio: $$\nu = \frac{\mu}{\rho}$$ where μ and ρ are the viscosity and density of the fluid, respectively.	Identifying the type of flow occurring in a system, also defines a relative flow velocity in terms of a characteristic length "l", defined according to the system under study.
The Schmidt number, Sc_i, is defined, for a species "i", as: $$Sc_i = \frac{\mu}{\rho\,D_i} = \frac{\nu}{D_i}$$ where D_i is the diffusion coefficient of the species "i" in the fluid.	The Schmidt number, Sc_i, is a dimensionless number associated with the mass-transfer properties of the fluid.
The Sherwood number, Sh, is defined, for species "i", as: $$Sh_i = \frac{k_i\,l}{D_i}$$ $$k_i = \frac{i_{lim_i}}{n\,F\,C_{b_i}}$$ where, C_{bi} =Bulk Concentration. Then, the Sherwood number can be rewritten in terms of the limiting current density as: $$Sh_i = \frac{i_{lim_i}\,l}{n\,F\,D_i\,C_{b_i}}$$	The Sherwood number, Sh, is a dimensionless group associated with the mass-transfer coefficient, k_i, of a specific species in the fluid.

Hydrodynamic analyses have shown that the Re, Sc_i and Sh_i dimensionless numbers can be correlated by the following expression:

$$Sh_i = D \, Re^x \, Sc_i^y$$

A good review of the electrochemical measurements in flowing conditions is presented by Poulson[44] which summarised results from rotating disc, rotating cylinder, impinging jet, orifice and tube apparatus.

Two most common hydrodynamic test systems used in the corrosion studies in flow environment are presented below.

2.2.4.1 The Rotating Cylinder Electrode (RCE).

The rotating cylinder electrode has been widely used as laboratory hydrodynamic test system in corrosion studies. This popularity is mainly due to some of its characteristics, such as being designed for working in turbulent flow conditions, its well-understood mass transfer properties, its ease of construction and operation, and low cost [45,46].

It has been found that for a RCE enclosed in a concentric cell, the transition between the laminar and turbulent flow occurs at low rotation rates. This transition has been suggested to occur at values of Reynolds number of approximately 200 [45,46]. This Reynolds value will be equivalent to a peripheral velocity of 0.02 m/s (approximately 38 rpm), for a cylinder of 0.01 m in diameter immersed in pure water. When the RCE is immersed in a fluid and rotated at a very low rotation rate, the fluid moves in concentric circles around the cylinder. As the rotation rate of the cylinder increases the flow pattern is disrupted and a cellular flow patterns, known as Taylor vortices, appear and the turbulent condition develops. These vortices enhance the mass momentum and heat transfer of the rotating electrode.

The RCE in corrosion laboratory studies is a useful tool for the understanding of mass-transfer processes, effects of surface films and inhibition phenomena taking place in turbulent flow conditions. However, its use in CO_2 corrosion studies has been questioned by some researchers[47]. The argument about the validity of the use of the RCE in CO_2 corrosion studies, arises from the differences found between the values of corrosion rates measured in pipe flow electrodes and in the RCE.

2.2.4.2 Mass-Transfer Expressions for the Rotating Cylinder Electrode.

In 1954, Eisenberg et al.[48] published what it is now considered the basic study on the mass transfer characteristics of the RCE. Based on the electrochemical study of the reduction-oxidation reaction of the $Fe(CN)_6^{-3}$ / $Fe(CN)_6^{-4}$ ions, they determined the relationship between the measured limiting current density of an electroactive species "i" in solution, (i_{lim_i}), and the rotation rate of the cylindrical electrode, (u_{RCE}). This relationship is given by the following equation:

$$i_{lim_i} = 0.0791 \, n \, F \, C_{b_i} \, d_{RCE}^{-0.3} \, v^{-0.344} \, D_i^{0.644} \, u_{RCE}^{0.7}$$

which can be rearranged to:

$$Sh_{i,RCE} = 0.0791 \, Re_{RCE}^{0.7} \, Sc_i^{0.356}$$

where, n is the number of electrons involved in the electrochemical reaction, F is the Faraday constant, d_{RCE} is the diameter of the cylindrical electrode, i.e. the characteristic length "l", C_{b_i} is the concentration in the bulk of the solution of the ionic species "i" involved in the electrochemical reaction, v is the kinematic viscosity of the environment and D_i is the diffusion coefficient of the species "i".

The equation for the RCE proposed by Eisenberg and co-workers predicts at a constant temperature, a linear relationship between the measured i_{lim_i} and the rotation rate of the electrode to the power of 0.7:

$$i_{lim_i} = A\, u_{RCE}^{0.7}$$

where the constant A is equal to:

$$A = 0.0791\, n\ F\ C_{b_i}\ d_{RCE}^{-0.3}\ \nu^{-0.344}\ D_i^{0.644}$$

2.2.4.3 Wall Shear Stress and Mass-Transfer for the Rotating Cylinder Electrode.

In order to calculate a value of wall shear stress for the RCE, $\tau_{w_{RCE}}$, the following equation is used, developed initially for flow through a pipe: [49]

$$\tau_{w_{RCE}} = C_{f_{RCE}} \frac{1}{2} \rho\ u_{RCE}^2$$

where ρ is the density of the fluid, u_{RCE} is the peripheral velocity of the rotating cylinder and $C_{f_{RCE}}$ is the friction coefficient. Eisenberg [48] used the following empirical expression for $C_{f_{RCE}}$ in the turbulent regime, between $10^3 < Re_{RCE} < 10^5$:

$$\frac{C_{f_{RCE}}}{2} = 0.0791\ Re_{RCE}^{-0.3}$$

The expression for the wall shear stress can be written as:

$$\frac{\tau_{w_{RCE}}}{\rho\, u_{RCE}^{2}} = 0.0791\, Re_{RCE}^{-0.3}$$

This is the common expression used in the calculation of $\tau_{w_{RCE}}$. An alternative expression for the wall shear stress is obtained if the mass-transfer expression proposed by Eisenberg and the universal velocity profile concept are considered:

$$\frac{\tau_{w_{RCE}}}{\rho\, u_{RCE}^{2}} = 1.92\, Re_{RCE}^{-0.6}$$

The relationship between $\tau_{w_{RCE}}$ and the mass-transfer coefficient of the diffusing species "i" can be expressed as:

$$k_{i_{RCE}} = 0.225 \left(\frac{\tau_{w_{RCE}}}{\rho}\right)^{0.41} \left(\frac{\nu}{d_{RCE}}\right)^{0.18} Sc_i^{-0.644}$$

However, the results obtained for mild steel in CO_2 solutions under various conditions, using each rig, have been under extensive criticism, since there was no obvious correlation between them [47]. It was concluded that the RCE apparatus under-estimates corrosion rates when compared to a flow loop. However, Turgoose et al. [50] showed that the RCE provides baseline corrosion data comparable with that from an infinitely long pipeline. Test loop electrodes are usually of short length with not fully developed mass-transfer boundary layers, which vary with distance along the electrode. This results in much higher mass-transfer to and from the short electrodes. However, this may not affect the cathodic reaction rate, which, as stated previously, is not often mass-transfer controlled but it may affect the surface ferrous ion concentration leading to a lack of development of iron carbonate on pipe electrodes.

2.2.4.4 Pipe Flow

For flow in straight, smooth pipe, there are a large number of empirical mass transfer expressions in open literatures. For example, the expression due to Chilton and Colburn [51];

$$Sh = kd/D = 0.023 Re^{0.8} Sc^{0.33}$$

which can also be expressed in terms of the mass transfer coefficient

$$K = 0.023 \, D^{0.67} \, V^{-0.47} \, u^{0.8}/d^{0.2}$$

Other empirical expressions give similar results: Berger and Hau [52] give

$$Sh = kd/D = 0.017 Re^{0.86} Sc^{0.33}$$

However, in real systems pipes are not smooth and straight and hence the equation derived from smooth pipes does not apply. Nonetheless, the since the wall shear stress can be determined from pressure drop, an expression that relates shear stress to flow parameters was given by Chilton and Colburn [51].

The determination of average shear stress is important since it has been suggested by Silverman [53] that same mass transfer conditions prevail for systems with the same shear stress magnitude, same flow regime and satisfying the non-slip condition at the wall. It is found from the RCE and straight pipe tests, the overall scalar transport rate is identical with mean wall shear stress. However, the scalar transport mechanism in the two configurations was different. For the straight pipe, the scalar transport arises from turbulent convection and molecular diffusion, whereas in the turbulent flow of a rotating cylinder, it includes turbulent Taylor vortices.

2.3 CO₂ Corrosion Predictive Models for Carbon Steel

Predictive models are developed as an engineering design tool to be used ideally in all stages of project development and subsequent operation and maintenance of the plant. This is idealistic as there are many factors involved that complicate the matter. As such, although there are many different models available, they are developed from different philosophies and bases, namely:

- Worst case or maximum risk approach, which is based solely on laboratory test data; and
- Most probable risk approach that is partly based on field data.

Nesic et al. [15] presented a good review of the available models and categorised them into three groups:

1. Mechanistic models – Utilising firm theoretical background to describe the mechanisms of the underlying reactions;

2. Semi-empirical models – Partly based on firm theoretical background and partly based on empirical functions; and

3. Empirical models – Based mostly on best-fit parameters from experimental results, hence, relying on minimal theoretical background.

Nyborg [54] highlighted that the main difference in these models is in their treatment of the effect of protective films and the effect of oil wetting. The fact that these different models are based on different philosophies and parameters renders them neither equivalent nor interchangeable.

Table 2.4 below shows the parameters that are used by different models, as compiled from the open literature [38, 54].

38

Table 2.4: An overview of the parameters treated in the various predictive models

PARAMETERS	MODELS												
	DW 75	DW 91	DW 93	DW 95	CASSANDRA	NORSOK	CORMED	LIPUCOR	KSC (IFE)	USL/ULL	PREDICT	HYDROCOR	Ohio Model
P_{CO2}	•	•	•	•	•	•	•	•	•	•	•	•	•
Temperature	•	•	•	•	•	•	•	•	•	•	•	•	•
pH		•	•	•	•	•	•	•	•	•	•	•	•
Flow rate		•	•	•	•	•	•	•	•	•	•	•	•
Flow regime				•		•	?	•	•	•	•		
Scale factor		•	•	•		•	?	•	•	•	•	•	•
Total Pressure			•	•		•	?	•	•	•	•	•	•
Steel				•			?	•	•			•	
Water wetting		?	?	?			?	•		•	•		•
Ca/HCO₃					•		•				•	•	
H₂S							•	•		•	•		
Acetic Acid					?		?			?		?	
Field data						•	•	•		•	•		

• Parameters considered directly

? Parameters considered indirectly or not considered highly influential

Brief description of these models is presented in Table 2.5 with comment on the treatment of acetic acid in the model.

Table 2.5: Brief description of various models used in the oil and gas industry.

Models	Brief Description	Comment on HAc
de Waard et al. (DW)	First version published in 1975 [1] based only on temperature and P_{CO2}. Correction factors for the effect of pH, non-ideality of CO_2 at high pressures and protective film formation introduced in 1991[10]. A new model in 1993 [11] accommodates the effect of flow particularly on the effect of mass transport and fluid velocity. Latest version, in 1995 [55], includes the steel composition and also represents a best fit to the flow-loop data generated at IFE. The model was developed primarily for wet gas pipelines.	Not considered.
CASSANDRA [56]	This is BP's model based on de Waard models and own experiences. Spreadsheet on pH calculation module is included which requires CO_2 content, temperature and full water chemistry as inputs. The effect of protective corrosion films is set as a user-option. It gives three corrosion rates based on DW 1993, DW 1995 and the average of the both models setting DW 1993 as the minimum value.	Acetate determined from water analysis is an input into model for calculation of pH .
NORSOK [57]	This model is an empirical model based on laboratory data at low temperature and a combination of laboratory and field at temperatures above 100°C. The model predicts lower corrosion rates at high temperatures and pH values than de Waard models as it considers the effect of protective films.	Not considered.

CORMED	Developed in 1991 and predicts the probability of corrosion risks in wells in formation water and condensed water. This is based on field experiences of Elf's operations and others [25,58,59]. The corrosion risk is predicted to be either low, medium or high based on CO_2 partial pressure, potential corrosivity, in-situ pH, in-situ free acetic acid concentration and Ca^{2+}/bicarbonate ratio.	Free acetic acid is considered as a criterion in determining risk category and in pH calculation.
LIPUCOR	This is TOTAL'S model and is based on both laboratory results and field data whereby more than 90 case histories have been used [60].	Not considered.
KSC (IFE)	Based on mechanistic modeling of electrochemical reactions, transport processes and film formation processes. The properties of the corrosion films are correlated with loop experiments [61,62].	Not considered.
PREDICT	This is based on the de Waard-Milliams relationship with other correction factors and 'effective CO_2 partial pressure' calculated from the system pH [54].	Not considered.
HYDROCOR [63]	Developed by SHELL combining corrosion and fluid flow modelling to be used for predicting corrosion in pipelines. Caters for protective film formation, oil - wetting, H_2S content, top-of-line corrosion, oxygen corrosion, micro-biologically-induced corrosion and organic acid corrosion.	Considers the contribution of organic acid in the model. Not conclusive.
OHIO MODEL [64]	Predictive models to be used in multiphase flow conditions.	Not considered.

2.4 Morphology of CO_2 Corrosion

Carbon steel and low alloy steel in the aqueous CO_2 environment could be susceptible to general corrosion and localised forms of attack depending on various parameters, as highlighted previously. Kermani [38] categorised the localised corrosion as pitting, mesa attack and flow-induced.

1. Pitting

This is the main corrosion failure in CO_2 environments although there are no conclusive findings on the initiation and propagation of this failure. Nonetheless, in the field, some failures have been observed adjacent to non-metallic inclusions or incipient mesa attack. Schmitt et al. [65] studied the effects of temperature, chloride concentration, nature of anions and cations and corrosion inhibitors on the pit initiation.

2. Mesa type attack

This localized corrosion is prone to occur in low to medium flow conditions where the protective iron carbonate film is unstable. Higher temperatures promote corrosion by elongated corroded areas (mesas) oriented in the direction of flow. The most severe metal loss often occurs at areas of high fluid turbulence, such as welds, tubing joints, or ends/constrictions in piping. It is rare to lose significant amounts of metal uniformly.

3. Flow-induced localized corrosion

This is an extension of pitting and mesa attack by the local turbulence created by the protrusions.

42

2.5 Literature Review of Acetic Acid

Organic acid, especially acetic acid, in oil reservoir formation water could be formed from organic matter by thermogenic processes called heterotrophic acetigenesis [66]. The presence of organic acids termed as carboxylic acids, and hence their corrosive roles in CO_2 corrosion, have been known since 1940s. This subject has then been dormant for thirty years until re-examined in 1980s. The conclusion at that time was that these organic acids played a secondary role in CO_2 corrosion [67].

Organic acids present in formation water could be in the form of acetic, propionic, butyric and lactic acids that could be regarded as equivalent since they have approximately the same dissociation constants (pKa) and solubility of their salts. The typical pKa values of some organic acids are shown in Table 2.6 below.

Table 2.6: Typical Organic acids in the formation water

Structure	IUPAC Name	Common Name	pKa
CH_3COOH	Ethanoic acid	Acetic acid	4.76
CH_3CH_2COOH	Propanoic acid	Propionic acid	4.86
$CH_3(CH_2)_2COOH$	Butanoic acid	Butyric acid	4.83

Since 70% of the total amount of these species is acetic acid species, they are termed as total acetates.

Crolet [25, 67] concluded that since the concentrations of CO_2 and bicarbonate ions are always greater, the carbonic acid buffer plays the major role. As highlighted again by Crolet [25], as long as the concentrations of acetate and acetic acid are lower than bicarbonates, any addition of acetic species will not contribute to the pH value.

Crolet and Bonis [25] concluded by virtue of the following buffer system
H_2CO_3 + Ac $\leftrightarrow$ HCO_3^- + HAc that:

43

- Addition of acetate (Ac) will produce a buffering action by conversion of acetate to undissociated acetic acid.

- Although acetates can contribute to the alkalinity of waters when bicarbonate (HCO_3^-) are already present, the addition of acetic species has no influence on pH.

- Acetates could partially re-associate to acetic acid under CO_2 pressure that increases the oxidizing power of the solution. Hedges [14] also observed this effect with 100 ppm NaAc increasing the corrosion rate, although pH also increases. The corrosion rate increased from 4.0 to 6.5 mm/yr in the solution without HCO_3^- and from 3.0 to 5.0 mm/yr in the solution with HCO_3^-.

Thus, as long as these compounds remain at a low level, either acetic acid or acetate can be added indifferently. The practical consequence is that the in-situ pH depends only on CO_2 and bicarbonate content and not on the presence of acetic species. The only concern as stressed by Hedges [14] is the possibility of misinterpretation of bicarbonate analysis from the alkaline titration methods that include 2/3 of acetate as bicarbonate, which could falsify pH calculation.

From previous considerations, Crolet [59] presented the rules of prediction for oil and gas wells based on field data as follows:

1. at high CO_2 partial pressures, only CO_2 is corrosive;

2. at lower partial pressures, CO_2 remains the principal corrosive agent, because it enables the formation of acetic acid in-situ; and

3. at low P_{CO2}, the corrosivity is indeed due to the acetic acid, but only the in-situ acetic acid and not the total acetates analysed.

It is also reported [18] that under 100 kPa CO_2 solution of pH 5 with and without bicarbonates at 25°C and with the presence of 10 mM of acetate ions, the concentrations of undissociated acetic acid species are 0.75 mM and 2.4 mM respectively, which could contribute to the increase in cathodic current density. In a similar analysis, based on speciation analysis using PHREEQC 2.2 analysis software [68], the threshold value is

about 1 mM Ac which produces about 0.56 mM HAc that exceeds the concentration of bicarbonate and proton concentration at pH 4.4 and 25°C [69]. Thus, for acetate concentrations of more than 1 mM Ac, the organic buffer will be more dominant.

Two recent studies of the effect of acetate on CO_2 corrosion concluded that acetate increases the corrosion rate [14,15]. Ueda and Takabe [70] studied the effect of organic acid on CO_2 corrosion of carbon and chromium-bearing steels and concluded that the corrosion rate increases without influence on the scaling temperature. Earlier than that, Crolet [59] regarded the effect of acetic acid as part of the criteria for predicting the corrosivity potential of wells.

In general, the presence of free acetic acid increases the corrosion rate substantially as highlighted by Hedges [14]: 100 ppm HAc increased the corrosion rate from 3.8 to 9.1 mm/yr and 300 ppm increased the corrosion rate from 2.8 to 14.1 mm/yr. It was concluded that the increase in the corrosion rate is not solely due to the bulk pH effect but due to Ac-influence. Since his work and the others were done with drift of pH, the real effect of acetic acid species could not be distinguished. Hedges [14], however, concluded that corrosion rate increases both due to decreasing pH and solubilisation of Fe^{2+} which then suppresses iron carbonate film formation.

In a similar way, Crolet [42] highlighted that at low CO_2 partial pressure, genuine acetic acid corrosion governs where the main effect is on the protectiveness of the corrosion layers. This is similar to the thinning effect advocated by Hedges in the sense that the majority of corrosion films is iron acetate, which is much more soluble than iron carbonate.

However, recent work by Garsany and Fletcher [37] provided interesting evidence that acetic acid species are more dominant in the CO_2 saturated solution than carbonic buffer. This is based on the dramatic increase in cathodic current density observed in the testing.

Garsany et al. [69] considered that the role of both the undissociated proton donors and the solution chemistry of the weak acid buffers has been much underestimated in the interpretations proposed for the acceleration of steel corrosion by acetate in the carbon dioxide saturated brines. Garsany and Fletcher [37] argued that the reduction of carbonic acid plays a minor role in the corrosion of steel in brines containing acetic acid. Garsany and Fletcher [37] reported that the partial cathodic current density increases substantially with the higher concentration of acetic acid and concluded that the limiting current is controlled by the mass transport of both proton and un-dissociated acetic acid to the electrode surface. Corrosion current densities increase linearly with increasing acetic acid concentration, which indicates that the corrosion rate is largely determined by the concentration of the HAc.

One thing in common on the research of acetic acid corrosion in CO_2 corrosion is that the mechanisms of corrosion are not altered. It only alters the kinetics of the reactions whereby it is concluded that the presence of acetic acid species accelerates the reactions. A number of field failures have been linked directly to acetic acid corrosion. As such based on the open literature, the following concentrations of organic acid have been recorded to cause failures:

1. BP's field experience revealed that at low partial pressure of CO_2 and high bicarbonate concentration (400 ppm), flowlines could fail by pitting with the presence of 100 ppm acetic acid species [14].

2. Elf's field experience shows that fields with CO_2 partial pressures below 5 bar and pH above 5.6 are non-corrosive, provided the concentration of free acetic acid is below 0.1-1 mM.

3. Shell also experienced failure due to the presence of organic acid as follows [71]:

   • The presence of 700 ppm organic acid caused the failure of a carbon steel inlet nozzle of an offshore flash vessel on a sweet natural gas platform. The nozzle

failed in less than two years, which corresponds to a corrosion rate of more than 3 mm/y. The partial pressure of CO_2 was almost zero.

- The second field case was due to the presence of 150 ppm organic acid which resulted in the failure (leak) of a water/condensate drainpipe in an onshore sweet natural gas plant. Failure occurred after one year of service, which corresponds to a corrosion rate of about 5 mm/yr.

Since no single predictive model incorporates acetic acid species in the calculation, and the fact that acetic acid is corrosive, a challenge is presented to the currently available predictive models concerning [14]:

- HAc decreases the pH and increases the corrosion rate, with the increase in the corrosion rate being greater than that predicted by some of the models;
- Ac increases the pH, but also increases the corrosion rate.

3.0 EXPERIMENTAL METHODS

3.1 Introduction

Electrochemical studies were performed under stagnant and dynamic conditions with the use of static electrodes and the rotating cylinder electrode (RCE) apparatus. Two types of electrochemical measurements were employed in the study, which are Linear Polarisation Resistance (LPR) and Polarisation Tests. Reproducibility of the results is ensured by accurate preparation of test samples and test solutions. The tests are repeated at least twice for each case.

3.2 Electrochemical Test methods

3.2.1 Linear Polarisation Resistance (LPR)

This method is based on the linear approximation of the polarisation behaviour at potentials near the corrosion potential. Rp is given by Stern and Geary [72] equation

$$R_p = \frac{\Delta E}{\Delta i} = \frac{\beta_A \beta_C}{(\beta_A + \beta_C)i_{corr}}$$

$$i_{corr} = \frac{B}{Rp}, \text{ where } B = \frac{\beta_A \beta_C}{(\beta_A + \beta_C)}$$

ba = 2.3 β_A and bc = 2.3 β_C ; B = babc/2.3(ba+bc)

ba and bc = Tafel slopes for anodic and cathodic curves respectively.

The Stern-Geary constant, B, is approximated as 25 mV for all pH. This is in agreement with the available data, such as Sun [73].

The corrosion current can be related directly to the corrosion rate from Faraday's law:

$$\text{Corrosion rate (mm/year)} = \frac{315 \times Z \times i_{corr}}{\rho \times n \times F}$$

where, Z = Atomic weight of iron, 56 g/mol

i_{corr} = Corrosion current density, $\dfrac{\mu A}{cm^2}$

ρ = Density of iron, 7.8 g/cm^3

F = Faraday's constant, 96,500 C/mole

Linear polarization resistance measurements were performed by firstly measuring the corrosion potential of the exposed sample and subsequently sweeping from -10 mV to +10 mV with respect to Ecorr at 0.5 mV/s.

3.2.2 Polarization Curves.

Anodic and cathodic polarization curves were performed on individual coupons in freshly prepared solutions. The sample was allowed to reach a steady-state, after 24 or 50 hrs and subsequently it was polarized either in the anodic or cathodic direction to a maximum of 500 mV which was the maximum applied potential by the instrumentation box. The sweep rate was 1 mV/s.

3.3 Experimental set-up

A schematic diagram of the set-up for both static and RCE experiments is shown in Figure 3.1. The reference electrode used is a saturated calomel electrode (SCE) (+0.242 V-SHE) and the auxiliary electrode is a platinum electrode.
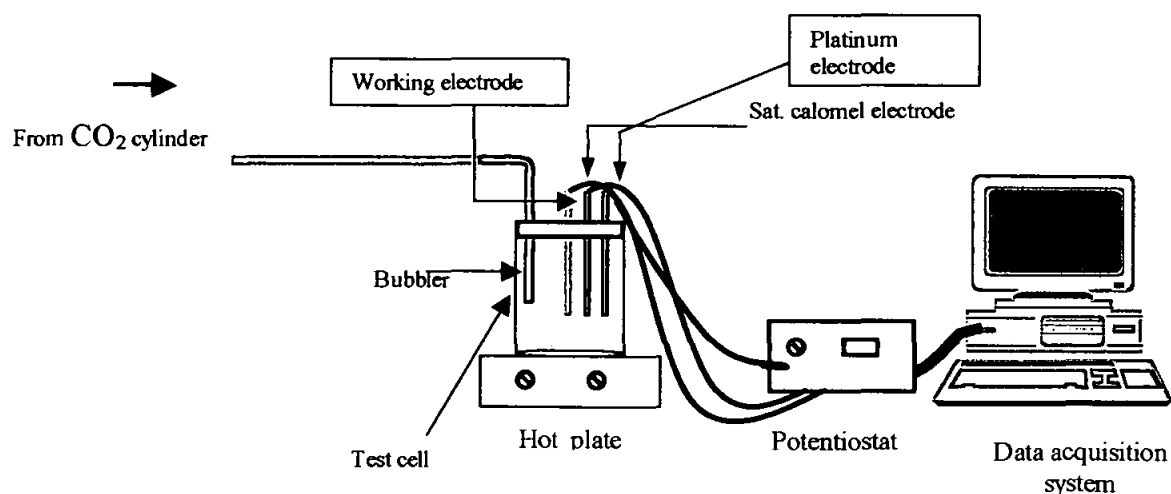
Figure 3.1: Experimental set-up

3.3.1 Static Test Set-up

The typical experimental set-up for the static test is shown in Figure 3.2 below.
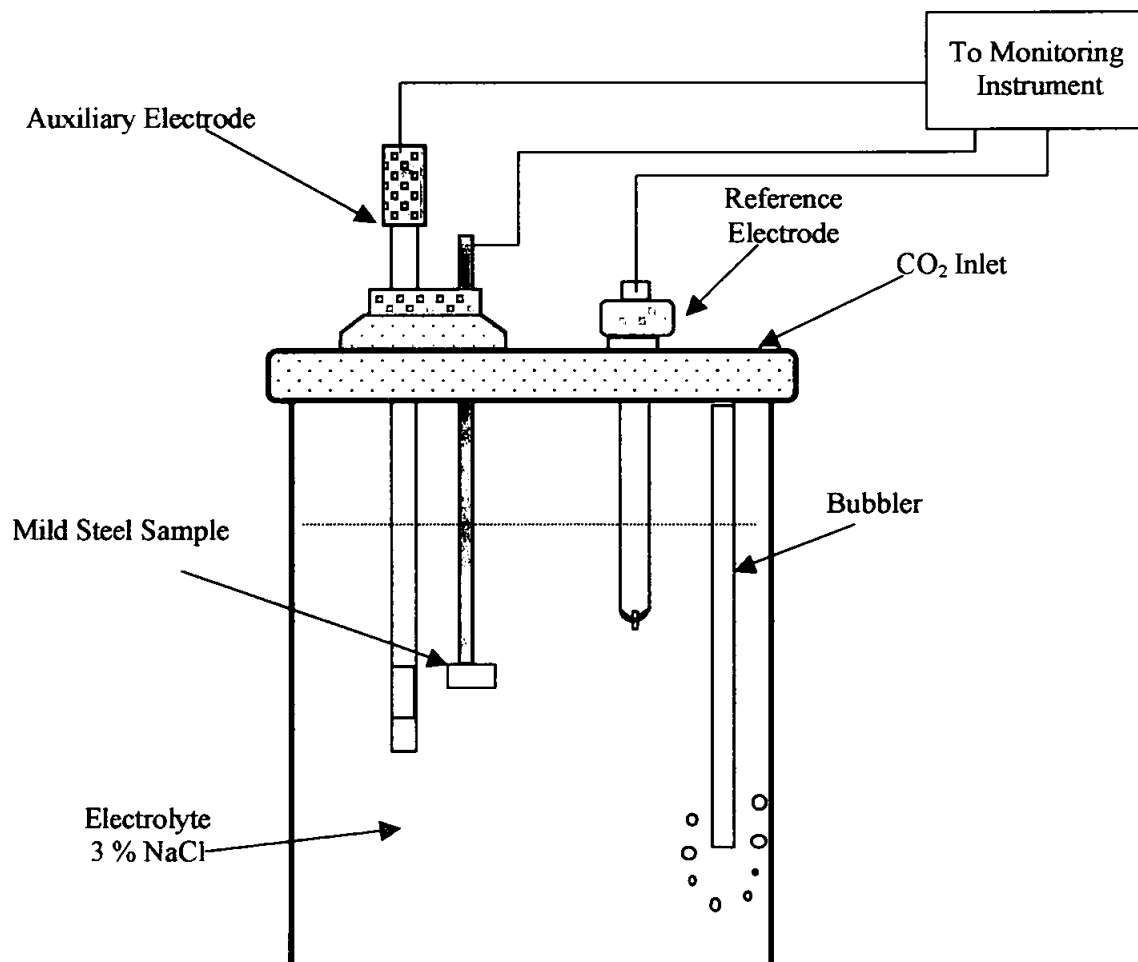
Figure 3.2 : Experimental set-up for static test.

The test assembly consists of a standard one-litre glass cell bubbled with CO_2. The required test temperature is set through a hot plate. The electrochemical measurements are based on a three-electrode system, using a commercially available potentiostat with a computer control system.

The working electrode is prepared from commercial mild steel cylindrical rod with 0.785 cm^2 cross sectional area. The sample was spot welded with nickel-chromium wire and mounted in araldite resin. The sample surface is then polished to 800-grade finish using silicon carbide papers. The specimen is degreased and rinsed with ethanol and deionised water prior to immersion.

3.3.2 Dynamic Experiments

Dynamic experiments were conducted in a 1-litre glass cell with polypropylene cell lids. Similar to the static experiments, a three-electrode arrangement was used. The rotating cylinder electrode apparatus used in this research was made by EG&G-PARC (Model 616) with rotation speeds from 1000 to 7000 rpm. The set-up is shown in Figure 3.3 below.

The shaft and the specimen holder of the RCE were made of 316 stainless steel and were embedded in a Teflon® tube. The cylindrical sample was held in position with the use of PTFE washers and an end cap screwed onto the end of the specimen holder. The cylindrical samples used in the RCE apparatus were machined from commercial mild steel grade. A schematic diagram of the specimen assembly, with dimensions of the samples, is shown in Figure 3.4.
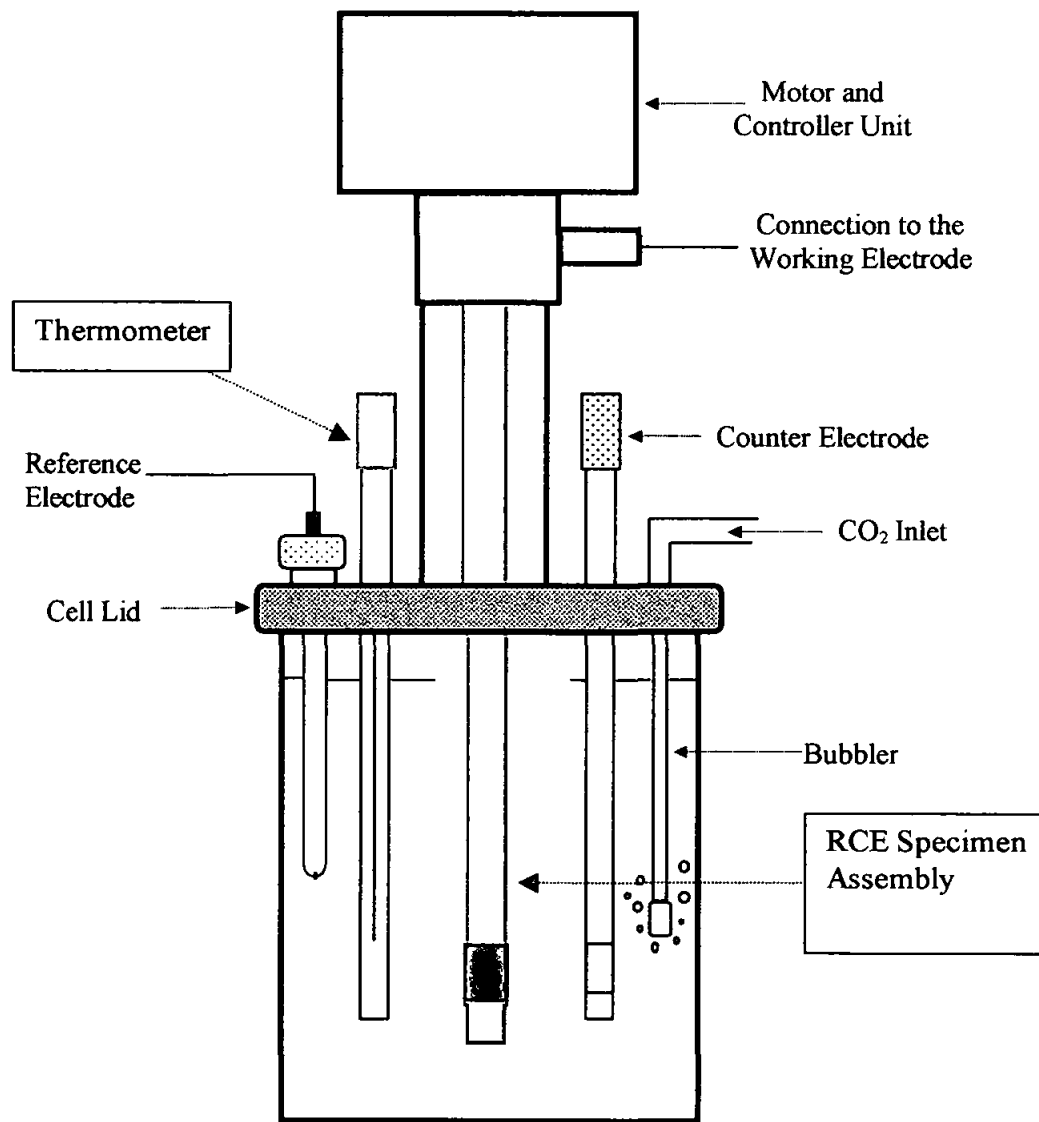
Figure 3.3: Experimental set-up for RCE test.
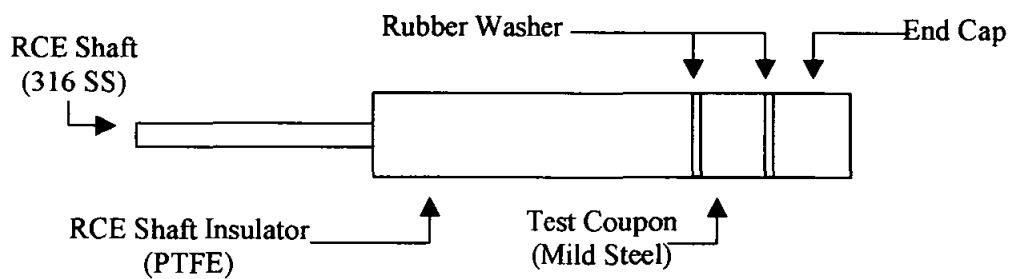
Figure 3.4: Details of the RCE specimen assembly with electrode diameter of 12 mm and length 8 mm.

The corresponding calculated wall shear stress is presented in Table 3.1.

Table 3.1 Wall shear stresses at different rotational speeds.

Rotation Speed (rpm)	Wall Shear Stress (Pa)
1000	2.1
2000	7.0
3000	13.9
4000	22.6
5000	33.0
6000	45.0
7000	58.6

3.4 Materials.

Experiments under static and dynamic conditions were conducted with mild steel (BS 970 : 080A15), provided by C & S Steels Ltd. with the following composition:

Table 3.2: Composition of steel 080A15, (BS 970).

Steel	C (%)	Si (%)	Mn (%)	P (%)	S (%)	Cr (%)	Mo (%)	Ni (%)
080A15	0.148	0.175	0.799	0.010	0.032	0.069	0.014	0.065

3.5 Test environment

3.5.1 Preparation of Solutions

The solutions were prepared from the following analytical reagent grade chemicals, namely glacial acetic acid (HAc), sodium acetate (NaAc), sodium bicarbonate ($NaHCO_3$)

Chemicals/Solvents	Specification
Deionised water	Elga Powerlab Option, resistivity more than 10 $Mohm.cm^2$
Sodium Chloride	Fisher Scientific, 99%
Glacial Acetic Acid	Fisher Scientific, 100%
Sodium acetate anhydrous	Fisher Scientific, 99%
CO_2	BOC, 99.8%
Sodium Bicarbonate	Fisher Scientific

The 3% NaCl solution is saturated with CO_2 by purging for at least one hour prior to the exposure of electrode. The pH of the solution could be adjusted by adding an amount of 1M $NaHCO_3$. The pH value was checked by microcomputer pH-meter HANNA Instruments Model HI 8424, which had been calibrated using standard buffer solutions.

3.5.2 Addition of Acetic Acid and Acetate

The amount of acetic acid/acetate added is determined by the Handerson-Hasselbach equation ($pH = pKa + \log_{10}$ [Base]/[Acid]) in order to maintain the required pH. For acetic acid buffer, this is given by:

$$pH = 4.76 + \log_{10} [CH_3COO^-]/[CH_3COOH]$$

The ratio of acetate ions and acetic acid at each pH is shown in the Table 3.3 below.

Table 3.3: Calculated ratio of base and acid

pH Value	Ratio	
	[CH$_3$COO$^-$]	[CH$_3$COOH]
3.8	1	10
5.0	2	1
5.5	5	1
6.0	17	1

3.6 Solution Composition

The variation of the concentration of carbonic species with temperature is calculated based on the equilibrium constants tabulated in Table 3.4 below.

TABLE 3.4 Chemical Reactions and Their Equilibrium Constants.

Description	Reaction	Equilibrium Constant	Constant
Dissolution of carbon dioxide	$CO_{2(g)} \rightleftharpoons CO_{2(aq)}$	$K_d = \dfrac{[CO_{2(aq)}]}{P_{CO_{2(g)}}}$	$\log K_d = 108.3865 + 0.01985076T - 6919.53/T - 40.45154 \log T + 669365/T^2$ Source: Plummer [69]
Hydration of carbon dioxide	$CO_{2(aq)} + H_2O \rightleftharpoons H_2CO_3$	$K_{hyd} = \dfrac{[H_2CO_3]}{[CO_2]}$ $K_{hyd} = \dfrac{k_1}{k_{-1}} = 0.00258$	$\log k_1 = 195.3 - 63.59\log(T) - 11715.8/T$ Source: Palmer van Eldik [17]
Dissociation of carbonic acid	$H_2CO_3 \rightleftharpoons H^+ + HCO_3^-$	$K_{a_1} = \dfrac{[H^+][HCO_3^-]}{[H_2CO_3]}$ $K_{a_1}' = \dfrac{[H^+][HCO_3^-]}{[H_2CO_3]+[CO_{2(aq)}]}$	$\log K_{a1} = 29688.2/T + 81.840\ln(T) - 0.0896488T - 2046790/T^2 - 522.461$ $K_{a1} = K'_{a1}(khyd + 1/khyd)$ Source: Palmer van Eldik [17]
Dissociation of bicarbonate anion	$HCO_3^- \rightleftharpoons H^+ + CO_3^{2-}$	$K_{a_2} = \dfrac{[H^+][CO_3^{2-}]}{[HCO_3^-]}$	$\log K_{a2} = -2730.7/T - 0.02199T + 5.388$
Dissociation of acetic acid	$HAc \rightleftharpoons H^+ + Ac^-$	$K_{HAc} = [H^+][Ac^-]/[HAc]$	$K_{HAc} = 10^{-(6.66104-0.0134916 \times T_K + 2.37856 \times 10-5 \times T_K^2)}$ molar Source: Kharaka [78] $k_f = 3.2 \times 10^5 s^{-1}$ Source: Vetter [79]

Both expressions for the dissociation of carbonic acid (K_{a1}' and K_{a1}) are used and the calculated concentrations of the carbonic species in solution are shown in Figures 3.5 and 3.6. As can be seen from the figures, there is not much difference in the carbonic species concentrations observed from both expressions.

It is evident from Figure 3.7 that as the temperature of the solution increases, the concentration of the dissolved CO_2 decreases and hence the concentration of carbonic acid decreases.
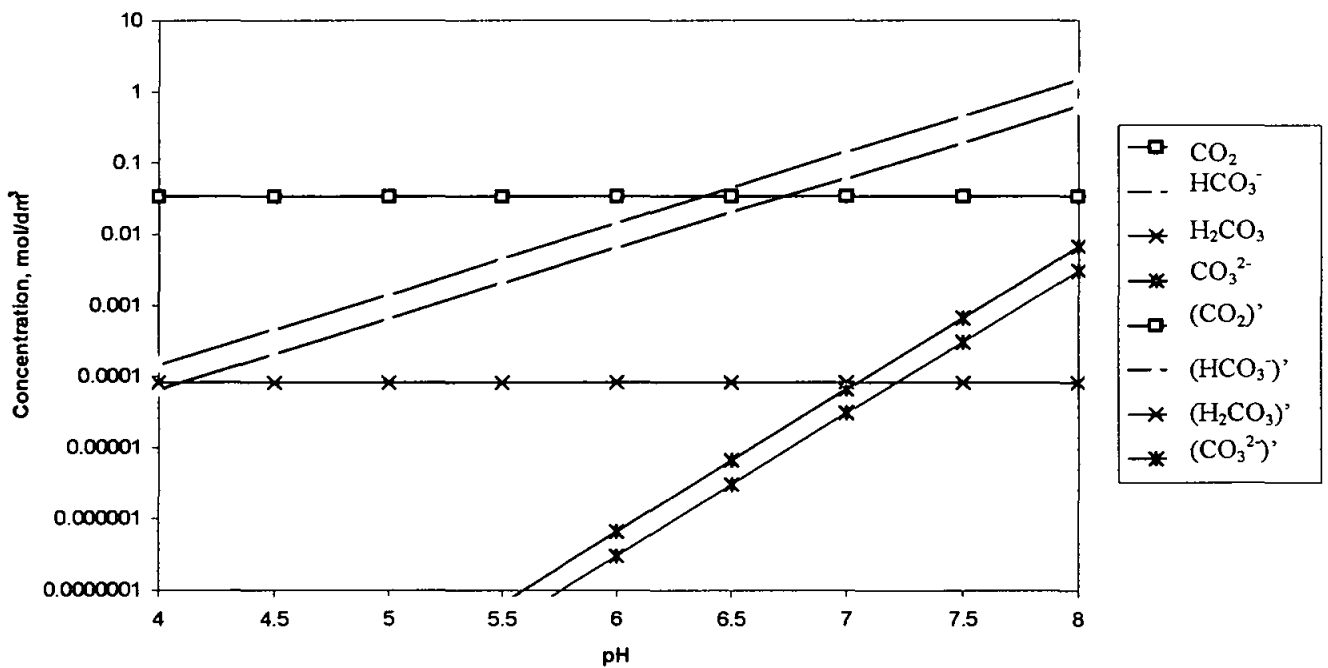
Figure 3.5: Concentration of carbonic species in water, as a function of pH, at 1 bar CO_2 and 25°C.
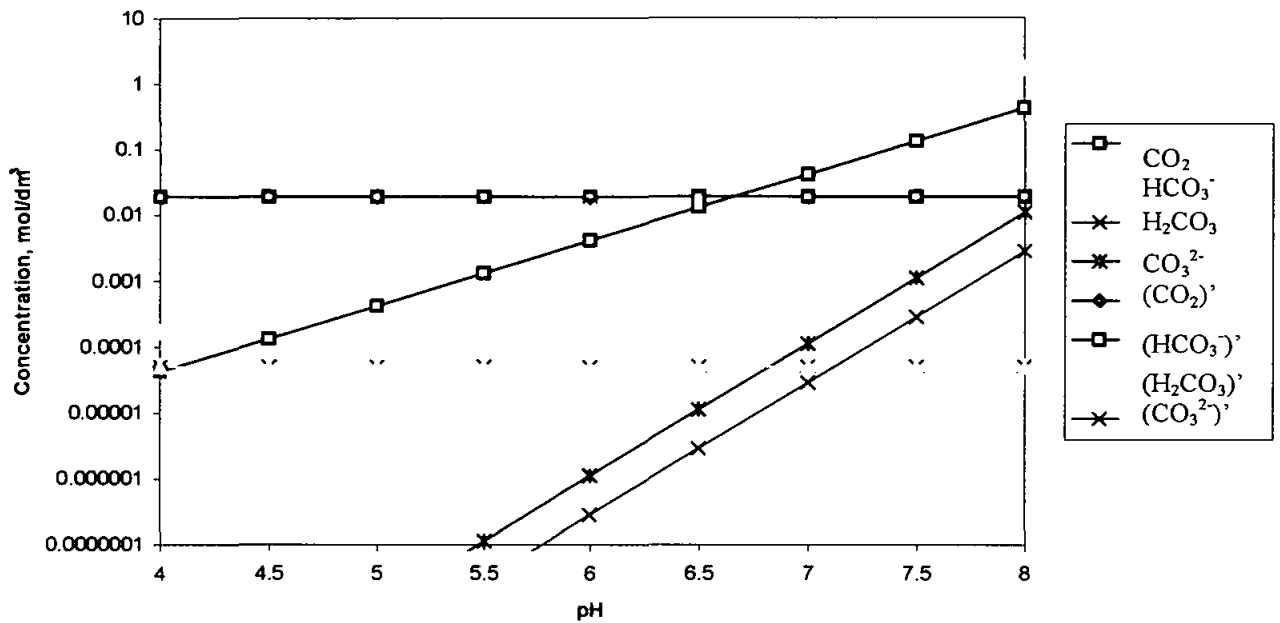
Figure 3.6: Concentration of carbonic species in water, as a function of pH, at 1 bar CO_2 and 50°C.
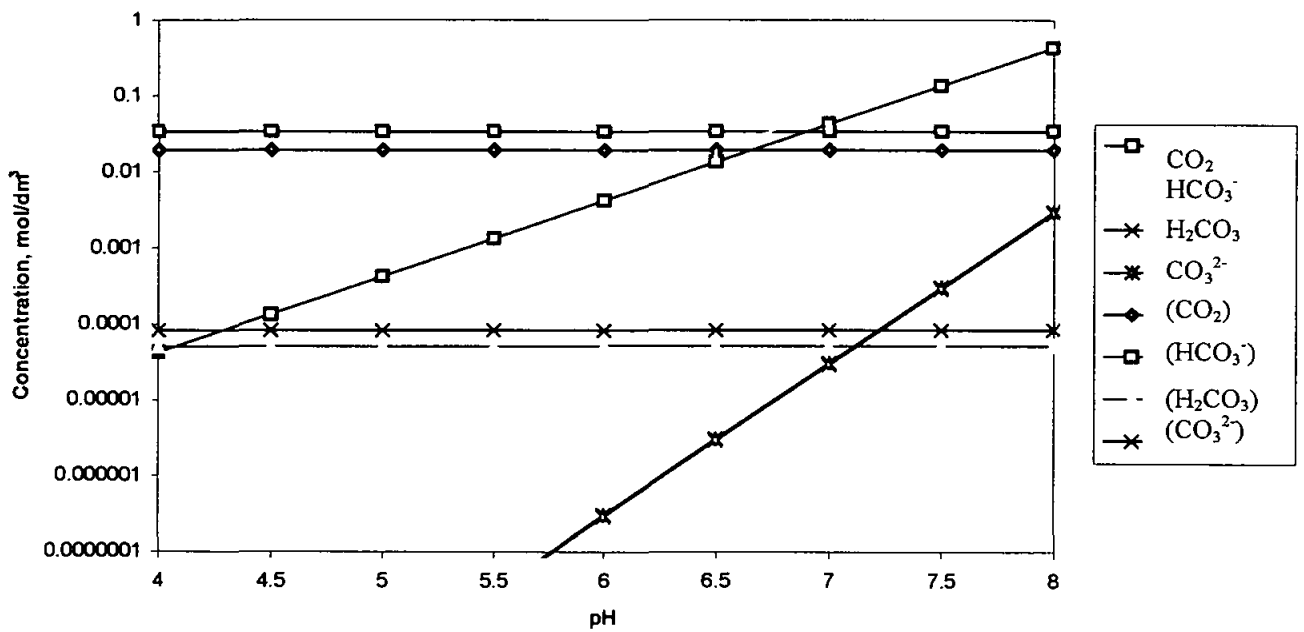
Figure 3.7: The effect of temperature (25°C and 50°C(in brackets)) on the concentration of carbonic species in water.

The calculation of the acetic acid species can be done similarly but since the experiment is done at a constant pH, the concentration of acetic acid and acetate ions is readily obtainable.

For 360 ppm acetic acid/acetate buffer, the initial amount of each species is shown in Table 3.5 below. At pH 5.5, this 360 ppm acetic acid/acetate buffer translates to 60 ppm of free acetic acid (HAc). As the equilibrium constant for acetic acid K_{HAc} varies a little with temperature, we could assume the concentration of the acetic acid species remain the same at different temperatures.

Table 3.5: Initial concentrate ion of chemical species of the buffered solution for 360 ppm HAc/Ac.

Initial Concentration of Added Species	Buffered NaCl Solution at different pH			
	pH 3.8	pH 5.0	pH 5.5	pH 6.0
Cl^-	18,000 ppm	18,000 ppm	18,000 ppm	18,000 ppm
CO_2	1 bar	1 bar	1 bar	1 bar
HCO_3^-	0	252 ppm	756 ppm	2268 ppm
HAc	300 ppm	120 ppm	60 ppm	20 ppm
Ac	60 ppm	240 ppm	300 ppm	340 ppm

3.7 Experimental Procedure

3.7.1 Linear Polarisation Measurements

The LPR procedure for static test and RCE test is conducted after sufficient CO_2 gas bubbling, adjusting the solution to the required pH and attaining the set temperature. The bubbling is reduced and maintained throughout the test.

1. Bubble CO_2 through the 1-litre 3% NaCl for at least 1 hour before inserting sample.
2. Adjust pH to the required values by adding solution of 1M $NaHCO_3$. pH is measured at room temperature by pH meter.
3. Set the temperature and maintain with an accuracy $\pm 5^{\circ}C$.
4. Add the mixture of HAc and Ac accordingly to the required pH values.
5. Insert the polished specimen.
6. Take readings every 15 minutes for at least 24 hours.

3.7.2 Cathodic Polarisation curves

1. Bubble CO_2 through the 1-litre 3% NaCl for at least 1 hour before inserting sample.
2. Adjust pH to the required values by adding solution of 1M $NaHCO_3$. pH is measured at room temperature by pH meter.
3. Set the temperature and maintain with an accuracy $\pm 5^{\circ}C$.
4. Add the mixture of HAc and Ac accordingly to the required pH values.
5. Insert the polished specimen. Set the rotation rate for the RCE apparatus..
6. Set the scan rate 30mV/minute.

3.8 Corrosion Prediction

Three readily available predictive models were used namely Cassandra, NORSOK and de Waard models. The molar percentage of CO_2 used in the calculation is adjusted to account of the water vapour pressure at respective temperatures as shown in Table 3.6 below.

Table 3.6: Vapour pressure of water [80]

Temperature ($^{\circ}$C)	Vapour pressure of water (mm Hg)	Corresponding mole % CO_2
22	19.8	97.4
50	92.5	88
70	233.7	70
80	355.1	53
85	433.6	43
90	525.76	31

4.0 RESULTS ANALYSIS : ACETIC ACID IN STATIC CONDITION

4.1 The Effect of Acetic Acid with Temperature and pH

The effect of the acetic acid and acetate (HAc/Ac), which are termed as acetic acid species, on the corrosion rate of mild steel in NaCl saturated with CO_2 at pH values of 3.8, 5.0, 5.5 and 6.0 tested at different temperatures is shown in Figure 4.1 below.
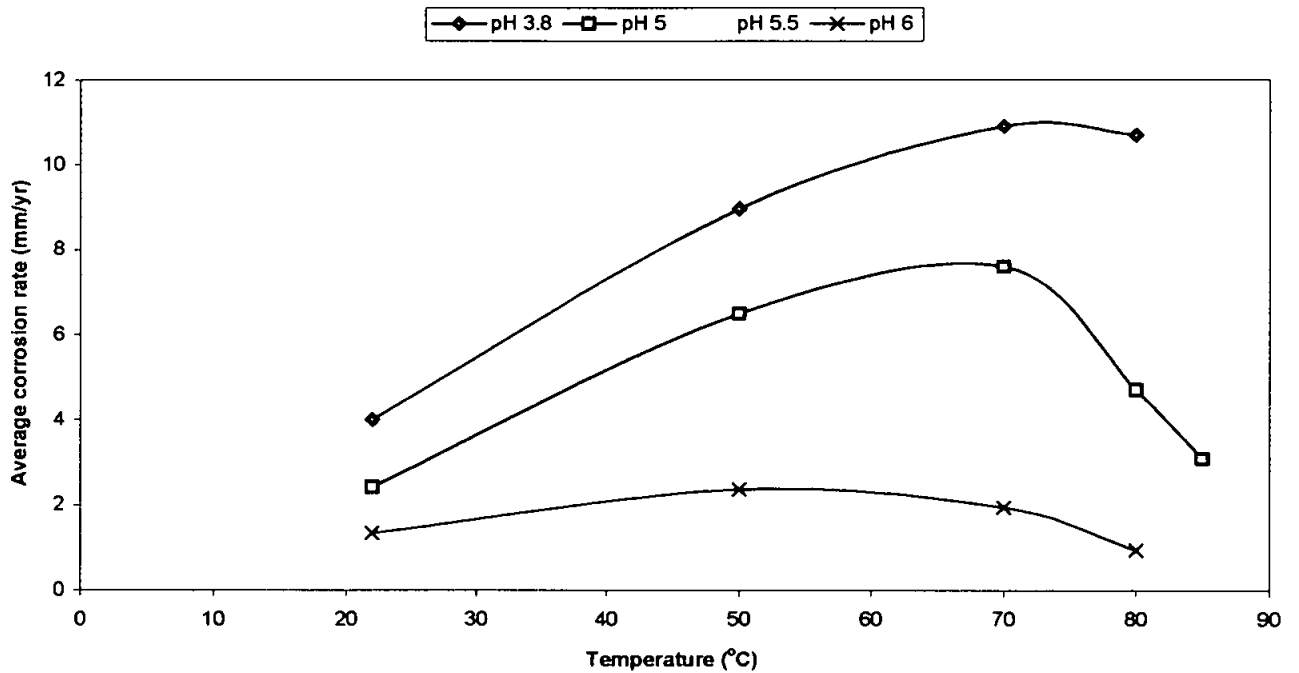
Figure 4.1: Average corrosion rate of mild steel in NaCl saturated with 1 bar CO_2 with 360 ppm acetic acid species at various pH values and different temperatures.

Distinct characteristics due to the effect of the 360 ppm acetic acid species on the mild steel in the CO_2 environment can be clearly seen when this is compared to the results of the blank solutions as shown in Figure 4.29(a-d) below.
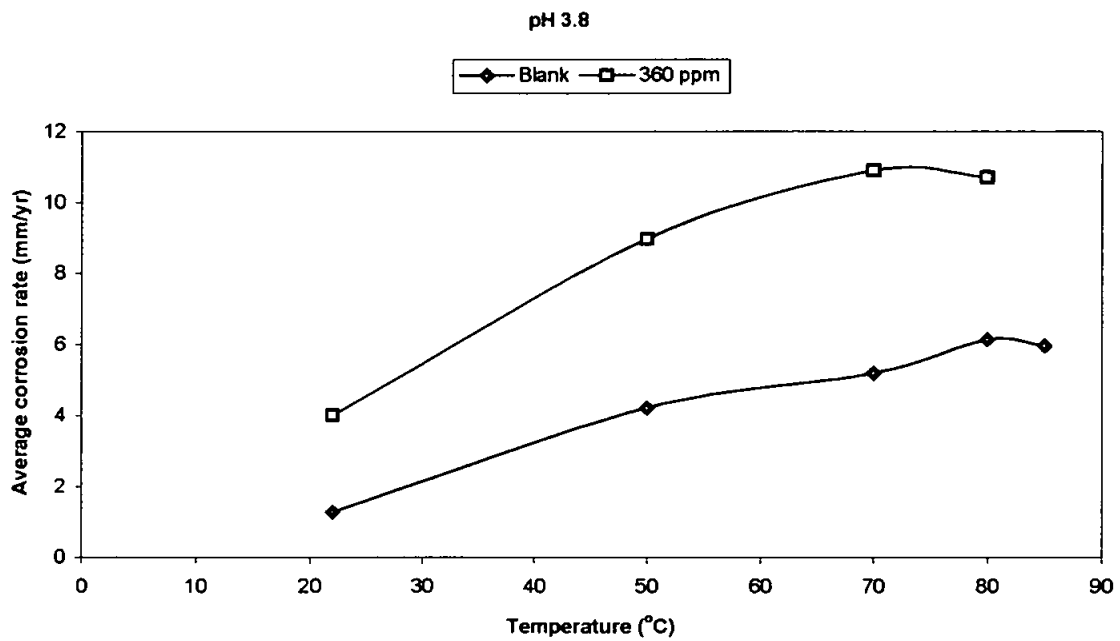
Figure 4.2(a): pH 3.8

Figure 4.2 (b): pH 5.0

63
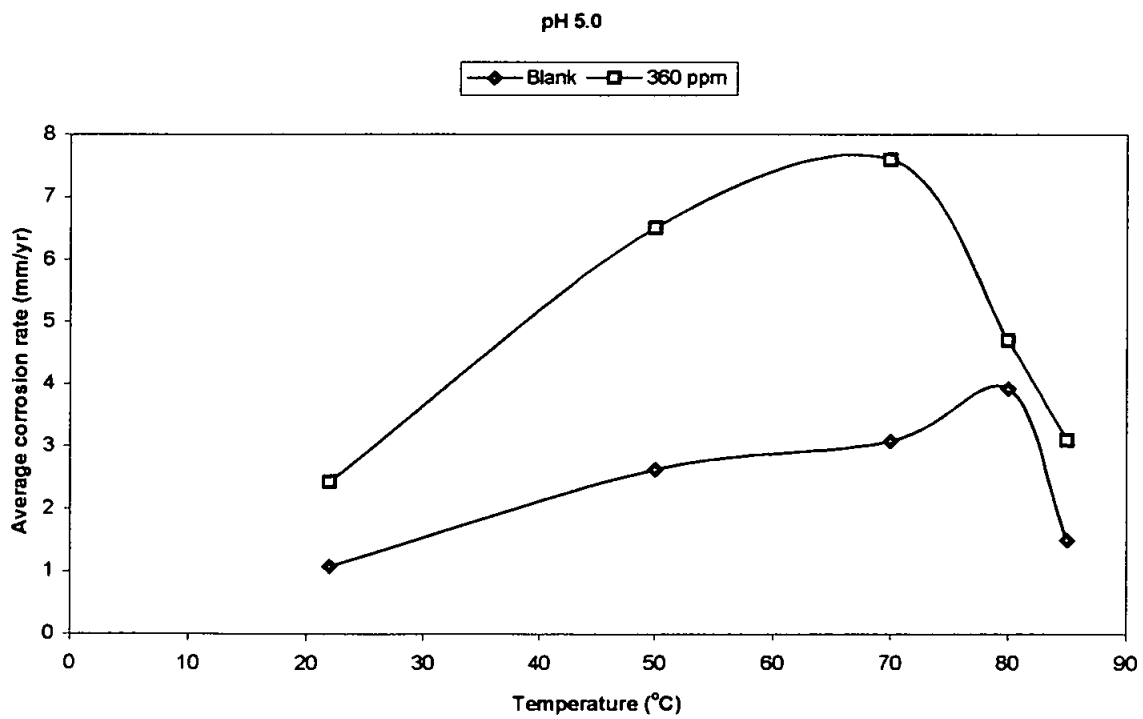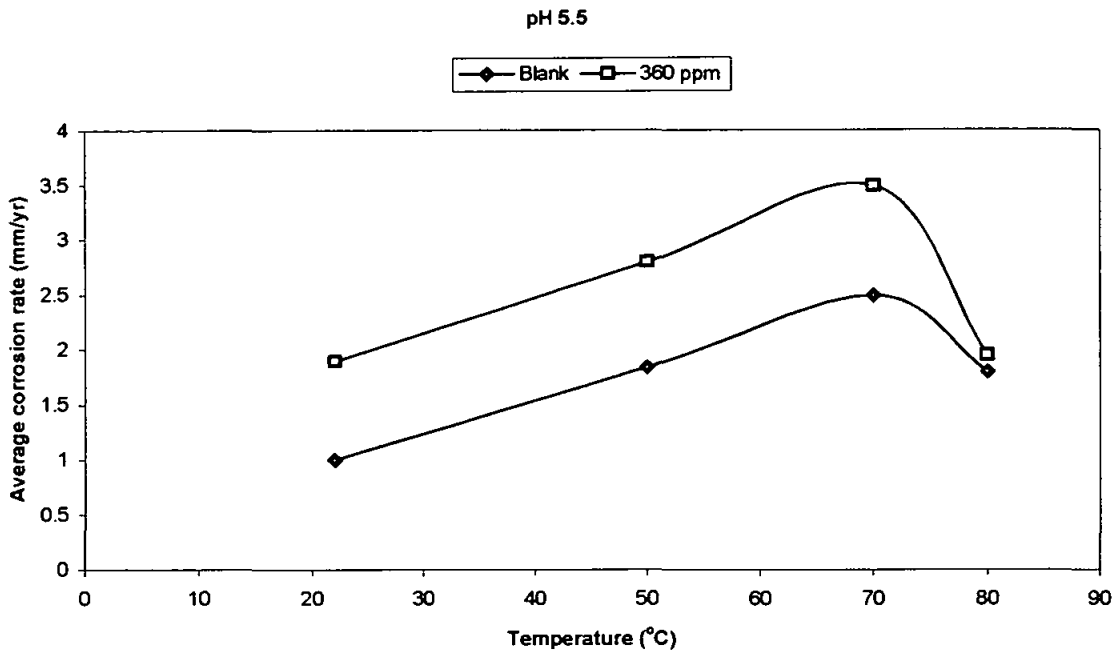
pH 5.5

Figure 4.2(c): pH 5.5
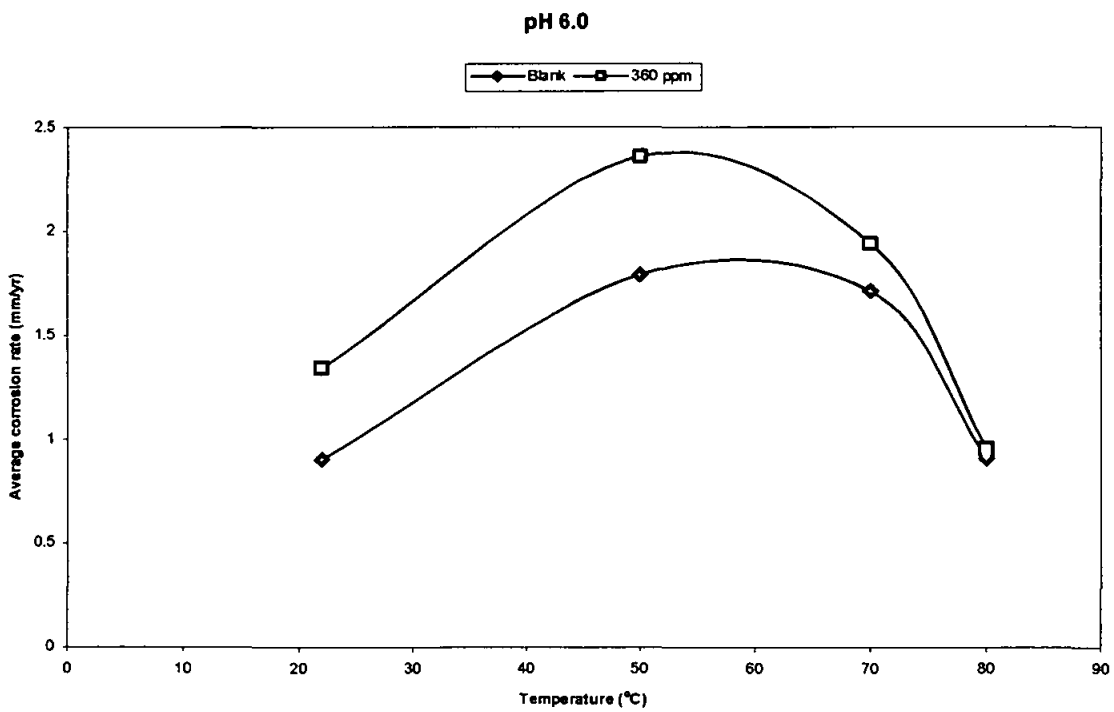
pH 6.0

Figure 4.2(d): pH 6.0

Figure 4.2(a-d): Average corrosion rate of mild steel in NaCl saturated with 1 bar CO_2 at various pH values and different temperatures for blank and 360 ppm acetic acid species.

The corrosion rate increases with temperature for both systems and reaches maximum values at the scaling temperatures (Ts) for pH 5, pH 5.5 and pH 6.0. Beyond the scaling temperatures, the corrosion rates decrease to low values. This is not distinctly observed for pH 3.8 since the test was only done up to 85°C, which indicates the scaling temperature is higher than this.

The effect of the acetic acid species can be divided into two domains - below and above Ts.

4.1.1 The Effect of Acetic Acid below Ts

The increase in corrosion rate below Ts due to the effect of acetic acid species is significant as shown in Table 4.1 below. For pH 3.8, the corrosion rate is increased from 80 % to 200%. For pH 5.0, the increase is in the range of 120% to 150%. At pH 5.5, the increase is between 40% and 90%. At pH 6,with 360 ppm acetic acid species in the solution, only slight increase of 40% is seen. This is expected since the free acetic acid concentration is only 20 ppm at pH 6.0.

Table 4.1: The effect of acetic acid species on the average corrosion rate below the scaling temperature.

	Average Corrosion Rate below Scaling Temperature (mm/yr)											
	pH 3.8				pH 5.0			pH 5.5			6	
	22°C	50°C	70°C	80°C	22°C	50°C	70°C	22°C	50°C	70°C	22°C	50°C
Blank	1.3	4.2	5.2	6.0	1.1	2.6	3.1	1.0	1.8	2.5	0.9	1.8
360 ppm total acetate	4.0	9.0	10.9	10.7	2.4	6.5	7.6	1.9	2.8	3.5	1.3	2.4
% increase	200	115	110	80	120	150	145	90	55	40	40	30

For example at pH 5.5, the corrosion rate increases substantially with the presence of 360 ppm acetic acid species (60 ppm HAc) in the solution, as shown in Figure 4.3 below. The increase is substantial as compared to the blank solution at the same pH. This increase is solely due to the effect of acetic acid species, which are the free acetic acid and acetate ions.
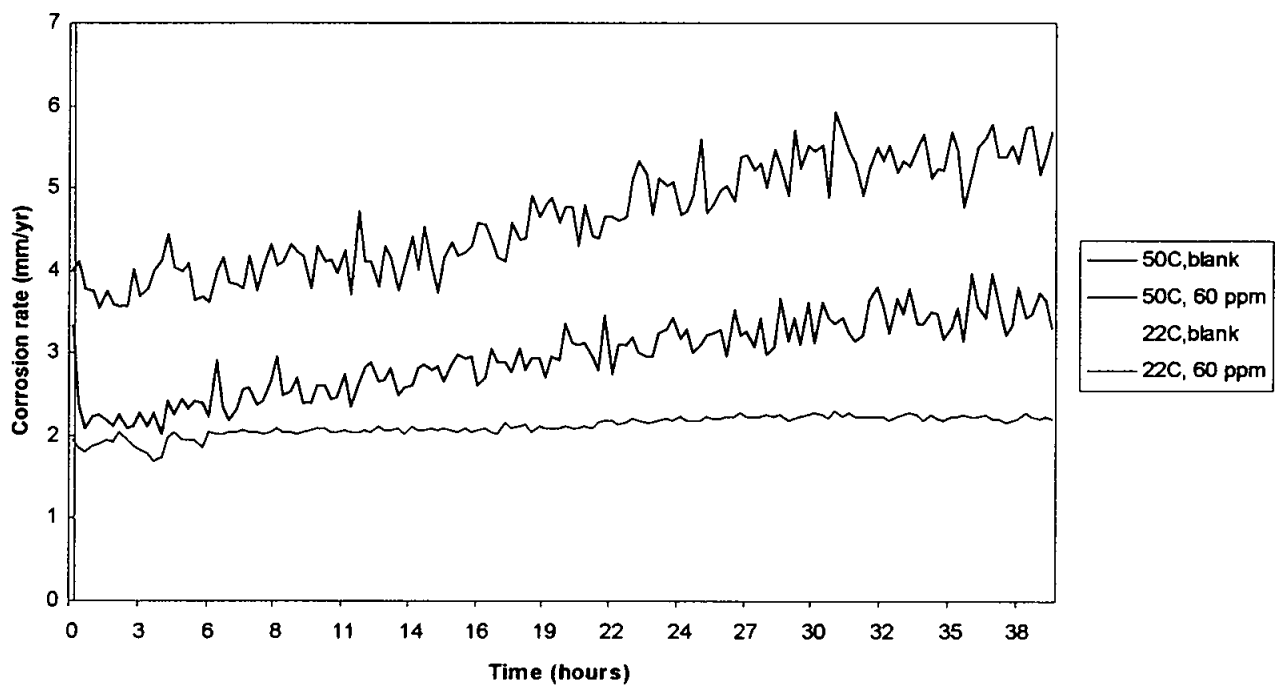
Figure 4.3: The increase in the corrosion rate due to addition of HAc at pH 5.5 for 22°C and 50°C.

4.1.2 The Effect of Acetic Acid above Ts

Above the scaling temperature, a protective corrosion film forms and the corrosion rate decreases gradually to a low value for both test solutions as summarised in Table 4.2 below.

Table 4.2 : The effect of acetic acid on corrosion rate above scaling temperature.

Test Solution	State of steel	Corrosion Rate above Scaling Temperature (mm/yr)				
		pH 5.0	pH 5.5		pH 6.0	
		$85^\circ C$	$75^\circ C$	$80^\circ C$	$70^\circ C$	$80^\circ C$
Blank CO_2	Before Formation	2.5	2.5	2.3	1.9	1.6
	After Formation	0.6	0.9	0.4	1.2	0.3
CO_2 + 60 ppm HAc	Before Formation	5.6	3.5	2.9	2.0	1.6
	After Formation	0.7	2.3	1.0	0.3	0.3

The scaling temperatures for all pH values are not affected by the presence of acetic acid species. However, the attainment of the stable protective film is delayed as can be seen for example at pH 5.5 and 75°C as shown in Figure 4.4 below.

The time taken to form protective film ranges from 20 to 25 hours depending on the temperature and pH of the solution. When substantial protective film forms, that is 80°C for pH 5.5 and 60°C for pH 6.0, the corrosion rate is reduced to approximately the

same value of those of blank CO_2 solutions.
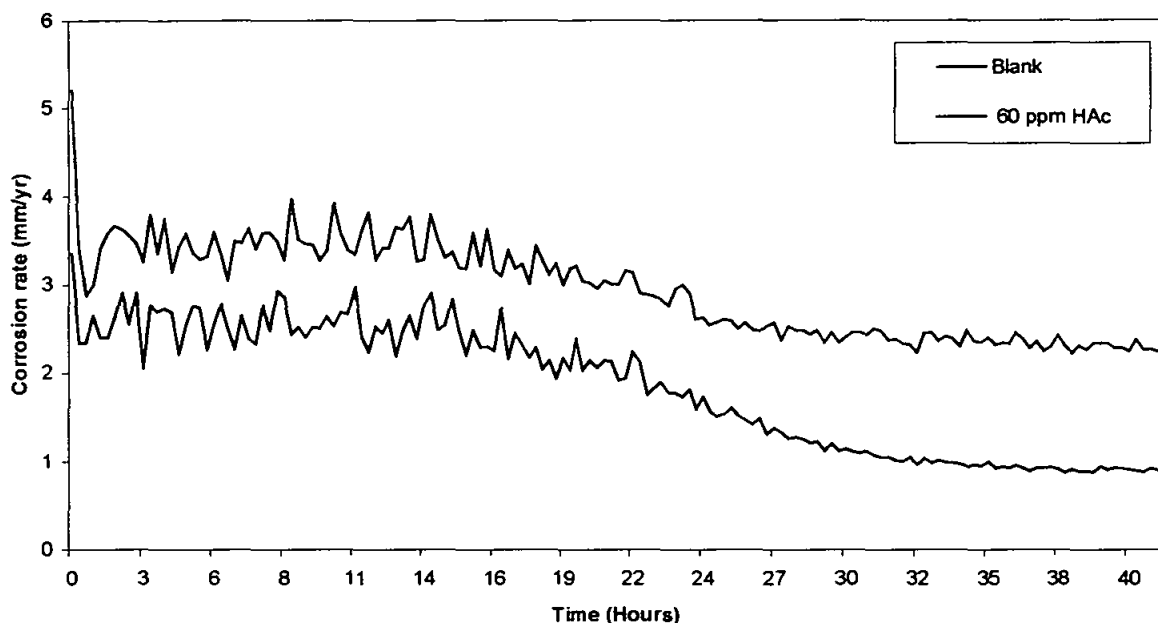
Figure 4.4: Corrosion rate vs time of mild steel in 3%NaCl solution saturated with CO_2, pH 5.5 at 75°C.

4.2 The Effect of Sequential Addition of Acetic Acid Species on Corrosion Rates

The effect of sequential additions of free acetic acid species (HAc) on the corrosion rate of the mild steel in the CO_2 solution below the scaling temperatures can be observed in Figures 4.5 and 4.6 below. The addition of acetic acid increases the corrosion rate approximately in a linear trend. This sequential addition is done prior to the formation of protective film.
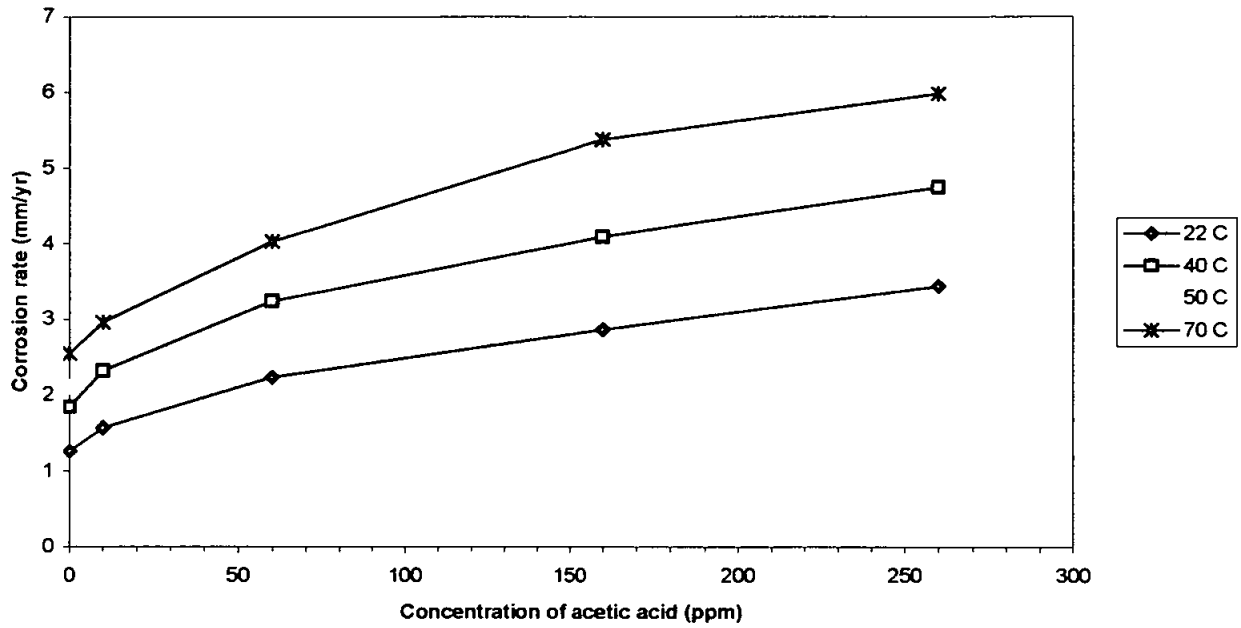
Figure 4.5: Average corrosion rates at different acetic acid concentrations below the scaling temperature; pH = 5.5 .
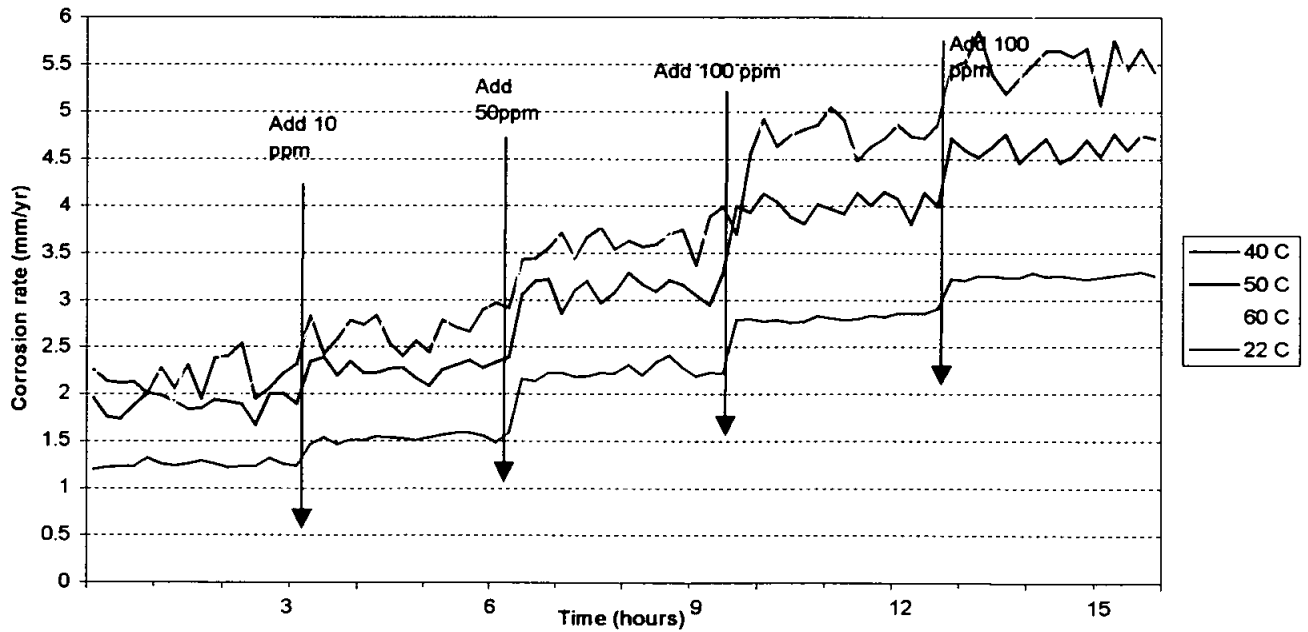
Figure 4.6: Corrosion rate variation with sequential additions of acetic acid below the scaling temperature; pH = 5.5

The same effect is found for higher temperature but before substantial film formation, as shown in Figures 4.7 and 4.8
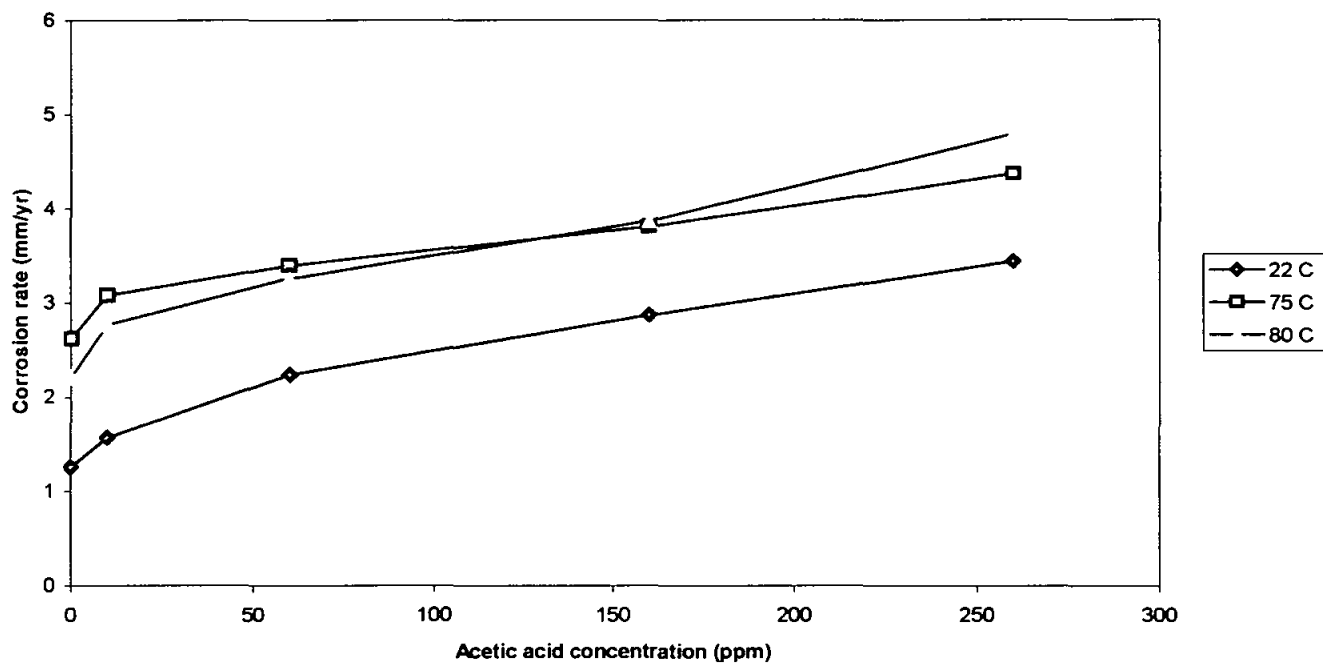
Figure 4.7: Average corrosion rates at different acetic acid concentrations at high temperatures; pH = 5.5
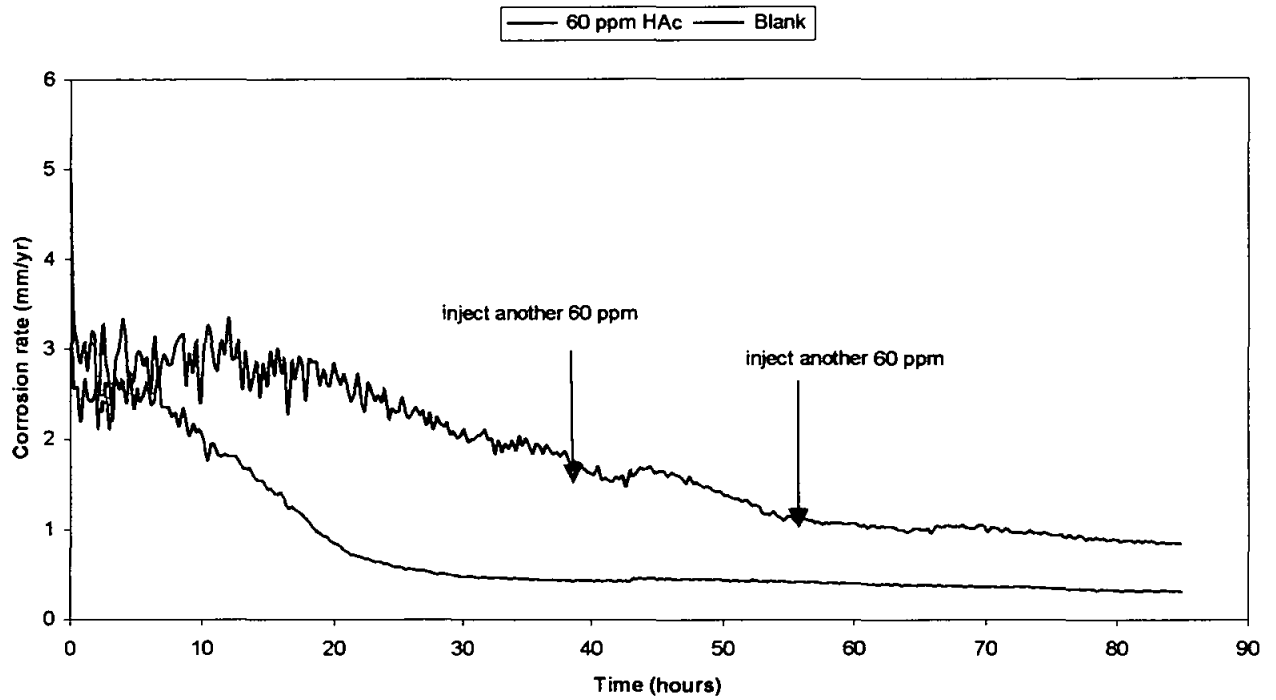
Figure 4.8: Corrosion rate with sequential addition of acetic acid at 80°C and pH = 5.5.

Once the protective film forms, the addition of HAc does not change the corrosion rate as shown in Figure 4.8 above.

4.3 Effect of HAc/Ac on Film Formation

The behaviour of the CO_2 corrosion process with the presence of the HAc/Ac above the scaling temperature at different pH values where stable and protective film forms can be inspected from the Figures 4.9, 4.10 and 4.11 below. Corrosion rates reduced to low values once protective films formed.
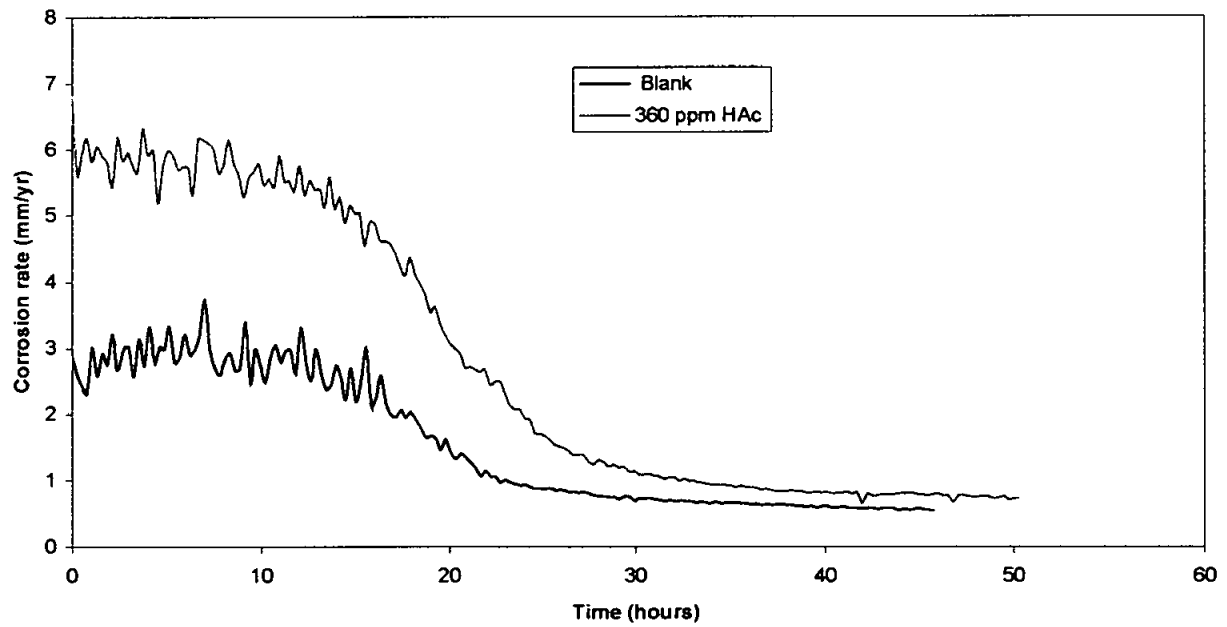
Figure 4.9: Effect of acetic acid species on film formation at 85°C and pH 5.0.
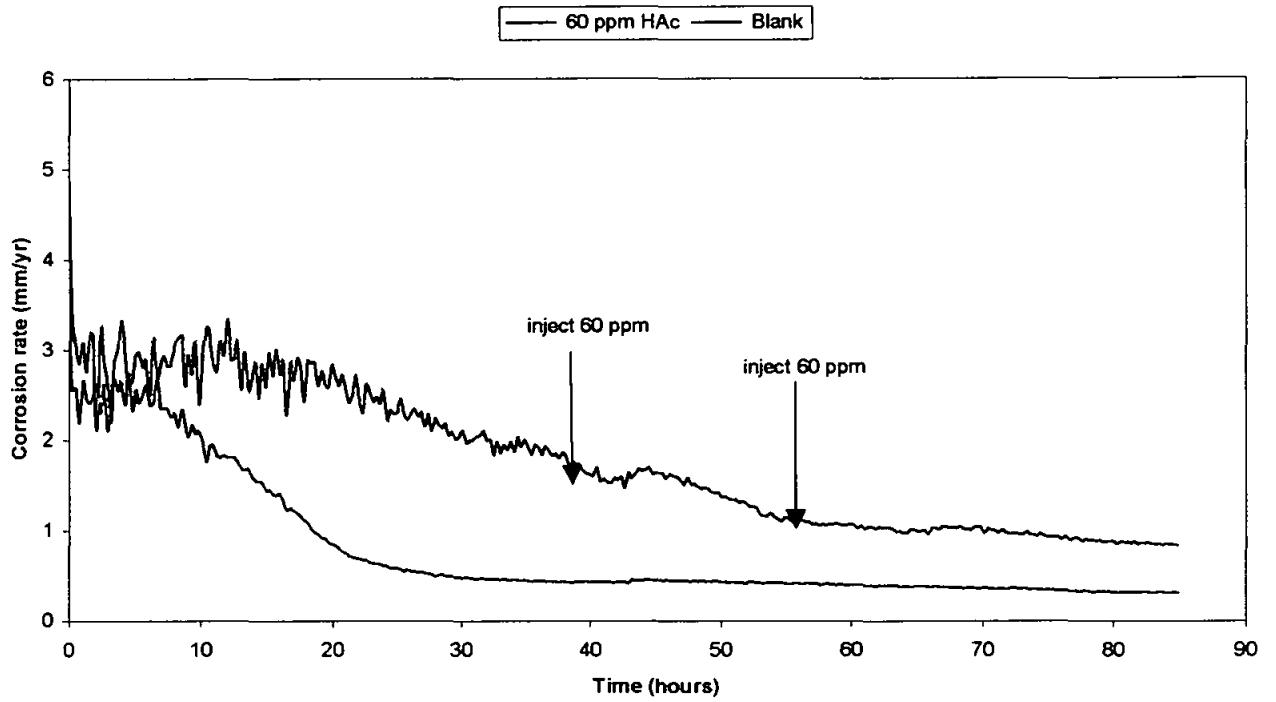
Figure 4.10: Effect of acetic acid species on film formation at 80°C and pH 5.5.
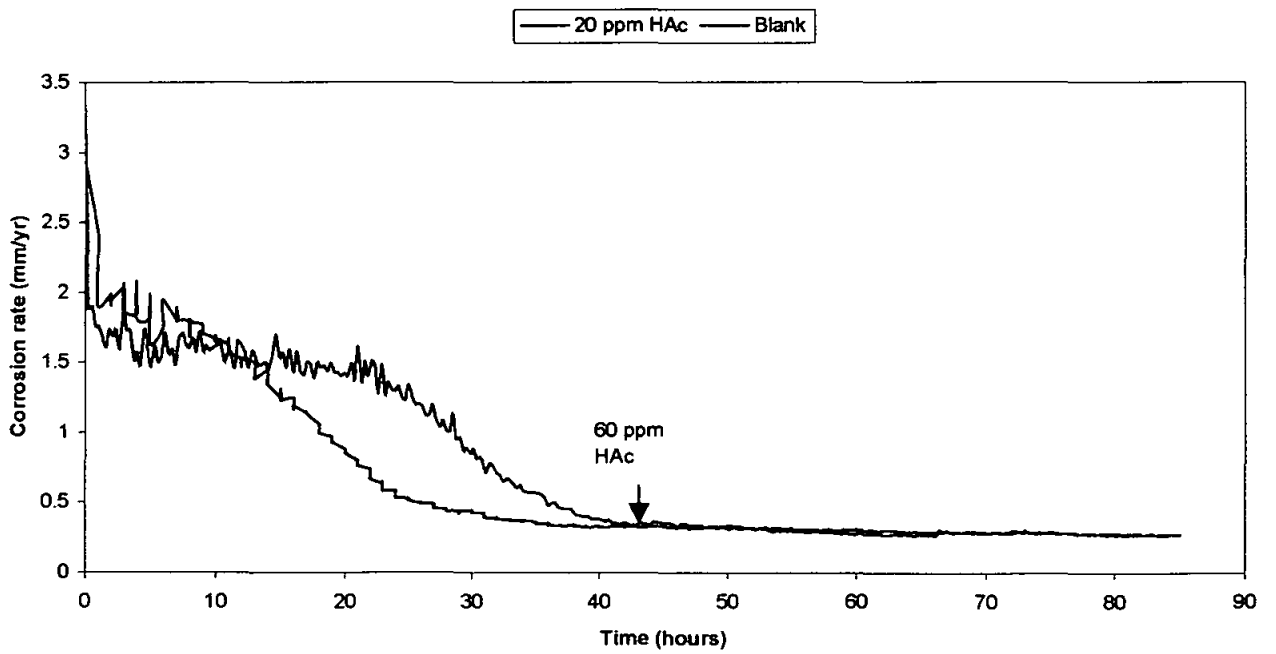
Figure 4.11: Effect of acetic acid species on film formation at 80°C and pH 6.0.

The time taken for the stable film to form for blank and HAc/Ac containing solutions differs. There is no drastic change in time taken for the blank solutions with the increase of the pH values. However, it is found that for the solutions containing 360ppm HAc/Ac, the time taken increases to 25 hours, 50 hours and 40 hours respectively for pH 5, 5.5 and 6. This is summarised in Table 4.3 below.

Table 4.3: Time taken to attain stable protective film formation

	pH 5.0	pH 5.5	pH 6.0
Blank	20 hours	20 hours	25 hours
360 ppm HAc/Ac	25 hours	50 hours	40 hours

4.4 Comparison with Predictive Models

The results were compared with two available models that are widely used in the industry, namely NORSOK and Cassandra. The comparison is based on the prediction at different pH values, as shown in Figures 4.13-4.16 below. For static tests, the results from blank and 360 ppm Hac/Ac cases were compared with the Cassandra using de Waard and Milliams 1993 version (Cassandra (DWM 93)), which does not consider flow effects in the model. The other predictive model used is the NORSOK model, whereby a shear stress of 1 Pa is approximated as the input.

The 360 ppm acetic acid species here represent the mixture of free acetic acid(HAc) and acetate ions(Ac). The concentration of each species varies with the pH of the solution. This concentration of HAc and Ac at the buffered pH is shown in Table 4.1 below.

Table 4.1: Concentration of chemical species of the buffered solution for 360 ppm HAc/Ac

Concentration	Buffered NaCl Solution at different pH			
	pH 3.8	pH 5.0	pH 5.5	pH 6.0
HAc	300 ppm	120 ppm	60 ppm	20 ppm
Ac	60 ppm	240 ppm	300 ppm	340 ppm

4.4.1 Corrosion Rates at pH 3.8

The experimental results at pH 3.8 with blank CO_2 show similar trends to that of Cassandra (DWM 93), with the corrosion rates being in reasonable agreement. The experimental results with 240 ppm HAc show similar upward trends as that of Cassandra (DWM 93) but with much higher corrosion rates.
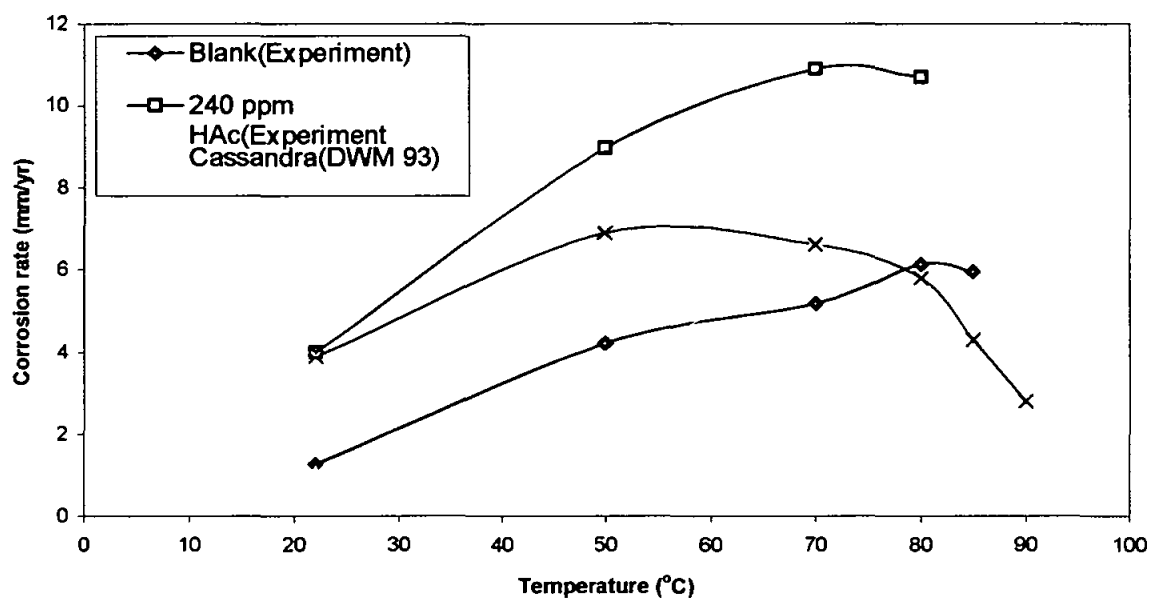
Figure 4.13: Comparison of experimental data with the predictive models at pH 3.8.

4.4.2 Corrosion Rates at pH 5.0

The experimental results at pH 5.0 of blank CO_2 shows a similar trend to that of Cassandra (DWM 93) with reasonable agreement of corrosion rates. The experimental results with 120 ppm HAc show higher corrosion rates than Cassandra (DWM 93) and NORSOK models.
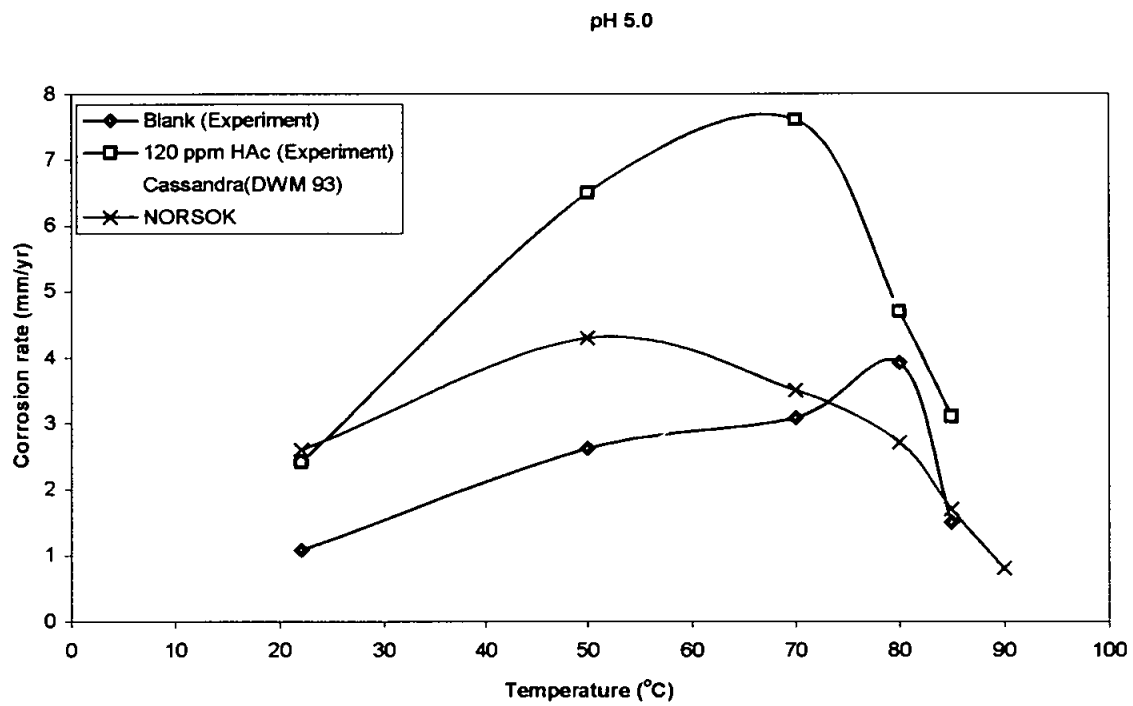
pH 5.0

Figure 4.14: Comparison of experimental data with the predictive models at pH 5.0.

4.4.3 Corrosion Rates at pH 5.5

The experimental results at pH 5.5 of blank CO_2 shows similar trend to that of Cassandra (DWM 93) with reasonable agreement of corrosion rates. The experimental results with 60 ppm HAc show similar upward trend and downward trend to those of NORSOK but with higher corrosion rates above 50°C.
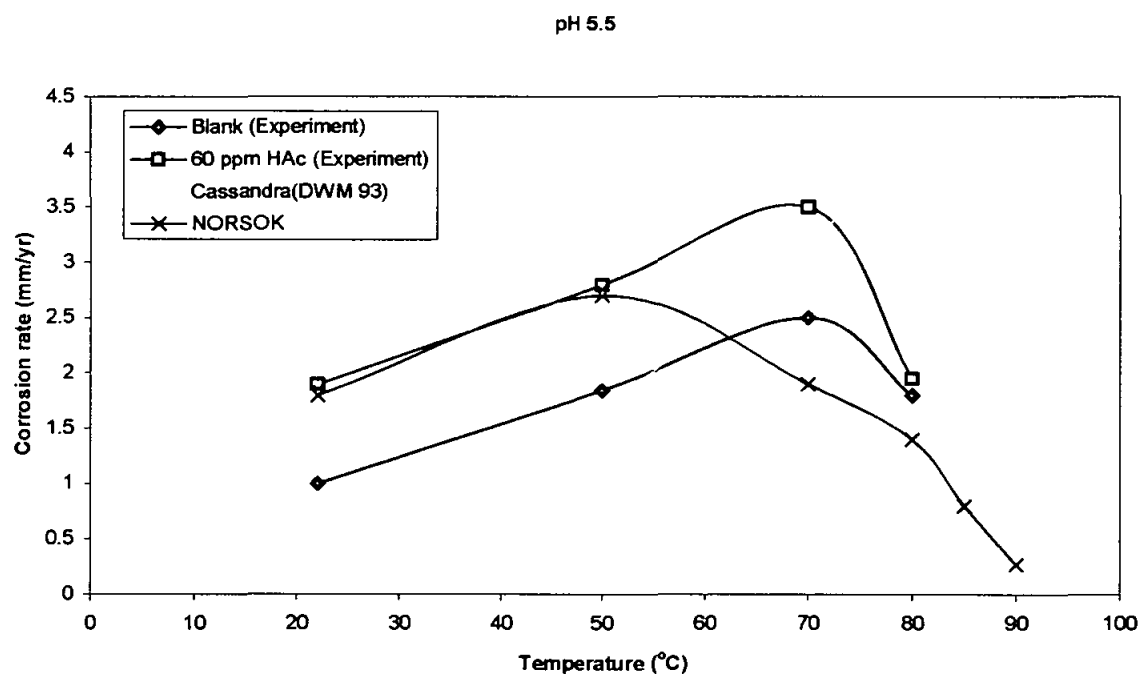
pH 5.5

Figure 4.15: Comparison of experimental data with the predictive models at pH 5.5.

4.4.4 Corrosion Rates at pH 6.0

The experimental results at pH 6.0 with blank CO_2 and 20 ppm HAc show similar trend to that of NORSOK both at low temperature and high temperatures. The experimental results with 20 ppm HAc show higher corrosion rates than both models considered.
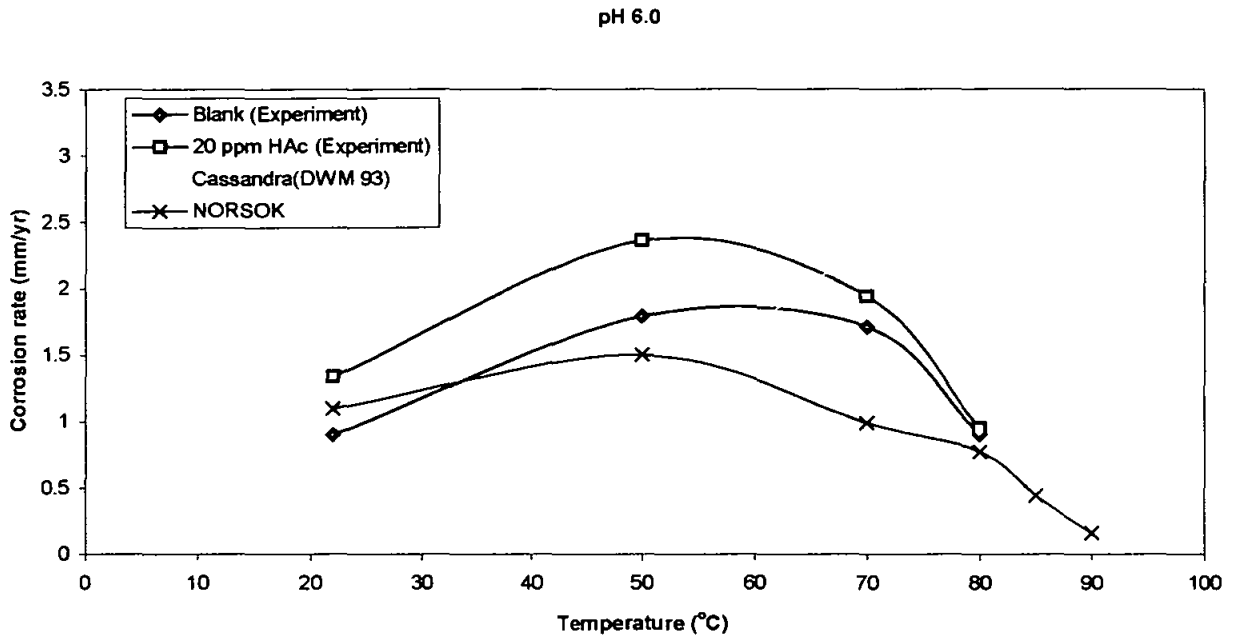
pH 6.0

Figure 4.16: Comparison of experimental data with the predictive models at pH 6.0.

5.0 DISCUSSION OF STATIC TESTS

5.1 The Effect of HAc/Ac on Corrosion rates with Temperature

The corrosion kinetics of carbon steel in both blank and acetic acid/acetate-containing solutions reveal similar trends with increase in temperature. The trends are influenced by the formation of protective films. Prior to any protective film formation, below the scaling temperature (Ts), the corrosion rate for both blank and HAc/Ac-added solution increases with temperature as described by de Waard & Milliam's equation, which has a temperature-dependent term following Arrhenius's relationship. Corrosion of carbon steel in CO_2-contained solution is presented in the form of nomogram by de Waard et al. [1] that shows the effect of CO_2 partial pressure and temperature. However, the corrosion rate of carbon steel in the presence of acetic acid/acetate increases significantly by 30 to 200 % compared to blank CO_2 corrosion. The increase in corrosion rates is due to the extra cathodic reactions of both the dissociations and direct reductions of acetic acid molecules.

Acetic acid also solubilises the ferrous ion (Fe^{2+}) in the iron carbonate ($FeCO_3$) corrosion film and dissolving ferrous iron by forming iron acetate film which is however soluble and not protective. These reactions compete with the usual reactions between iron and carbonic acid. Since the iron carbonate film is not protective, the acetic acid continuously reacts with iron ions forming iron acetate on the surface. Furthermore, iron acetate is known to be soluble, facilitating the corrosion.

It is found also that the scaling temperature (Ts) for both solutions is not altered, which indicates the acetic acid species are not forming protective film. The attainment of the Ts is associated with the lower solubility of Fe^{2+} and formation of iron carbonate film at high temperature. This is in agreement with the findings of Ueda [70] that Ts of low alloy steel is not altered by the presence of acetic acid. However, the time taken to attain a stable and protective film is longer by 5-20 hours in the presence of acetic. This is due to the thinning effect of the film and solubility of the iron acetate; acetic acid keeps on reacting with the substrate until sufficient iron carbonate film forms. This is also termed as

genuine acetic acid corrosion by Crolet [67] attacking the composition and structure of film. Above the scaling temperature, the corrosion rate reduces substantially for both solutions indicating significant protectiveness of the film.

5.2 The Effect of HAc/Ac on Corrosion Rate with pH

Based on the experimental results, the corrosion rate increases even with increasing pH confirming that the effect of acetic acid species is not due only to the acidification of the bulk solution. For pH 6, the addition of 360 ppm acetic acid species which adds only 20 ppm of free acetic acid (HAc) as shown in Table 4.1 does not change much the kinetics of the corrosion. However, with 2160 ppm acetic acid species in the system which contributes a significant concentration of 120 ppm HAc, the corrosion rate increases about 100% as shown in Table 4.2 below.

Table 4.2: The effect of HAc on the increase in corrosion rate at high pH.

Test Condition at pH 6	Average Corrosion Rate	
	22°C	50°C
Blank	0.9 mm/yr	1.8 mm/yr
120 ppm HAc	2.0 mm/yr	3.6 mm/yr
% Increase	100 %	100 %

5.3 The Effect on Corrosion Rates with Sequential Addition of Acetic Acid

For non-scaling conditions, the corrosion rate increases almost linearly with the sequential addition of the acetic acids. Above the scaling temperature, where a protective iron carbonate film forms, the sequential addition of acetic acid does not trigger much corrosion as the protective film hinders diffusion of acetic acid. The evidence of the competition of Hac/Ac with H_2CO_3 above the scaling temperature is in the delay of the formation of stable protective film. This effect is termed as 'thinning' by several authors.

80

It is worth noting that acetate also supplies a supplementary way for the transport of H^+ ions and re-associates into acetic acid under CO_2 pressure.

5.4 The Effect of Acetic Acid on Corrosion Mechanism

The corrosion mechanism is the same before and after film formation suggesting acetic acid species only affect the kinetics of corrosion. This is in conformity with other experimental data of many authors [14, 25, 81]. The acetic acid/acetate is found to substantially enhance the cathodic reaction by increasing the current density. The anodic reaction of both solutions does not show much difference confirming that anodic dissolution is not affected. This is in agreement with the findings of Hedges [14] and others, although Crolet [18] reported a slight effect on inhibition of anodic reaction. Cathodic current density is also found to increase linearly with increasing acetic acid. This is also reported by Garsany et al. [37] in voltammetry studies of carbon steel in similar environment. They reported that the reduction of carbonic acid plays a minor role in the corrosion of steel in brine containing acetic acid. It is well known that, CO_2 alone is corrosive and with the presence of acetic acid/acetate the reactions are synergistic. Obviously, the contribution of acetic acid species is dependent on the relative amount of the species in the environment.

5.5 Film Formation in the Presence of Acetic Acid Species

Iron carbonate film growth depends primarily on the precipitation rate. High pH results in a decreased solubility of iron carbonate, an increase in super saturation and consequently higher precipitation rate and surface scaling tendency. This applies to both solutions with and without the presence of acetate ions. Nonetheless, with the presence of acetate ions, competition between iron carbonate and iron acetate occurs which delays film formation below Ts and thins the film above Ts.

Thus at temperatures below 70°C, which are typical operating temperatures, substantial corrosion rate increase is seen with the presence of acetic acid species. Furthermore, if the film is damaged or ruptured, corrosion rate can increase rapidly and cause localised corrosion of the pipe. Local acidification due to the presence of acetic acid was also

suggested by Crolet [67] to cause localised corrosion. Thus, inaccurate prediction of the roles of acetic acid in the CO_2 corrosion is detrimental.

5.6 Performance of Predictive Models with the Presence of Acetic Acid

The comparison of corrosion rates from the experimental results with the predictive models, on the blank solution and the solution with acetic acid, is shown on the Table 5.1 below.

Table 5.1: Summary of the performance of protective models.

pH and Test Conditions	PREDICTIVE MODELS	
	CASSANDRA (DWM 93)	NORSOK
3.8 Blank	Good agreement	Over prediction
3.8 HAc/Ac	Under prediction	Under prediction
5.0 Blank	Good agreement	Over prediction
5.0 HAc/Ac	Under prediction	Under prediction
5.5 Blank	Good agreement	Over prediction
5.5 HAc/Ac	Under prediction	Good agreement
6.0 Blank	Under prediction	Good agreement
6.0 HAc/Ac	Under prediction	Under prediction

The experimental results of the pure CO_2 corrosion (blank solution) agree quite well with the Cassandra (DWM 93)'s prediction for most of the cases except for pH 6, which agree more with the NORSOK. However, the corrosion rates of carbon steel in 3% NaCl saturated with CO_2 and containing 360 ppm HAc/Ac predicted by those models are substantially lower, 40-200 %, as compared with the experimental results.

It is concluded by Nyborg [54] that the effect of protective corrosion films on the predicted corrosion rate varies between models. For example, NORSOK considers the effect of protective corrosion films more than de Waard models. It is apparent that

NORSOK predicts lower corrosion rates model at high temperature and high pH than the de Waard model.

From the two models considered, only Cassandra uses acetate as one of the inputs in the pH calculation. This is not unusual as from the review of predictive models available only two other models, namely, Cormed and Hydrocor, utilise the input of acetic acid/acetate. In general, all models considered in this exercise underestimate the effect of acetic acid/acetate ion on CO_2 corrosion of steel at all pH values typical of oilfield formation water.

5.7 Conclusions

Based on the experimental findings, the following points are observed:

1. Corrosion rates of carbon steel in brine containing acetic acid increase by 40 –200 %, depending on the concentration of acetic acid and pH value, under non-scaling conditions. The corrosion rates even increase with increase in pH of the solutions in the presence of acetic acid.

2. Corrosion rates with acetic acid follow similar trends to the blank CO_2 corrosion with regard to temperature showing the effect of the scaling temperatures (Ts). Corrosion rates increase with increasing temperature below Ts, and decrease gradually to low values after Ts.

3. Corrosion rates increase almost linearly with sequential increase of acetic acid as long as no protective film is formed. Once a stable protective film forms, sequential addition of acetic acid has no or minimal effect on corrosion.

4. Acetic acid species could attack exposed substrate at any temperature and pH with the absence of protective films. This could result in localised corrosion.

5. Acetic acid/acetate does not alter the scaling temperature at the respective pH values but delays the attainment by 5- 20 hours. This is termed as the thinning of the corrosion film.

6. Corrosivity of acetic acid /acetate is not primarily due to acidification of the solution but more an effect of solubilisation of iron by acetate, direct corrosion of acetic acid on iron and thinning of corrosion film.

7. Acetic acid influences the cathodic reactions but not the anodic reactions.

8. Standard industrial predictive models, Cassandra model and NORSOK model, predict much lower corrosion rates in the presence of acetic acid than the experimental results.

9. Experimental results of blank solutions show similar trends to the predictions of Cassandra (DWM 93) model in most cases.

10. Incorporating acetic acid/acetate in pH calculation is not enough to realise the true effect of the acetic acid/acetate.

6.0 EFFECTS OF ACETIC ACID IN FLOW-SIMULATED CONDITIONS

6.1 Results and Analysis

The effects of acetic acid (HAc) of various concentrations from 30 ppm to 1200 ppm on the corrosion behaviour of mild steel in 3% NaCl solution saturated with CO_2 are presented below in terms of LPR and polarisation tests. The tests are conducted at a constant pH 5.5 at two different temperatures below the scaling temperatures.

6.1.1 Linear Polarisation Resistance (LPR) Tests

The effect of different concentrations of acetic acid on the corrosion rates as obtained by LPR tests at different rotation rates from 1000 rpm to 6000 rpm are shown in Figure 6.1-6.5 below. The tests are conducted below Ts at two different temperatures, namely 22°C and 50°C.
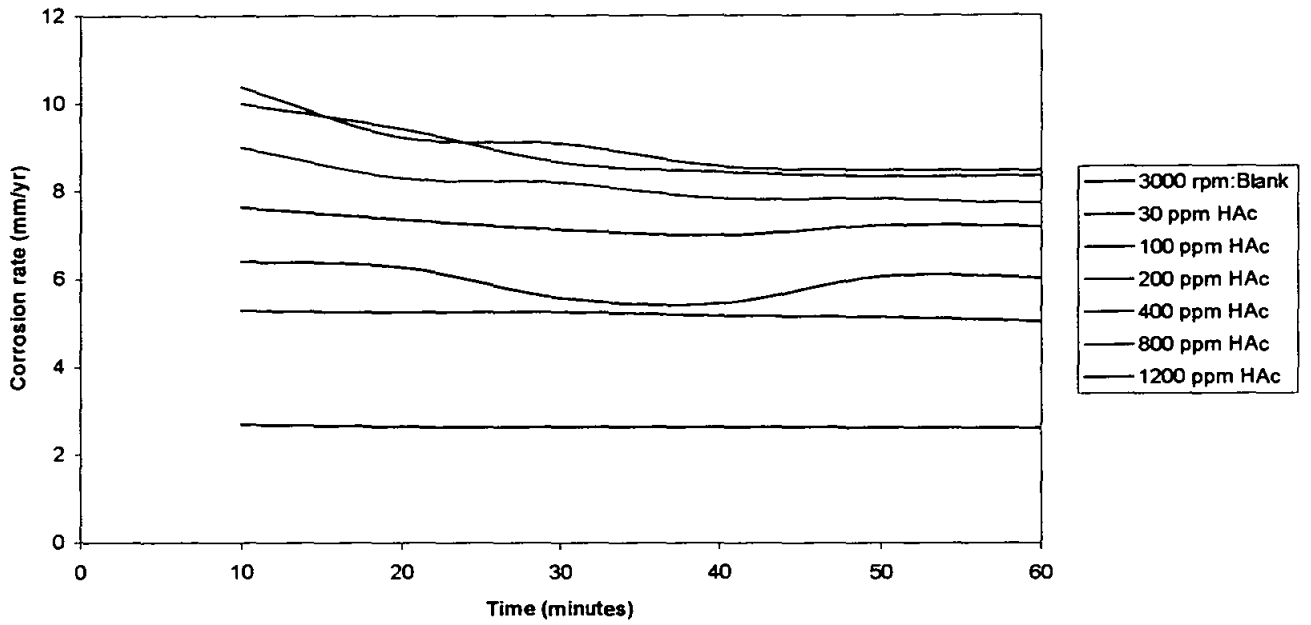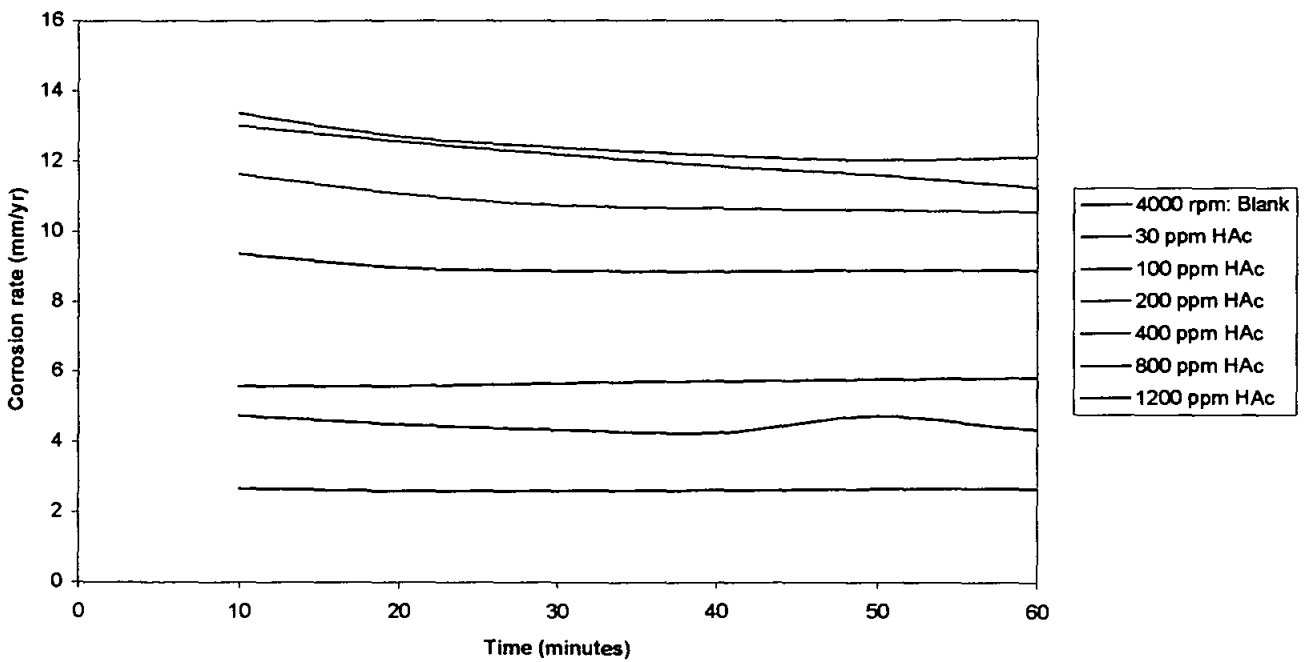
6.1.1.1 LPR Test at 22°C
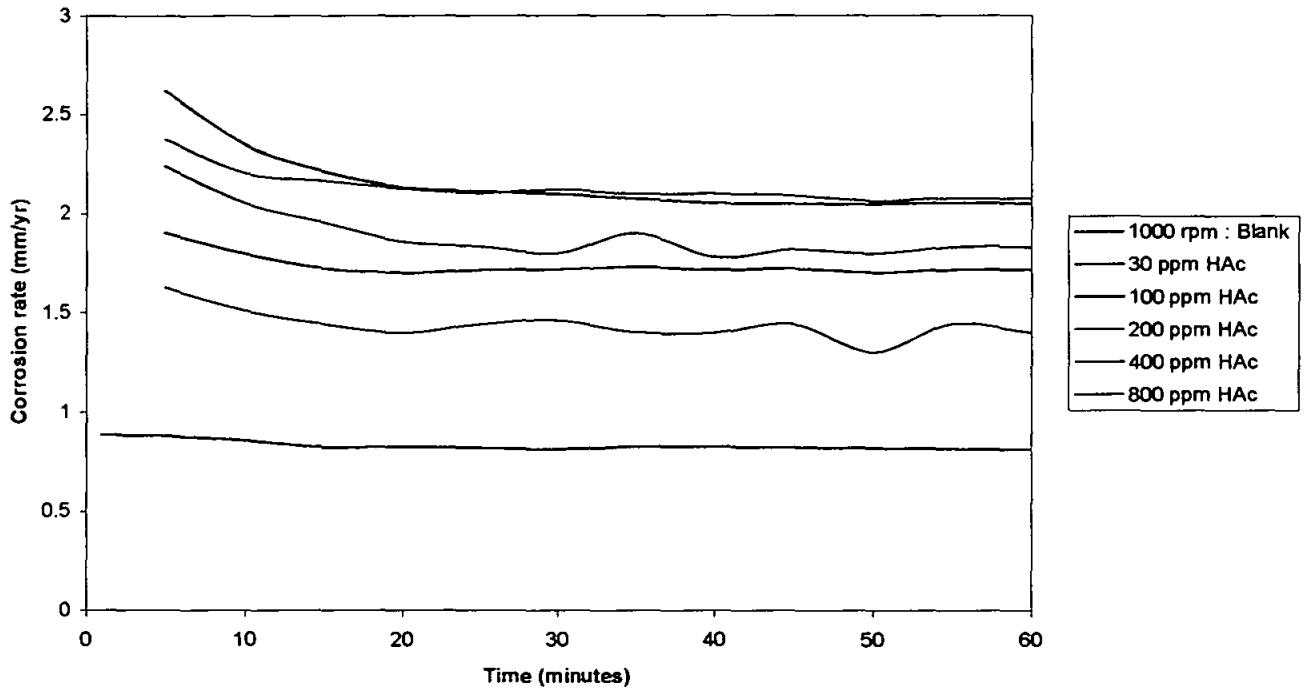
Figure 6.1: Average corrosion rate of mild steel in CO_2–saturated NaCl solution at pH 5.5, 22°C, and 1000 rpm.
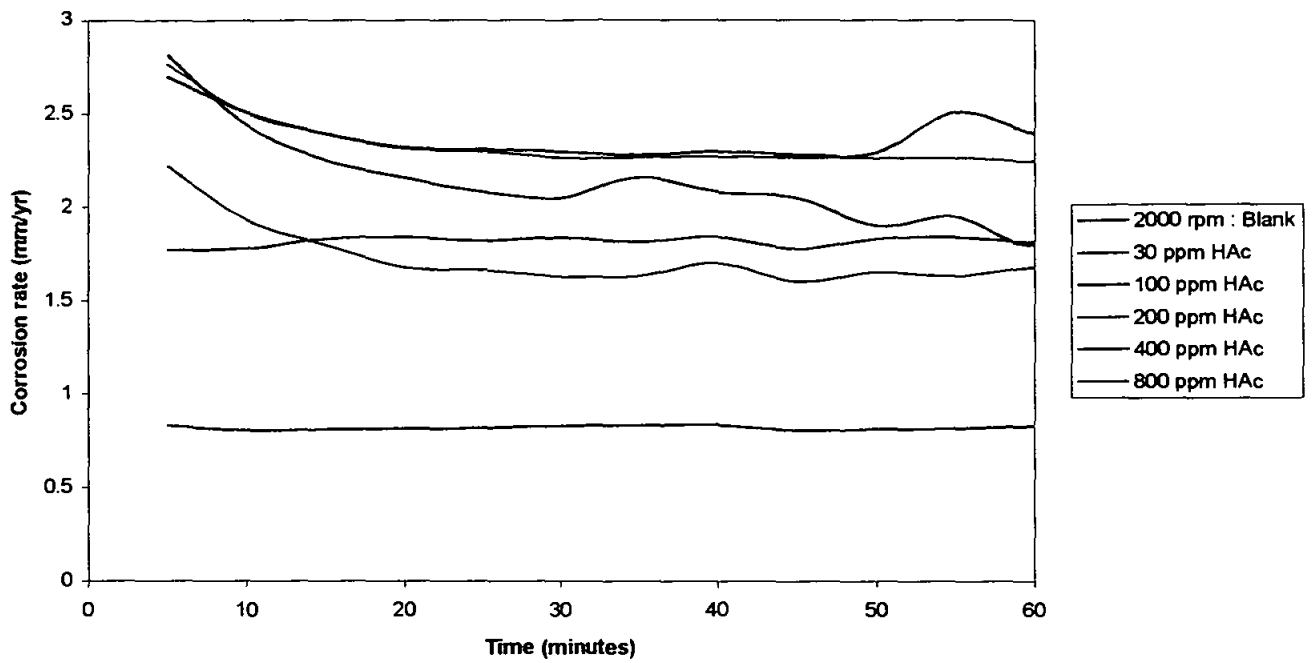
Figure 6.2: Average corrosion rate of mild steel in CO_2–saturated NaCl solution at pH 5.5, 22°C, and 2000 rpm.
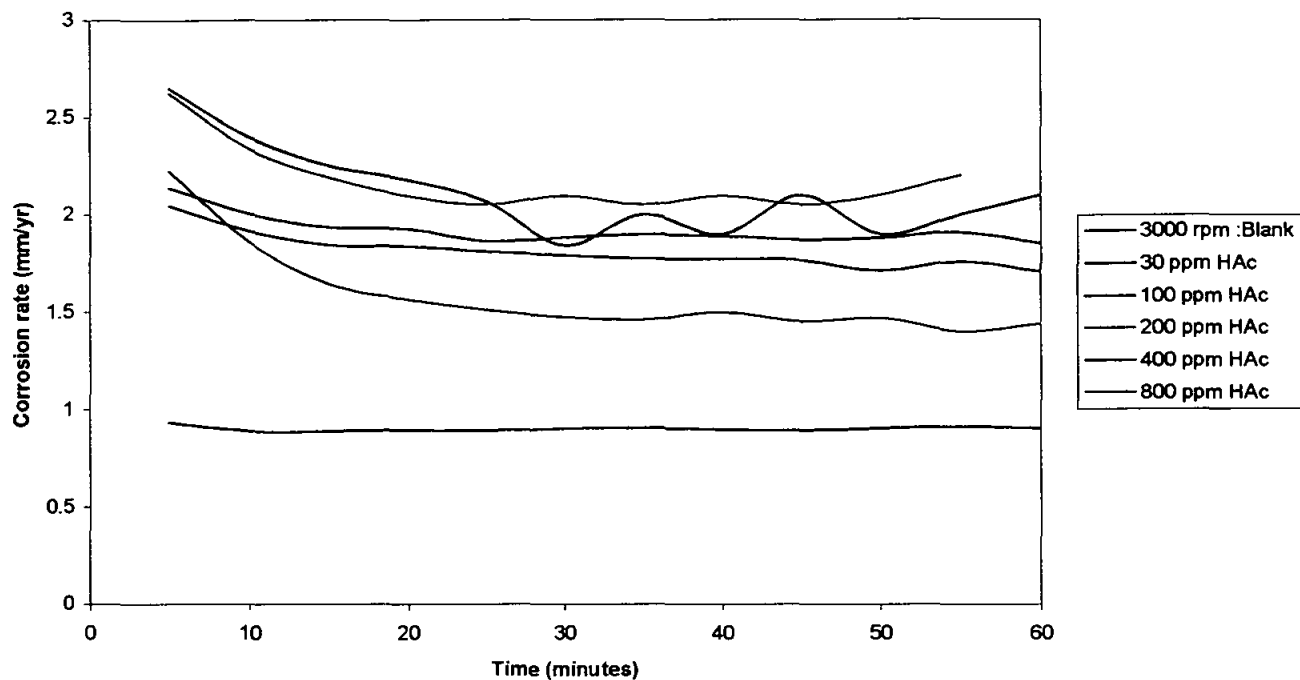
Figure 6.3: Average corrosion rate of mild steel in CO_2-saturated NaCl solution at pH 5.5, 22°C, and 3000 rpm.
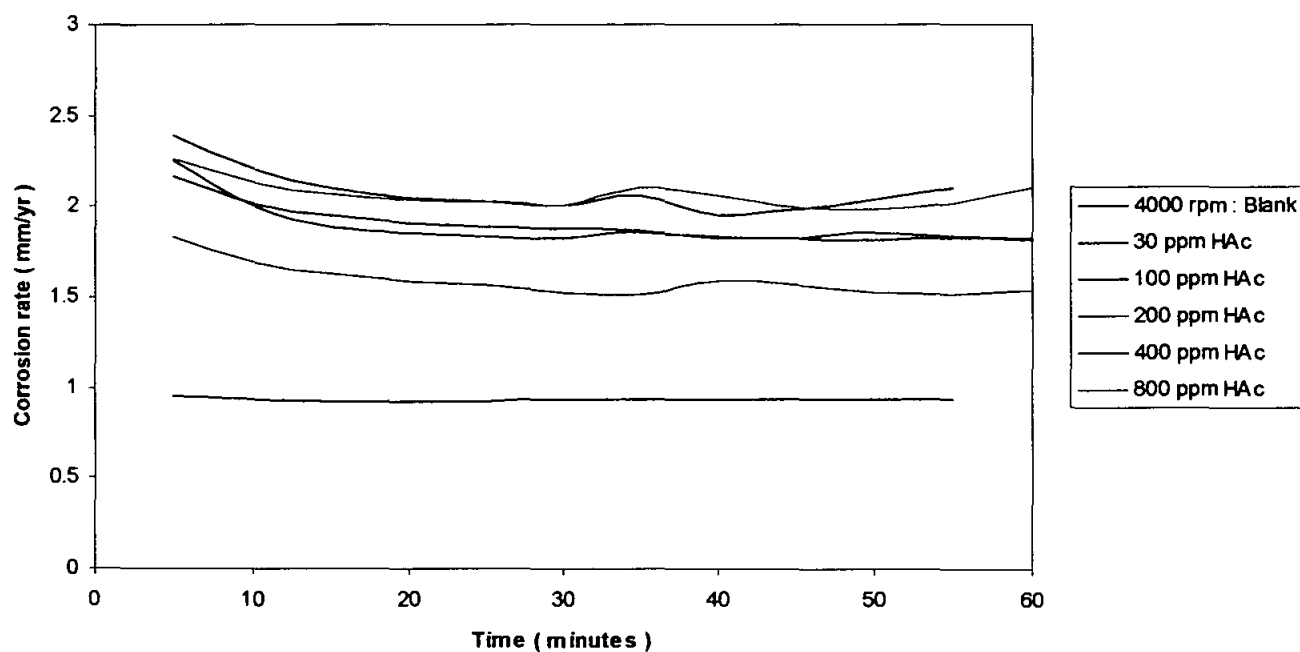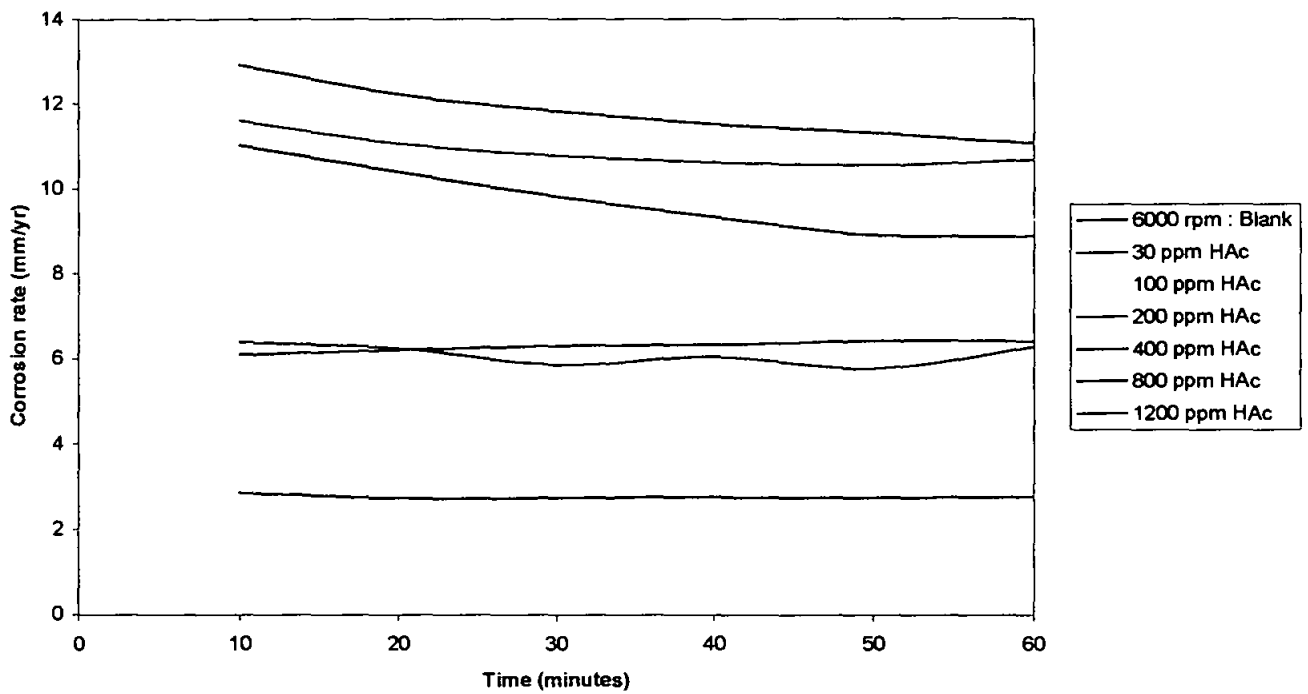

Figure 6.4: Average corrosion rate of mild steel in CO_2-saturated NaCl solution at pH 5.5, 22°C, and 4000 rpm.
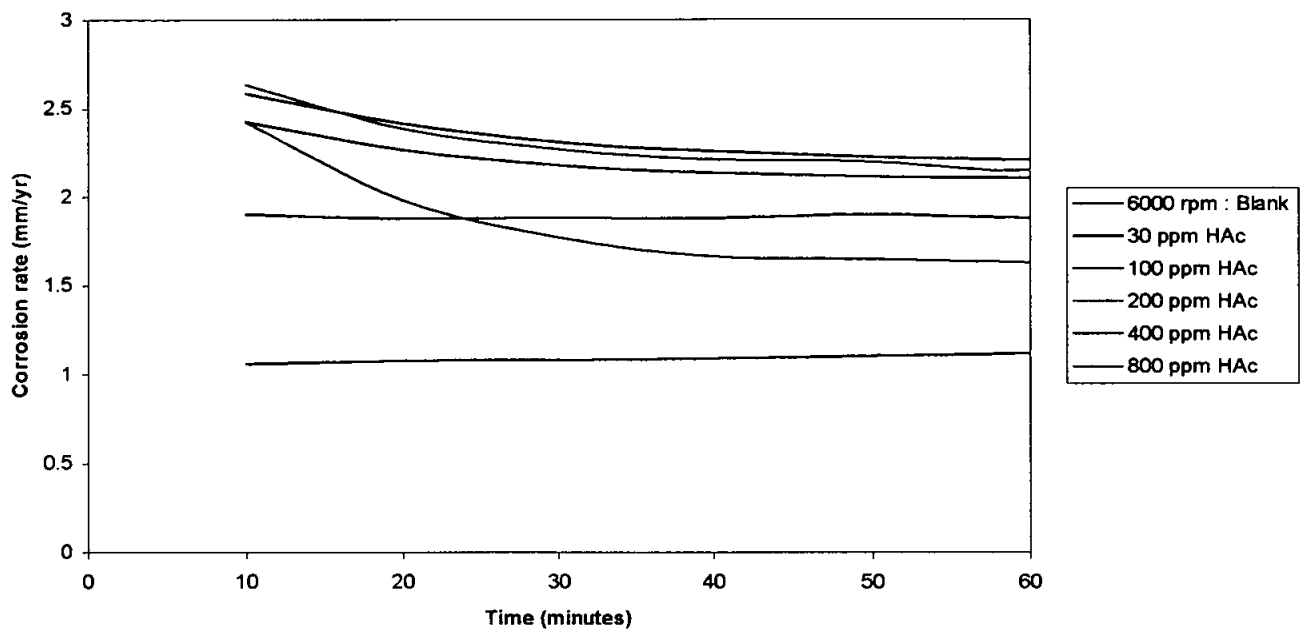
Figure 6.5: Average corrosion rate of mild steel in CO_2-saturated NaCl solution at pH 5.5, 22°C, and 6000 rpm.

The corrosion rate increases by more than 100 % with addition of 30 ppm HAc at all rotation rates as summarised in Table 6.1 below. However, not much increase in corrosion rate is observed with the presence of higher HAc concentration, i.e. more than 100 ppm. In fact, the corrosion rate tends to decrease with the presence of more than 200 ppm HAc. This is apparent with 800 ppm HAc where the corrosion rate decreases to approximately to that of the blank solution. This trend is true for all rotation rates tested 1000 – 6000 rpm.

Table 6.1: Percentage increase in corrosion rates with the increase in HAc concentration at pH 5.5, 22°C.

Rotation speed	Blank (mm/yr)	Percentage increase compared to the blank solution				
		30 ppm	100 ppm	200 ppm	400 ppm	800 ppm
1000 rpm	0.84	110%	150%	150%	140%	90%
2000 rpm	0.82	120%	180%	180%	170%	110%
3000 rpm	0.9	120%	140%	150%	100%	90%
4000 rpm	0.93	100%	130%	130%	100%	70%
6000 rpm	1.1	100%	110%	120%	70%	60%

This corrosion trend with the increase addition of HAc is shown in Figure 6.6. In summary, the corrosion rate increases drastically with 30 ppm HAc and reaches plateau with the presence of 100 ppm to 200 ppm and decreases beyond that threshold. This trend is true for all rotation rates.

pH 5.5, 22 deg. C, 1000- 6000 rpm
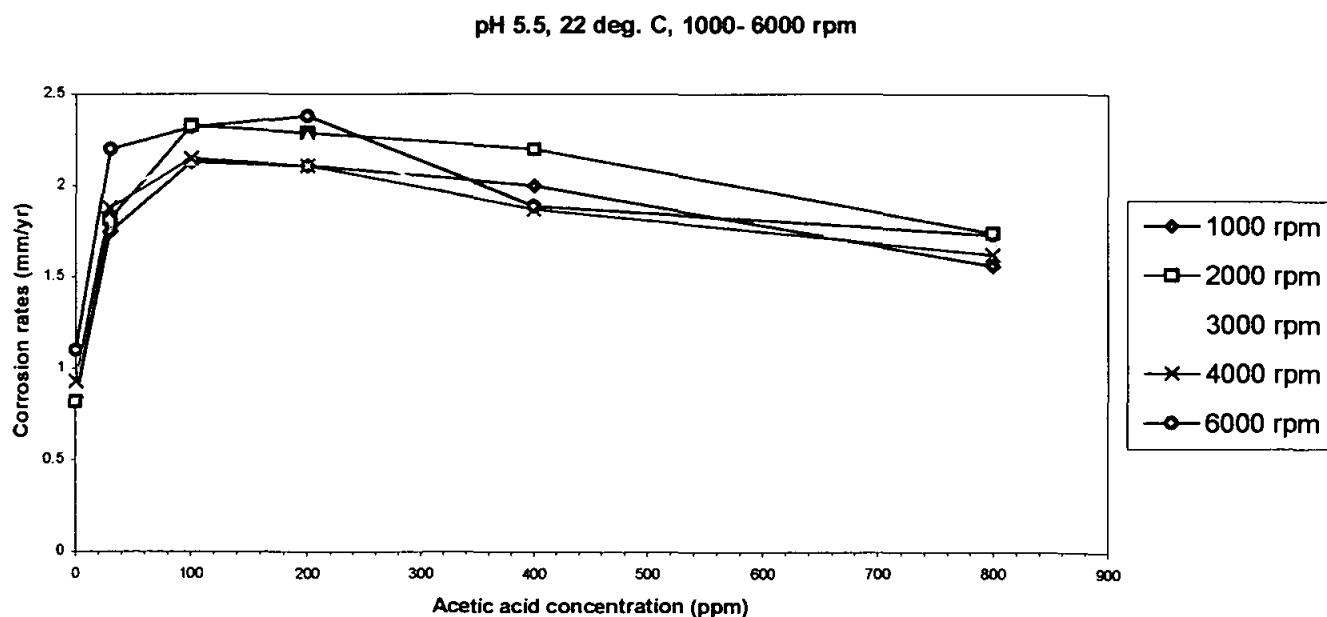
Figure 6.6: Corrosion trend with the increase of HAc concentration.

6.1.1.2 LPR Test at 50°C
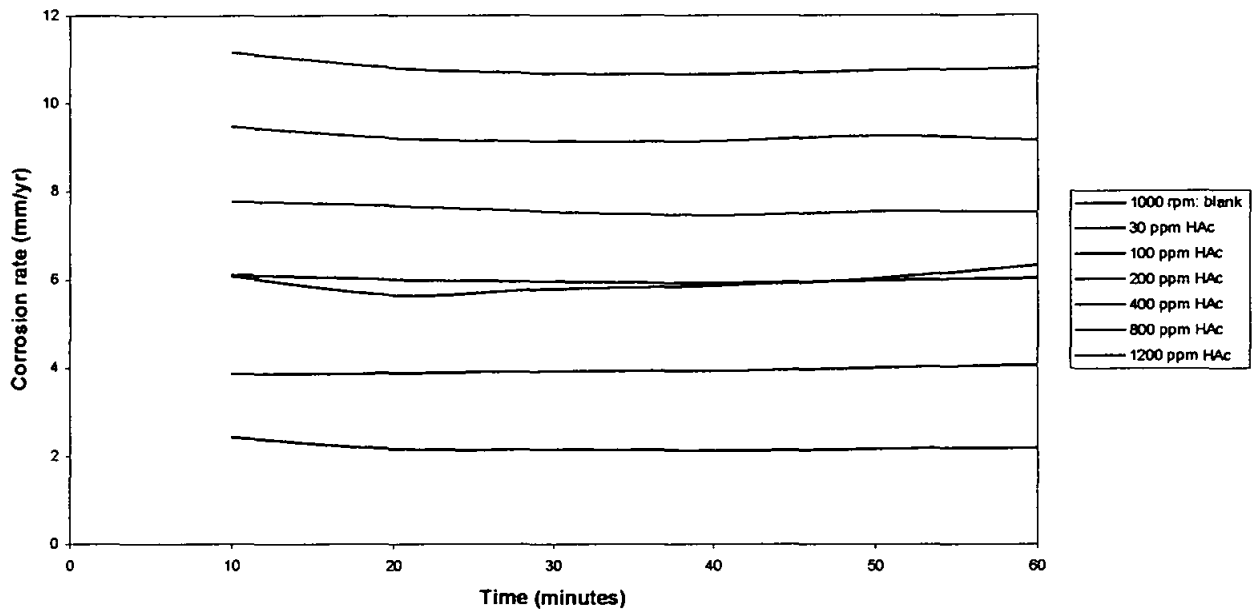
Figure 6.7: Average corrosion rate of mild steel in CO_2–saturated NaCl solution: pH 5.5, 50°C, 1000 rpm
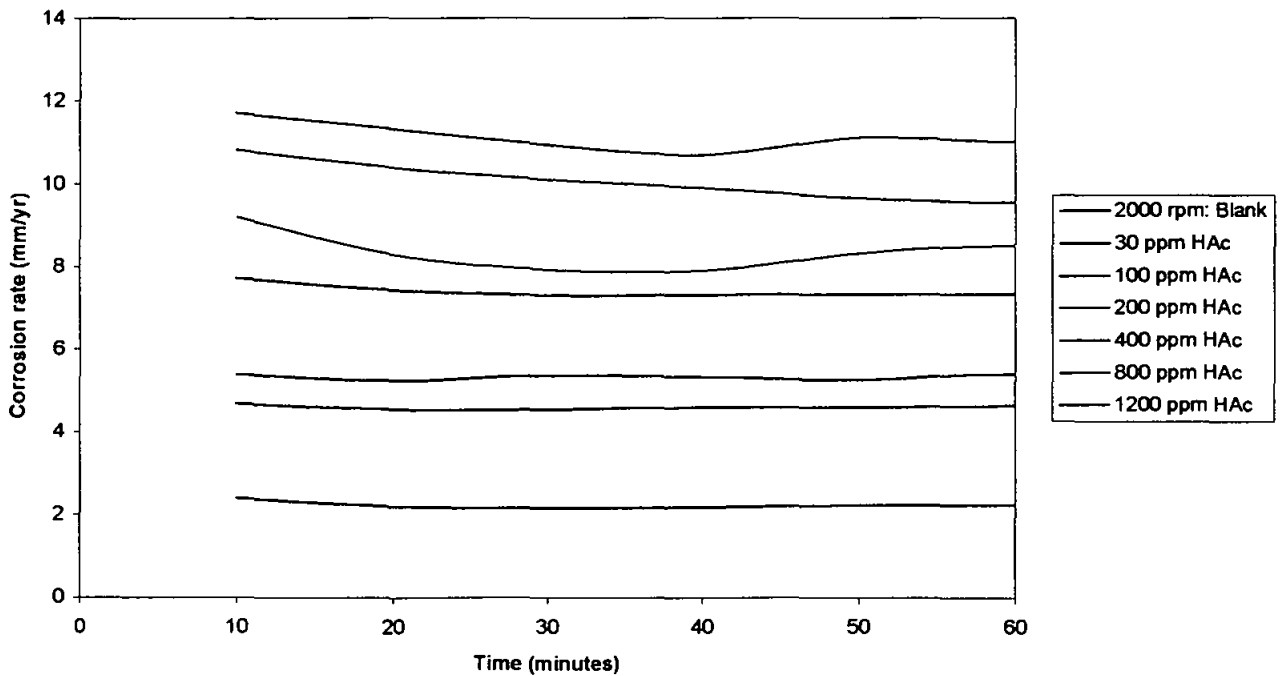
Figure 6.8: Average corrosion rate of mild steel in CO_2–saturated NaCl solution: pH 5.5, 50°C, 2000 rpm.

Figure 6.9: Average corrosion rate of mild steel in CO_2-saturated NaCl solution: pH 5.5, 50°C, 3000 rpm.

Figure 6.10: Average corrosion rate of mild steel in CO_2-saturated NaCl solution: pH 5.5, 50°C, 4000 rpm.

Figure 6.11: Average corrosion rate of mild steel in CO_2–saturated NaCl solution at : pH 5.5, 50°C, 6000 rpm.

At 50°C, the corrosion rates increase substantially with the addition of HAc. The corrosion rate increases by more than 100% with addition of 30 ppm HAc, 200 % with 100 ppm and linearly with the increase in HAc concentration. The increase is summarised in Table 6.2 below.

Table 6.2: Percentage increase in corrosion rates with the increase in HAc concentration at pH 5.5, 50°C.

Rotation speed	Blank (mm/yr)	% increase compared to blank solution					
		30 ppm	100 ppm	200 ppm	400 ppm	800 ppm	1200 ppm
1000 rpm	2.2	82%	170%	250%	320%	390%	170%
2000 rpm	2.2	110%	240%	280%	360%	400%	130%
3000 rpm	2.6	100%	180%	220%	240%	260%	120%
4000 rpm	2.6	120%	250%	320%	380%	360%	100%
6000 rpm	2.8	125%	240%	290%	320%	260%	125%

The corrosion trend with the addition of HAc is shown in Figure 6.12. Corrosion rate increases linearly with increasing HAc until about 800 ppm HAc, when a downward trend is observed. Similar to tests at 22°C, there seems to be a threshold value of 800 ppm where the corrosion rate reaches a maximum corrosion rate of about 12-14 mm/yr. Beyond that, for example, at 1200 ppm HAc, the rate reduces to lower values, about that of 30 ppm.
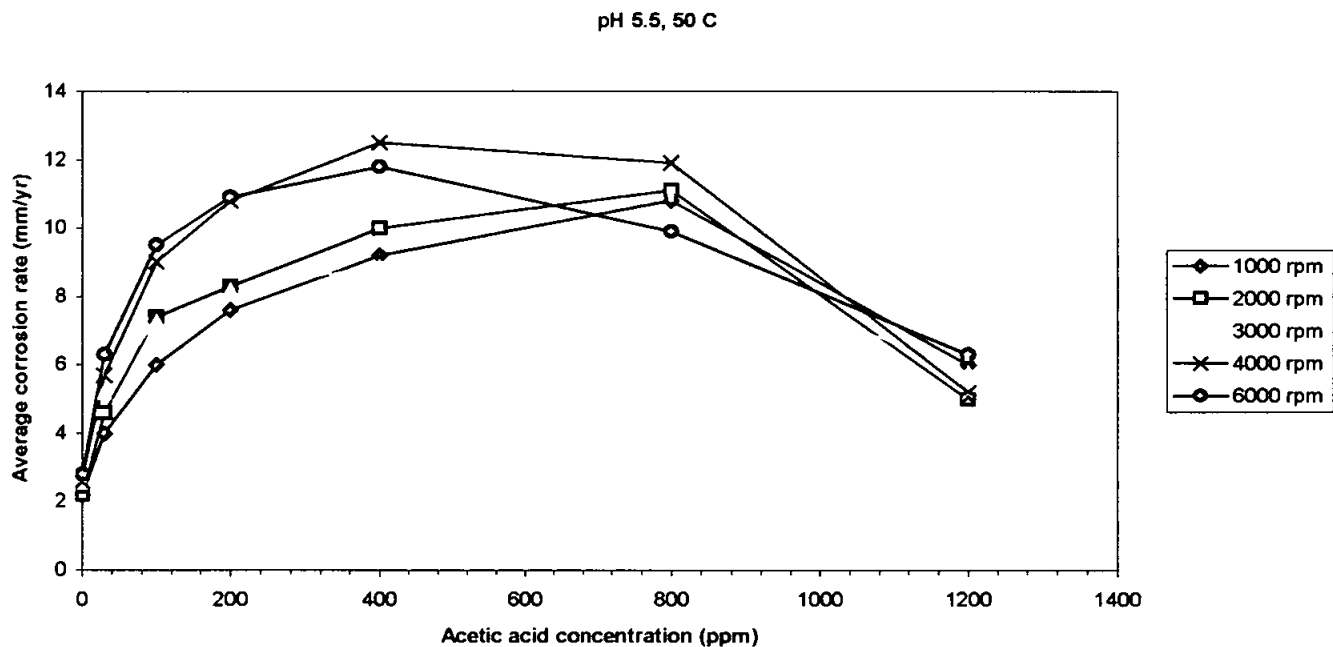
Figure 6.12: Corrosion trend at pH 5.5 and 50°C.

6.1.2 Cathodic Polarisation Tests

Cathodic polarization tests at different rotation rates and acetic acid concentrations are carried out at two different temperatures below the scaling temperature.

6.1.2.1 Cathodic Polarisation Tests at 22°C

Cathodic polarisation tests of the carbon steel in blank CO_2 solutions and in the presence of various HAc concentrations are presented in Figures 6.13-6.17.
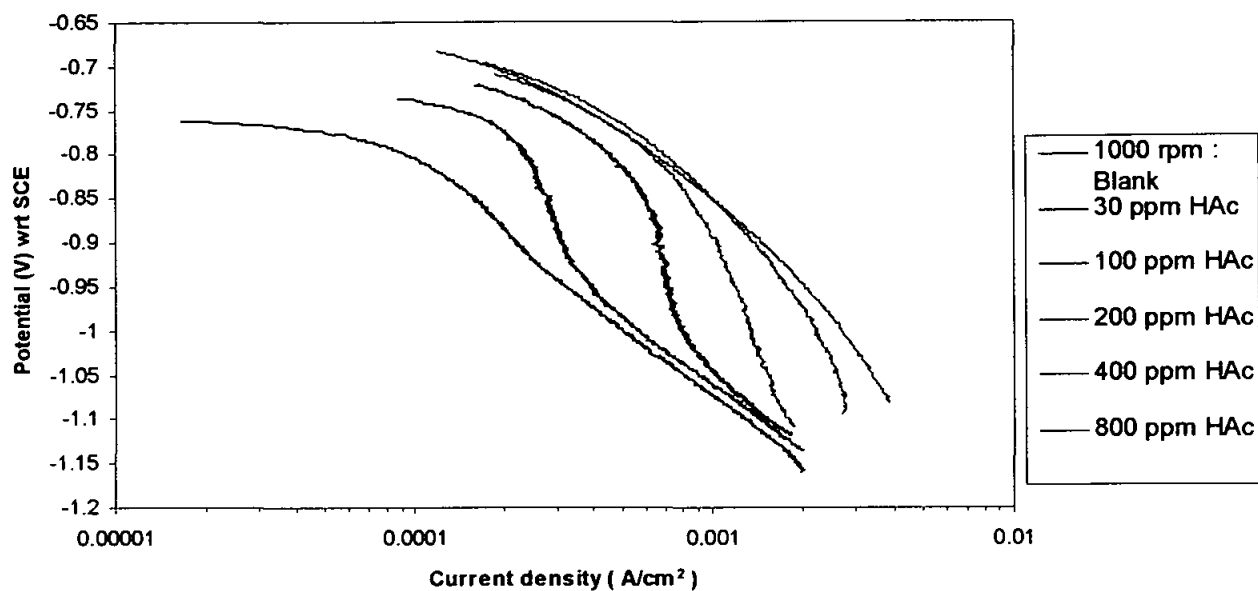
Figure 6.13: Cathodic polarisation curves for different HAc concentrations at pH 5.5, 22°C and 1000 rpm.
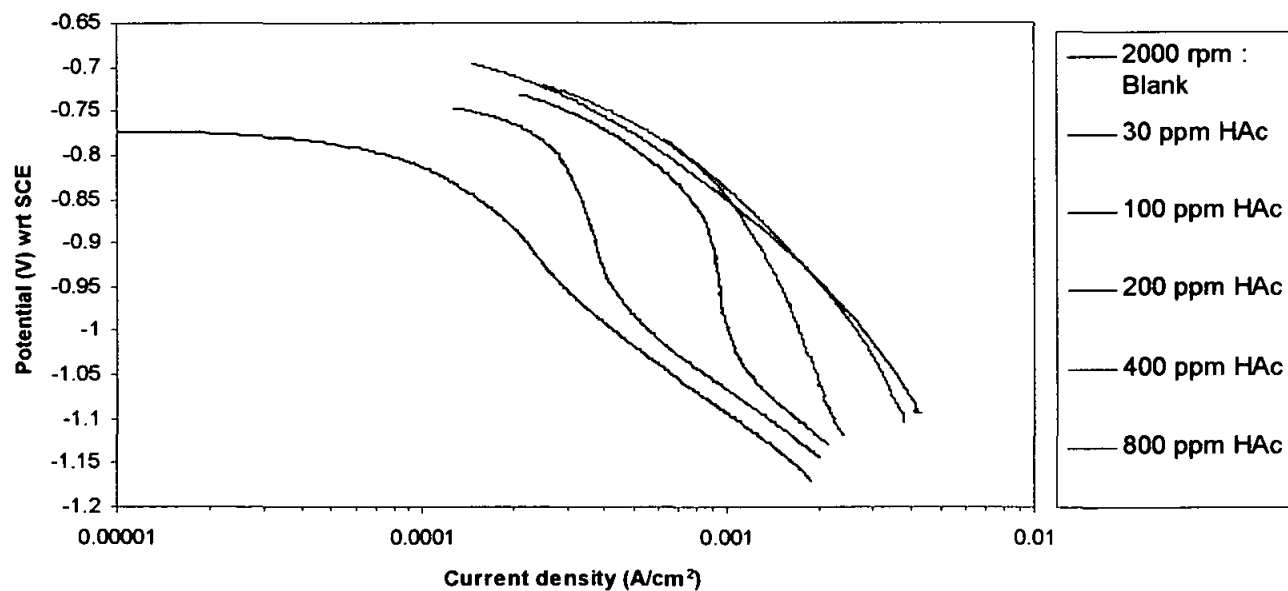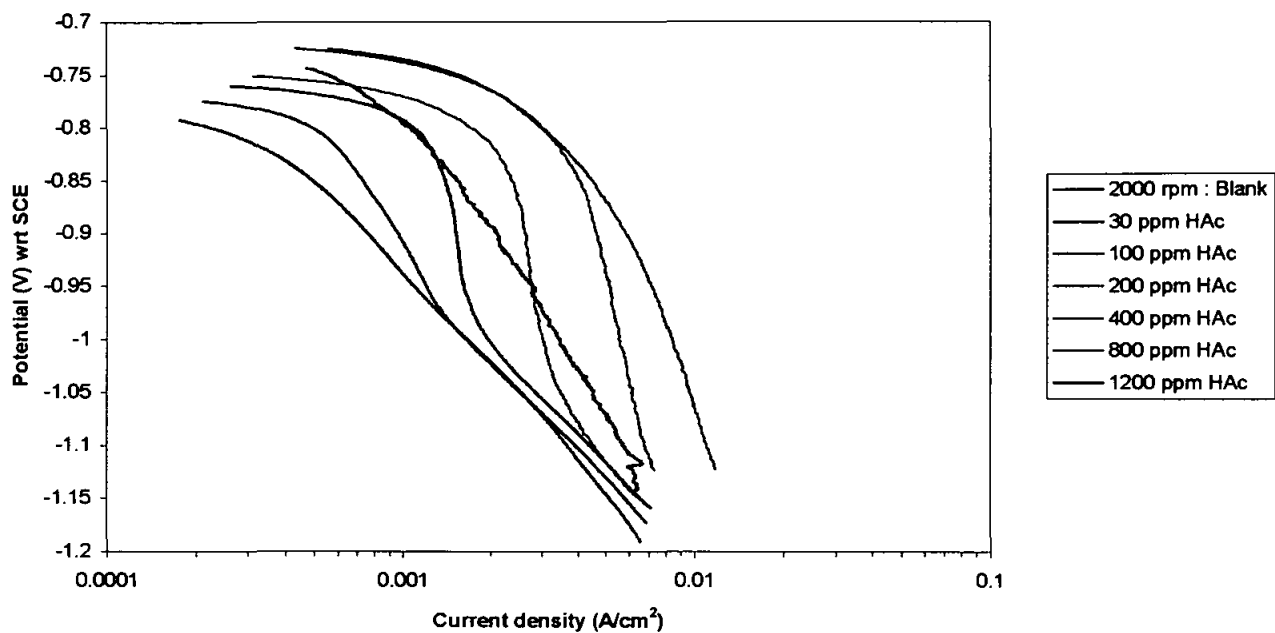

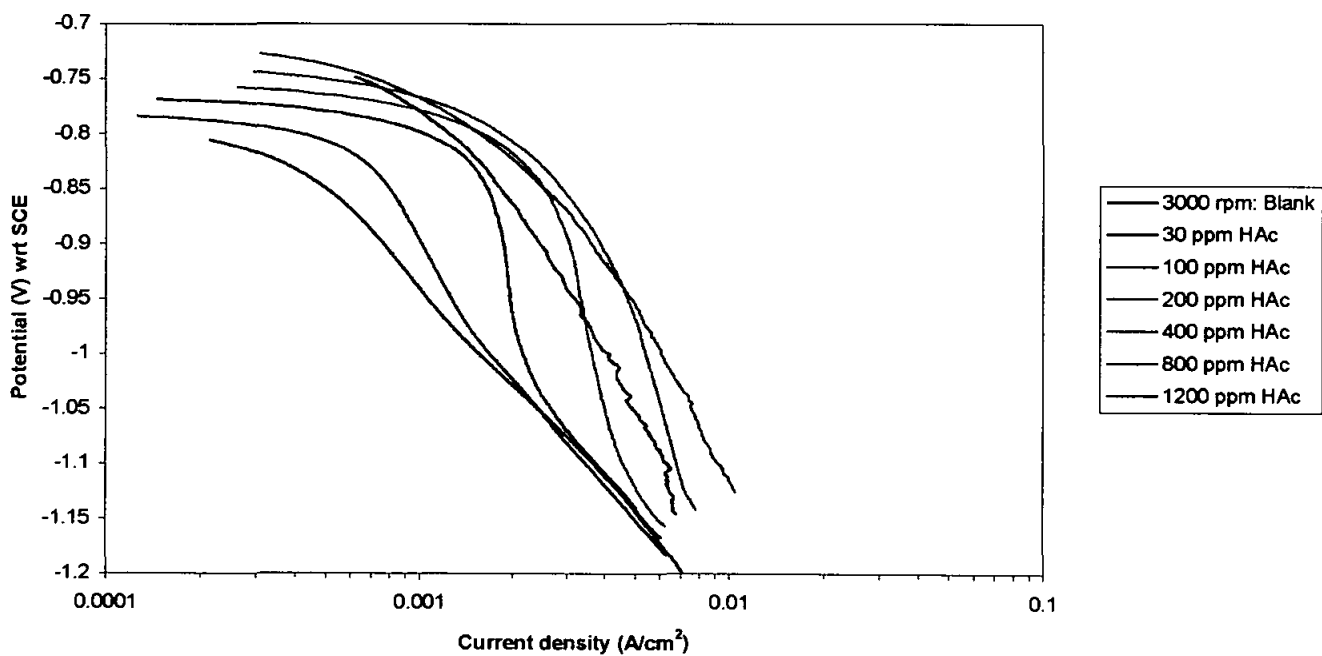Figure 6.14: Cathodic polarisation curves for different HAc concentrations at pH 5.5, 22°C and 2000 rpm.
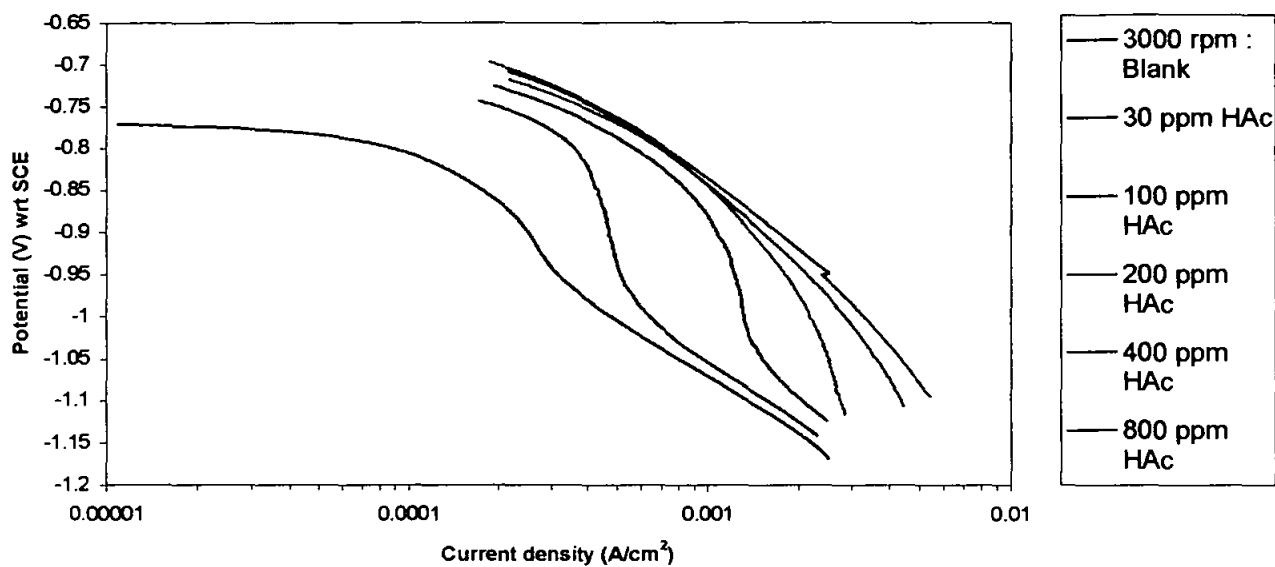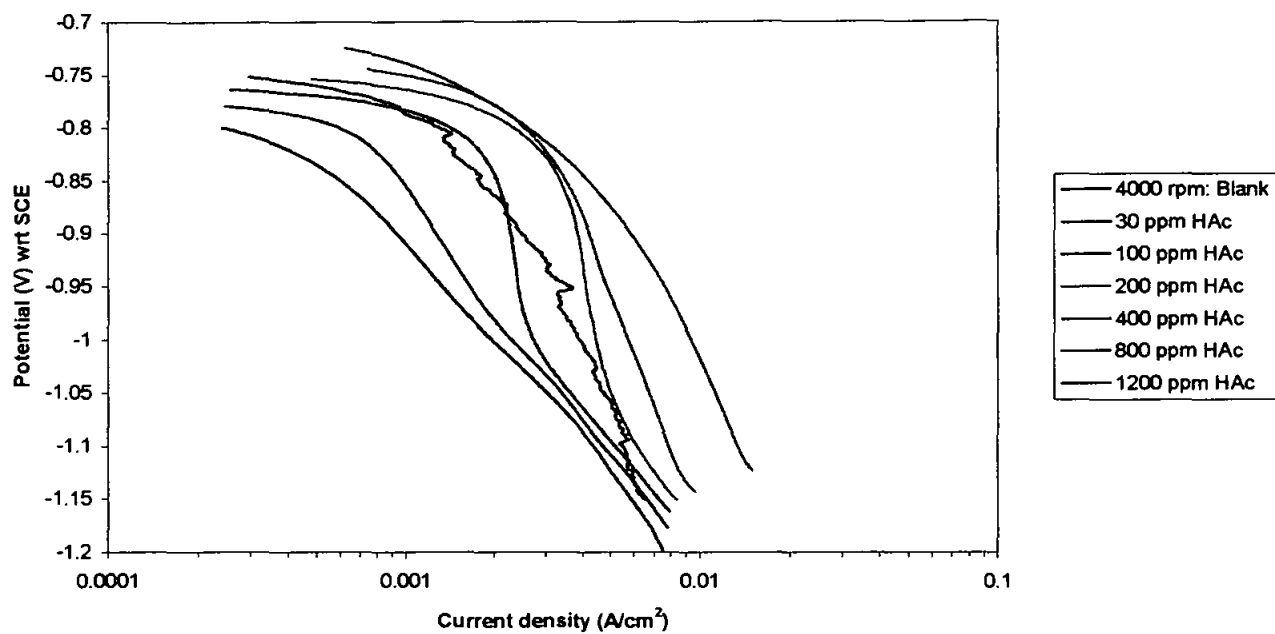
Figure 6.15: Cathodic polarisation curves for different HAc concentrations at pH 5.5, 22°C and 3000 rpm.
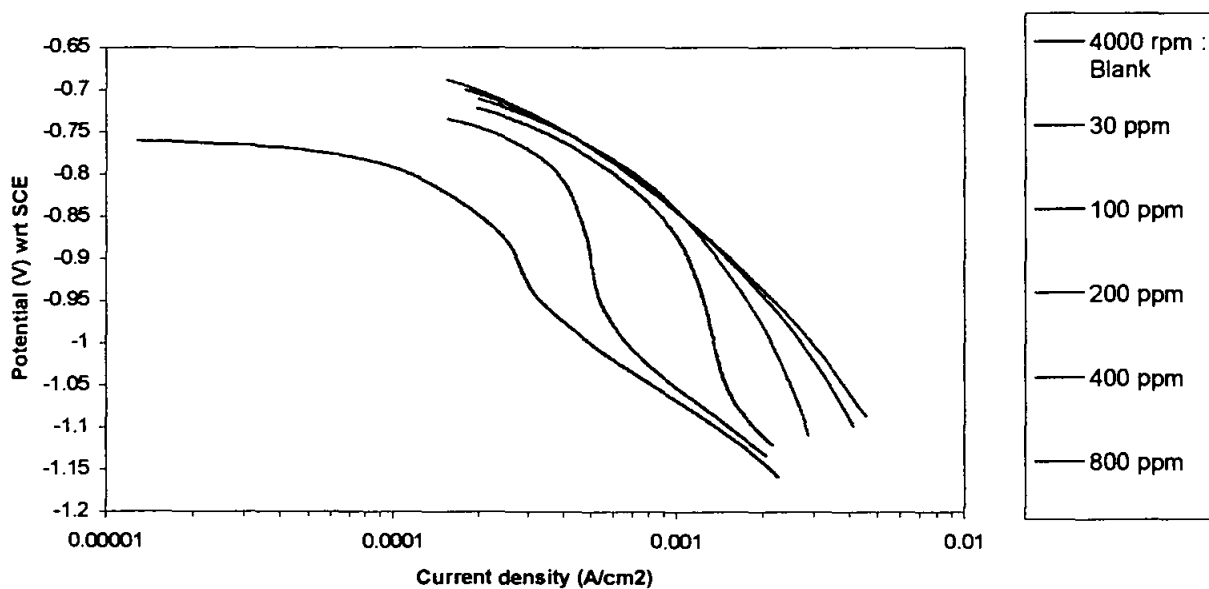
Figure 6.16: Cathodic polarisation curves for different HAc concentrations at pH 5.5, 22°C and 4000 rpm.
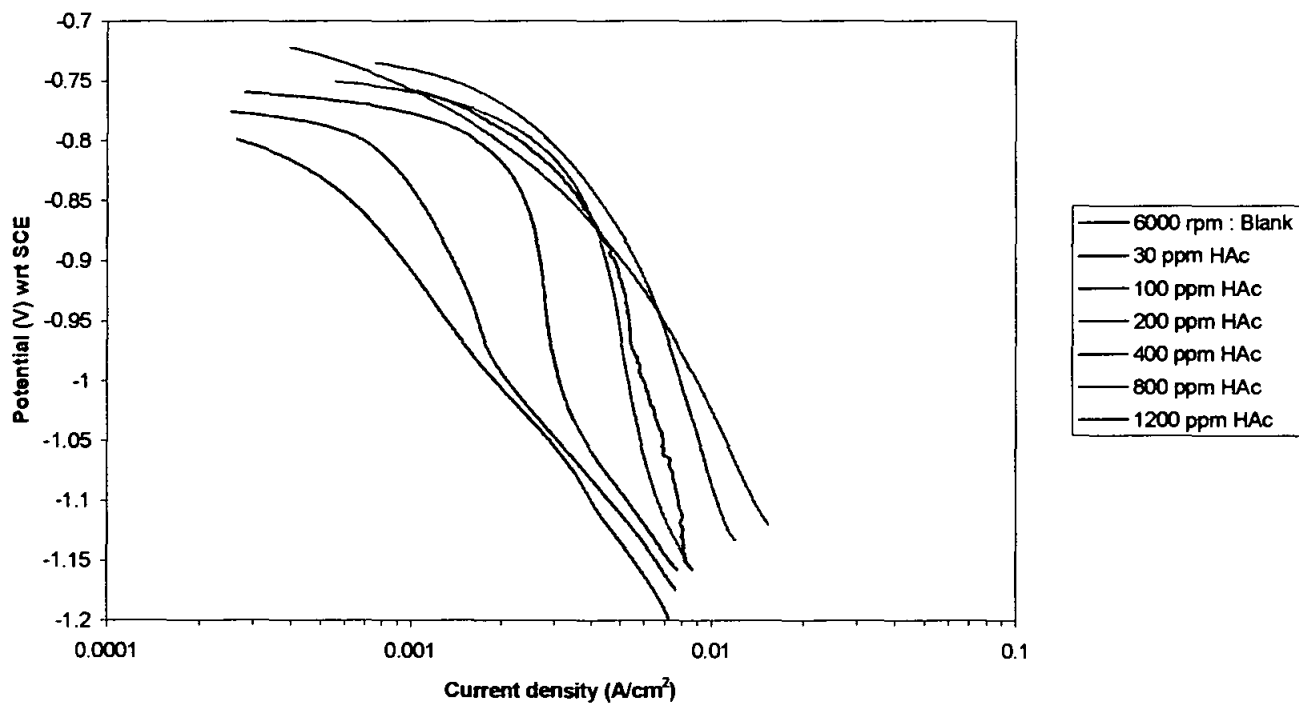
pH 5.5, 6000 rpm, 22 C
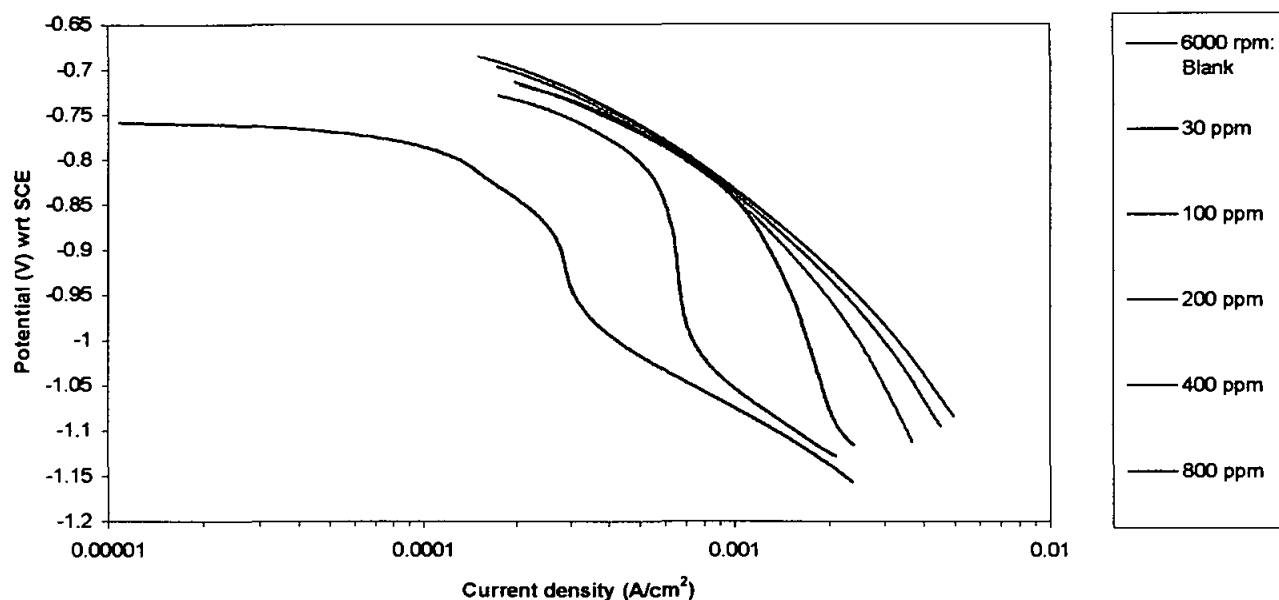
Figure 6.17 : Cathodic polarisation curves for different HAc concentrations at pH 5.5, 22°C and 6000 rpm.

Cathodic polarisation curves for solutions with no HAc(blank) do not show a well-defined limiting current density (ilim) which suggests a mixed cathodic processes of diffusion and activation occurring on the surface of the electrode. However, with the presence of 30ppm HAc, the cathodic polarisation curves show distinctive limiting current density (ilim) regions. With the HAc concentration of 100 ppm, the limiting current density region is not well-defined and falls between -0.85V and -0.95 V. Beyond 100 ppm HAc, the cathodic polarisation curve changes from a distinct mass transfer ilim to that of charge transfer or a mixture of mass transfer and charge transfer at a threshold concentration of 200 ppm HAc. The limiting current density increases with the increase in HAc concentration up to 200 ppm.

6.1.2.2 Cathodic Polarisation Test at 50°C

Cathodic polarisations of the carbon steel in CO_2 corrosion with the presence of acetic acid are presented in Figures 6.18-6.22.
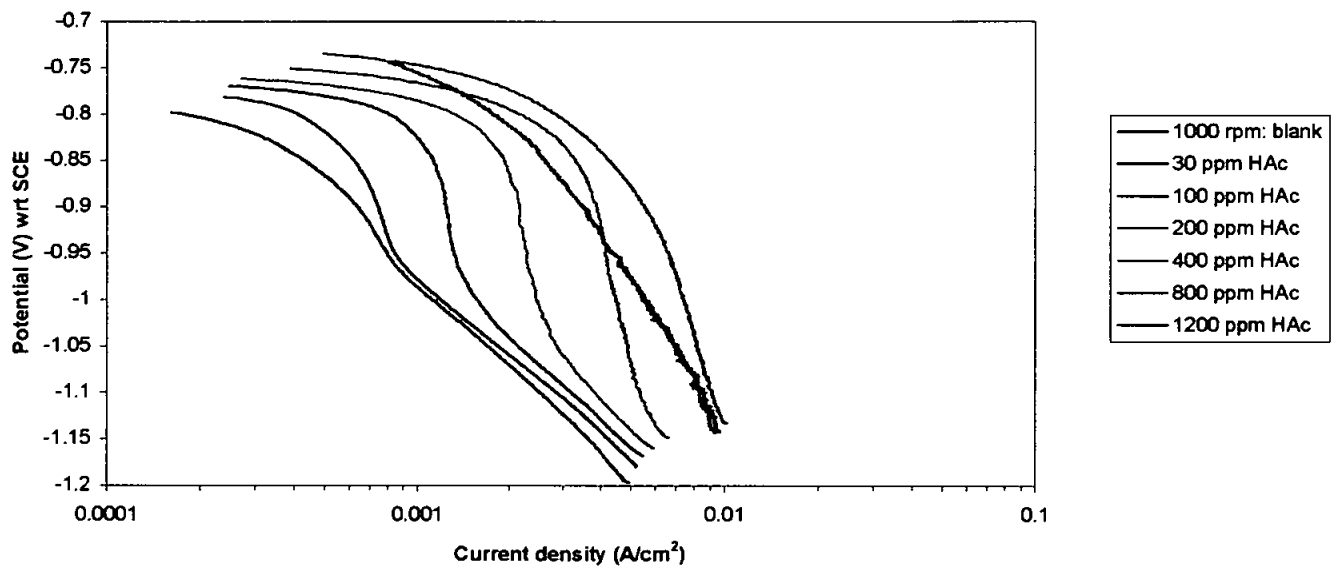
Figure 6.18: Cathodic polarisation curves for different HAc concentrations at pH 5.5, 50°C and 1000 rpm.

Figure 6.19: Cathodic polarisation curves for different HAc concentrations at pH 5.5, 50°C and 2000 rpm

Figure 6.20: Cathodic polarisation curves for different HAc concentrations at pH 5.5, 50°C and 3000 rpm.

100

Figure 6.21: Cathodic polarisation curves for different HAc concentrations at pH 5.5, 50°C and 4000 rpm.

Figure 6.22: Cathodic polarisation curves for different HAc concentrations at pH 5.5, 50°C and 6000 rpm.

Similar to the cathodic polarisation curves at 22°C, the cathodic polarisation curves for blank solution at 50°C shows a mixed cathodic process behaviour. As for 30 ppm to 200 ppm HAc, the curves show distinctive limiting current density (ilim) regions. The limiting current density increases with the increase in concentration up to 200 ppm. Beyond that threshold, the cathodic polarisation curve changes from a distinct mass transfer ilim to that of charge transfer or a mixture of both charge transfer and mass transfer.

6.2 Flow Effect in CO_2 Corrosion and with the Presence of HAC

With the presence of HAc, the limiting current densities, ilim, increase with the rotation rates as shown in Figures 6.23-6.26 below. As for blank solutions at 22°C and 50°C, the ilim does not change much with rotation rate.
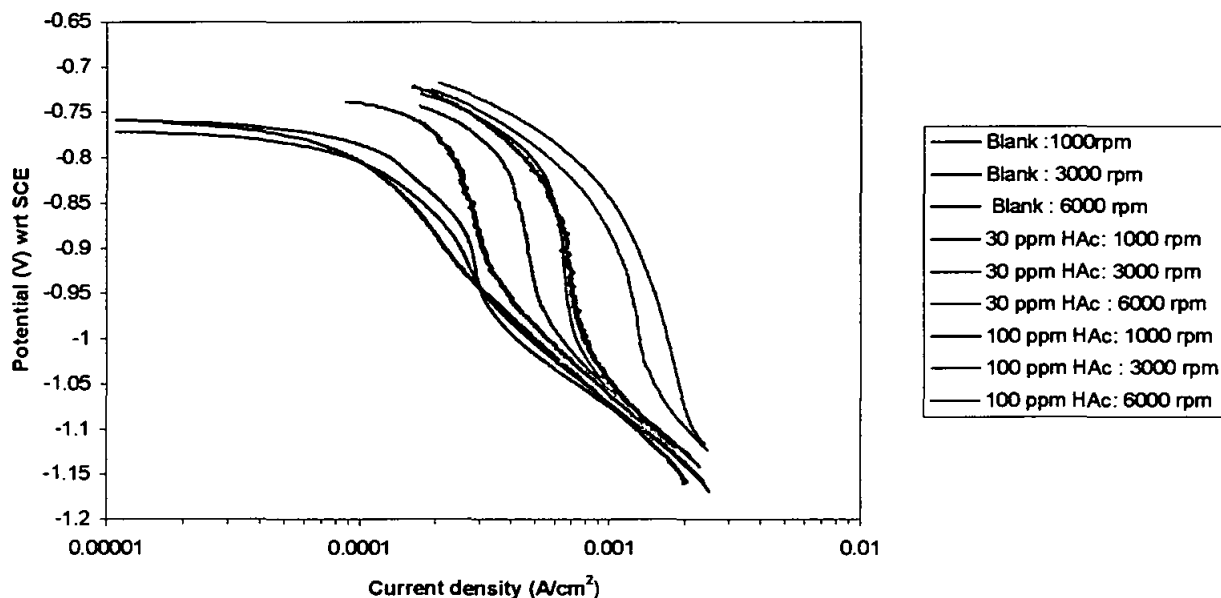
Figure 6.23: Flow effect on limiting current density at pH 5.5, 22°C.
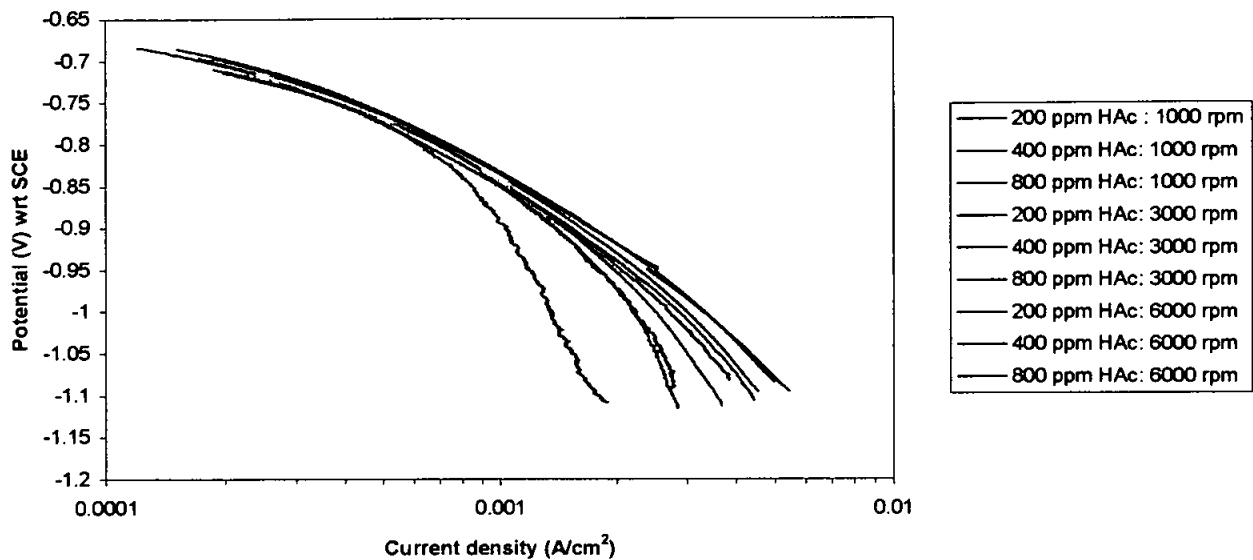
Figure 6.24 : Flow effect on charge-transfer current density at pH 5.5, 22°C.
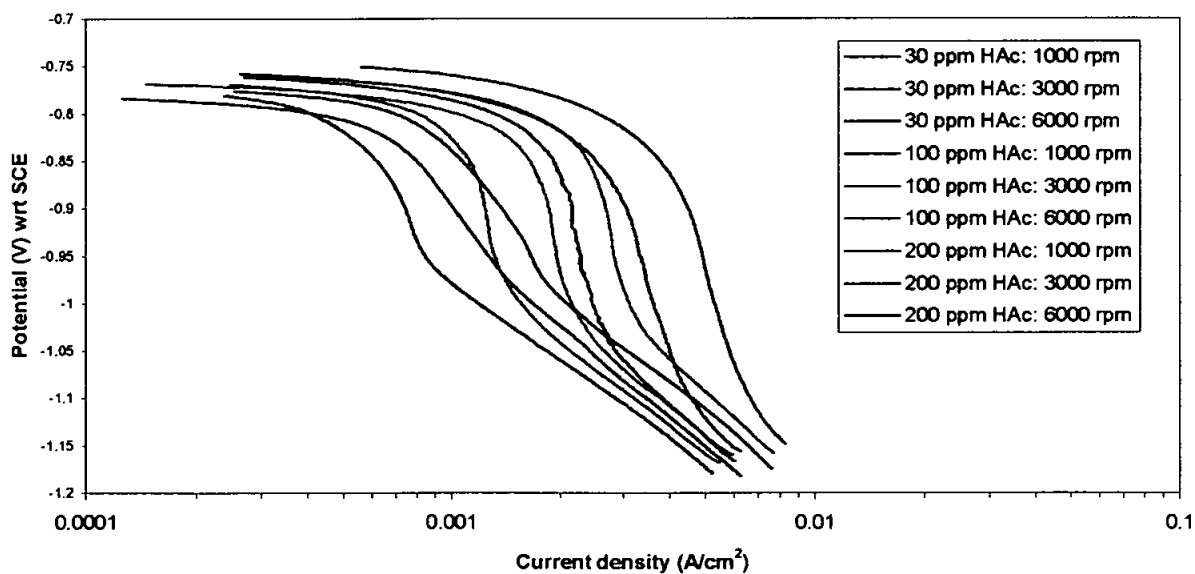
Figure 6.25: Flow effect on limiting current density at pH 5.5, 50°C.
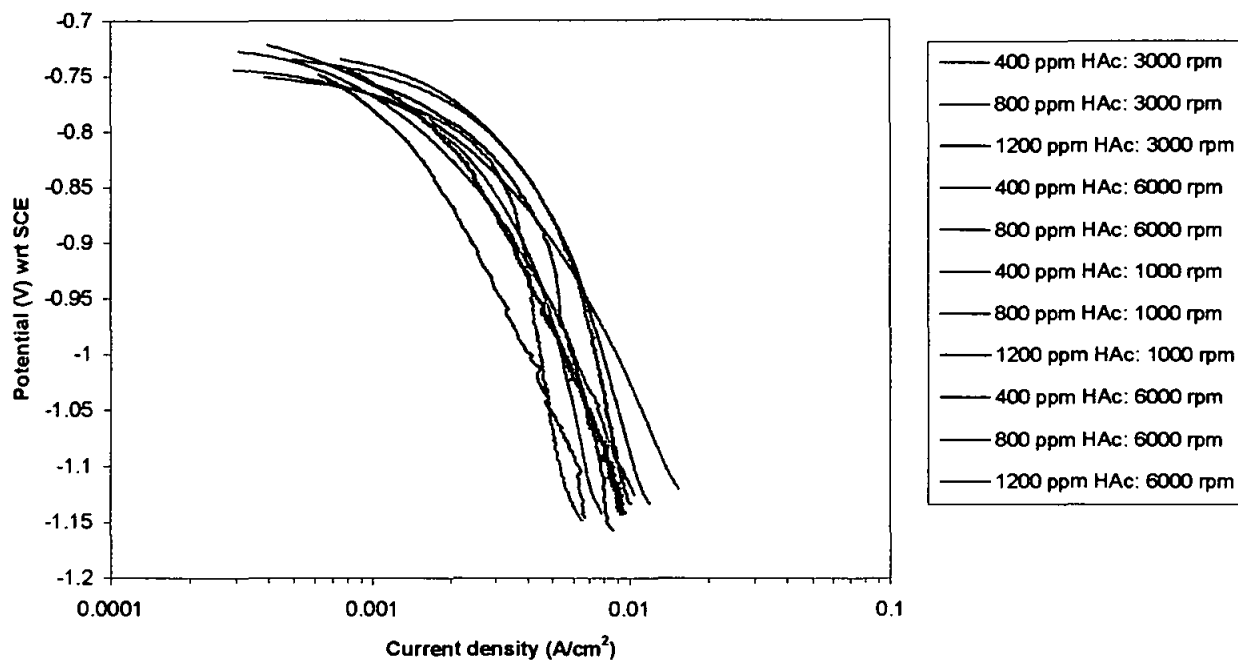
Figure 6.26 : Flow effect on charge transfer current density at pH 5.5, 50°C.

Beyond the threshold HAc concentration of both temperatures, the current densities do not change with the rotation rates as shown in Figures 6.24 and 6.26. This suggests that the cathodic reactions are not mass-transfer controlled beyond the threshold HAc concentrations.

6.3 Anodic Polarisation Behaviour

Figure 6.27 shows the anodic polarisation of the blank solution at different rotation rates tested at pH 5.5 and 22°C. The anodic polarisation curves indicate approximately the same mechanism at all rotation rates.
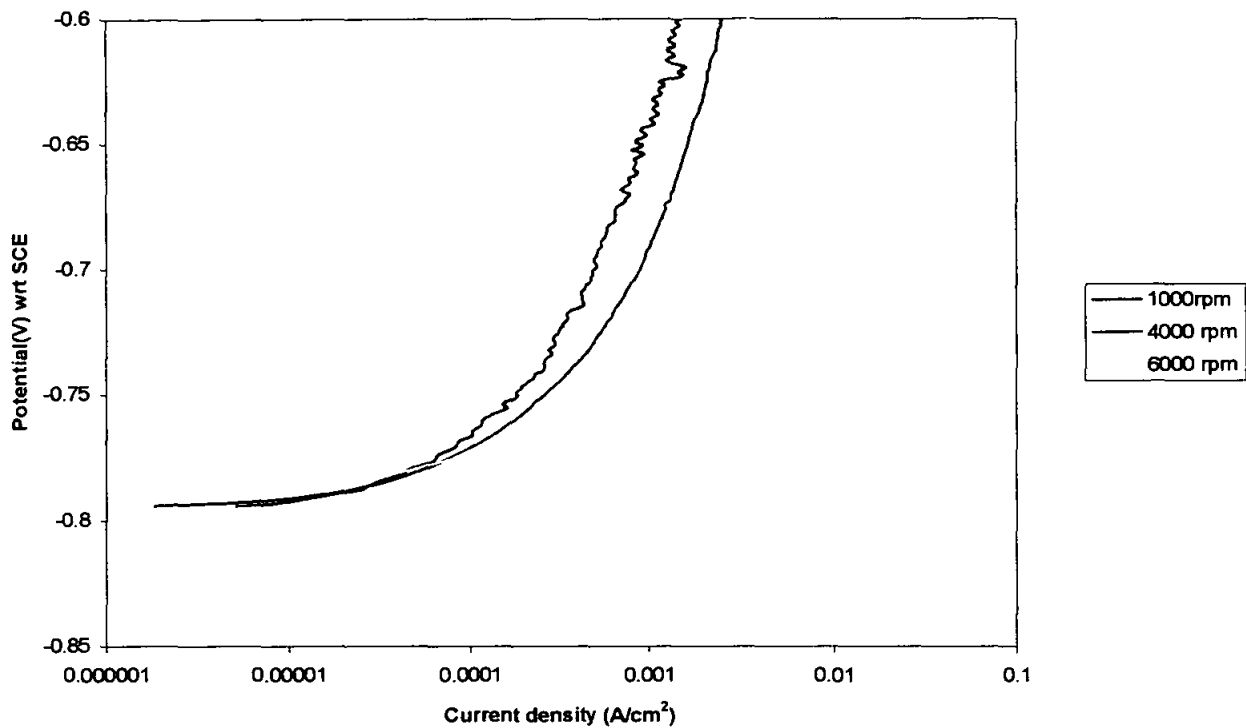
Figure 6.27: Anodic polarisation for blank solution at different rotation rates, pH 5.5, 22°C.

The anodic polarization behaviour of the carbon steel in CO_2 corrosion with the presence of acetic acid is shown in Figures 6.28-6.31 below.
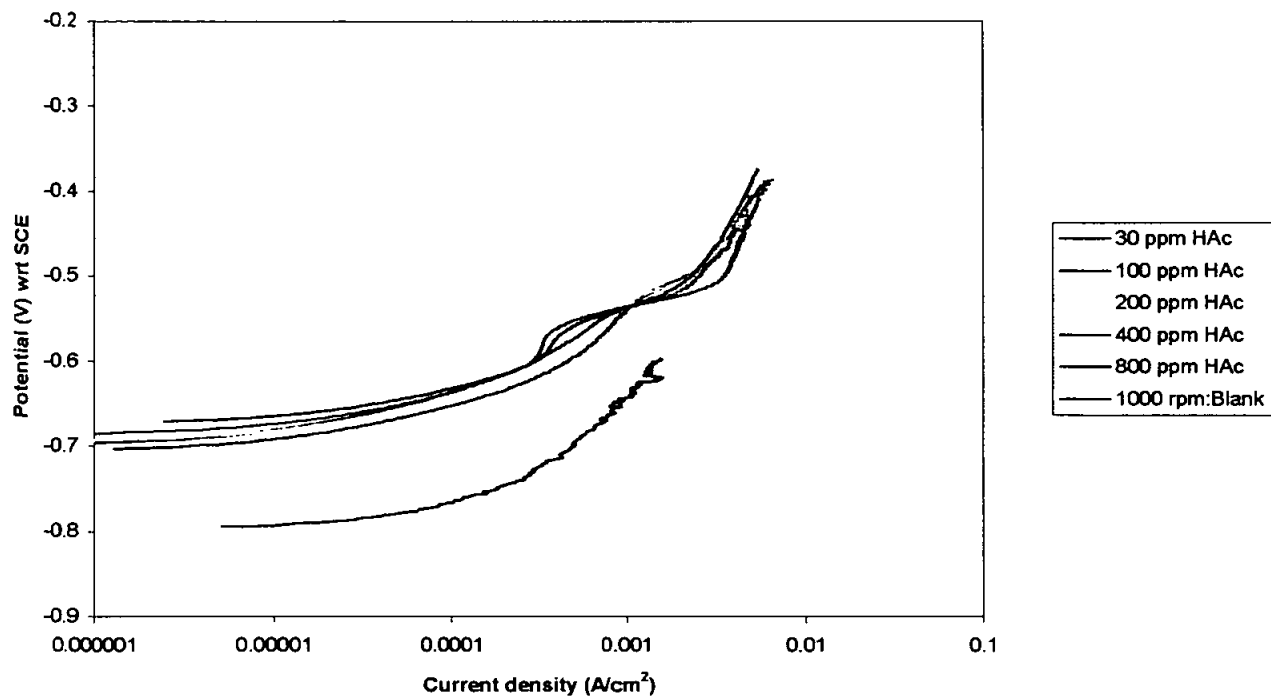
Figure 6.28: Anodic polarization for solution with HAc at 1000 rpm, pH 5.5, 22°C.
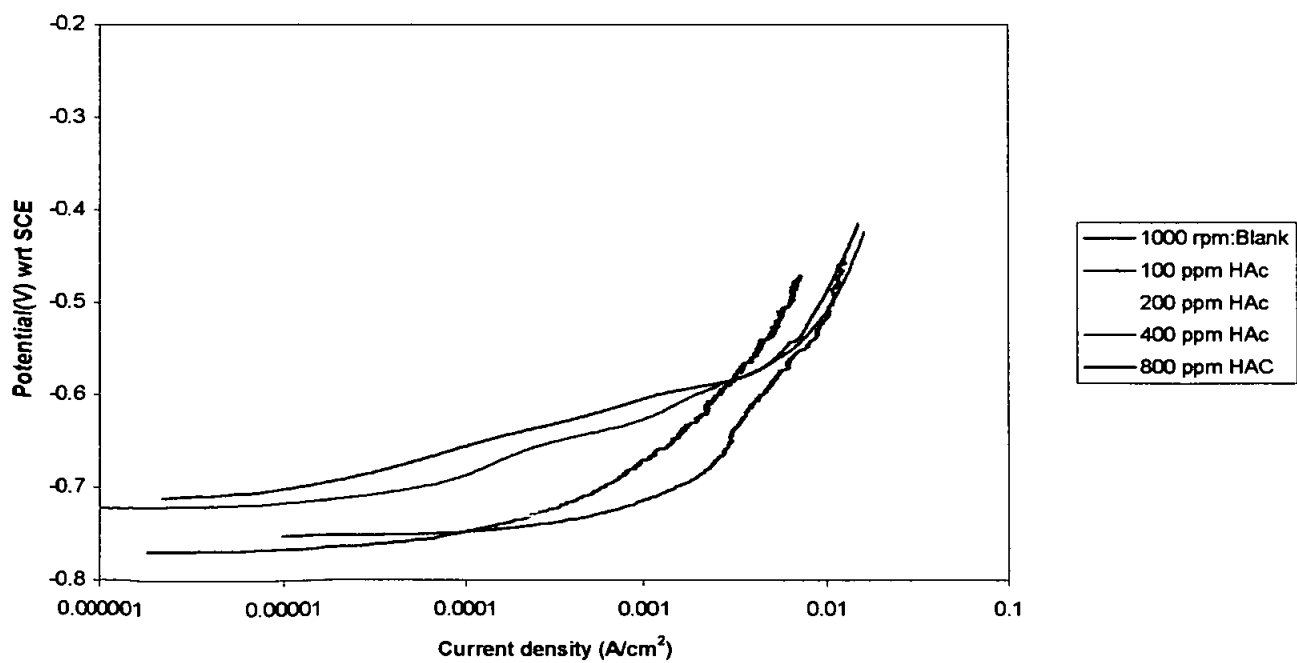

Figure 6.29: Anodic polarization for solution with HAc at 1000 rpm, pH 5.5, 50°C.
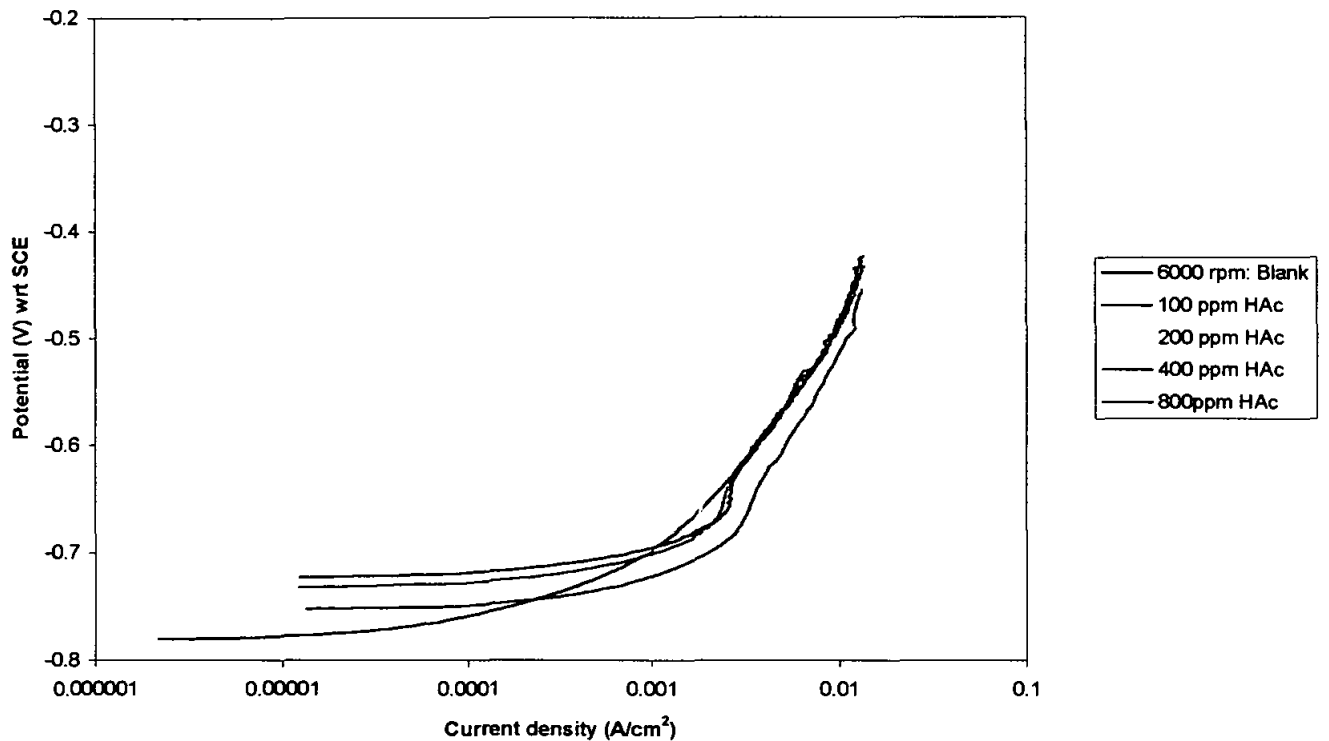
Figure 6.31: Anodic polarization for solution with HAc at 1000 rpm, pH 5.5, 50°C.

6.4 Discussions

Based on the results of the presence of various concentrations of HAc tested at different temperatures and rotation rates, there seems to be a threshold concentration of HAc beyond which an inhibition occurs. This threshold concentration increases with temperature due to the fact that inhibition is less effective at higher temperature. Therefore, the effect of HAc on CO_2 corrosion of mild steel below inhibitive levels is investigated in terms of the cathodic behaviour and corrosion rate behaviour.

In the presence of low concentrations of HAc in the range of 30 –100 ppm at 22°C, and 30-200 ppm at 50°C, the effects described in section 6.41 and 6.42 on the cathodic polarization behaviour and corrosion rate are observed.

6.4.1 Cathodic Polarisation Behaviour

Cathodic limiting current density (ilim) in turbulent flow conditions of CO_2 corrosion with the presence of HAc species could have contributions from two components, as presented below. This approach follows the findings of Rothman [65], and later by Mendoza [28].

i)   Flow-independent limiting current component or 'chemical reaction' limiting current.

ii)   Flow-dependent diffusion of main electro-active species, such as H^+ ions, H_2CO_3 and HAc species.

6.4.1.1 Flow-independent Limiting Current Component or 'Chemical Reaction' Limiting Current

By following Eisenberg's expression, a linear relationship exists between the limiting current densities (ilim) and the rotation rate to power of 0.7. Figures 6.32 and 6.33 show that the measured ilim is affected by the rotation rate of the electrode in a linear trend as predicted.

The salient point of the plot is the intercept is not zero that indicates a flow independent contribution to the total measured cathodic limiting current density. Thus as in CO_2 corrosion, there seem to be flow-independent and flow–dependent components.
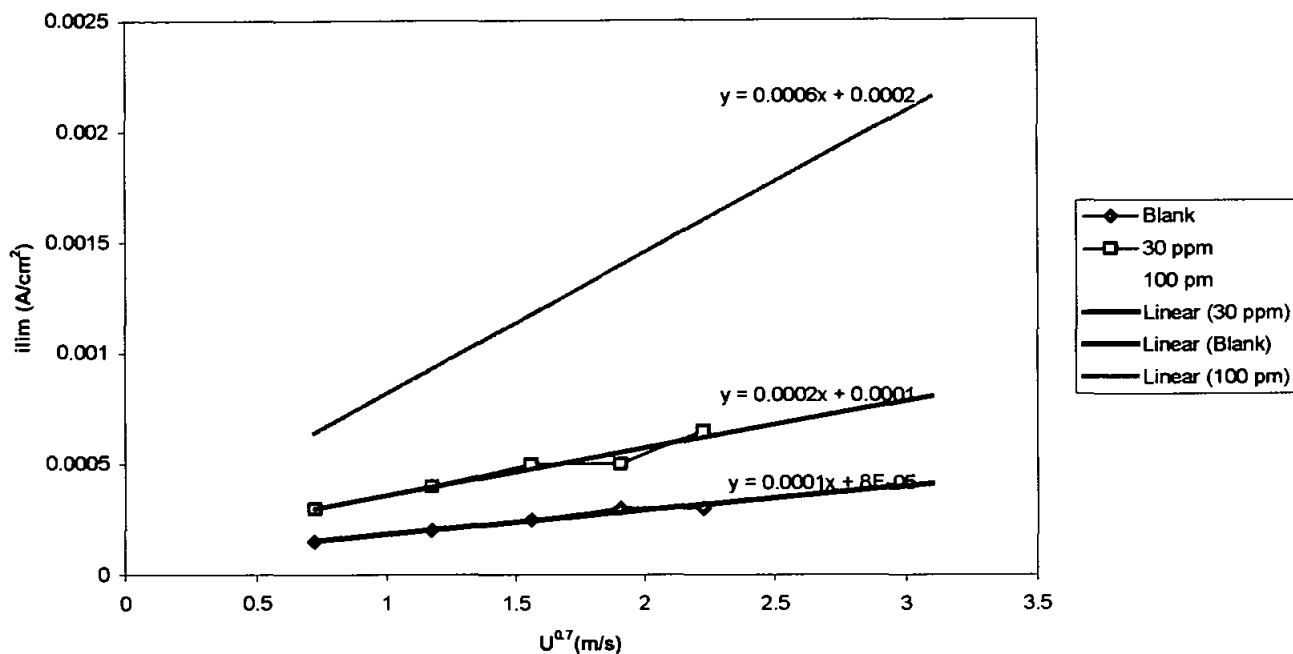
Figure 6.32: Limiting current densities (ilim) as a function of the peripheral velocity (U) to the power of 0.7, 22°C, pH 5.5
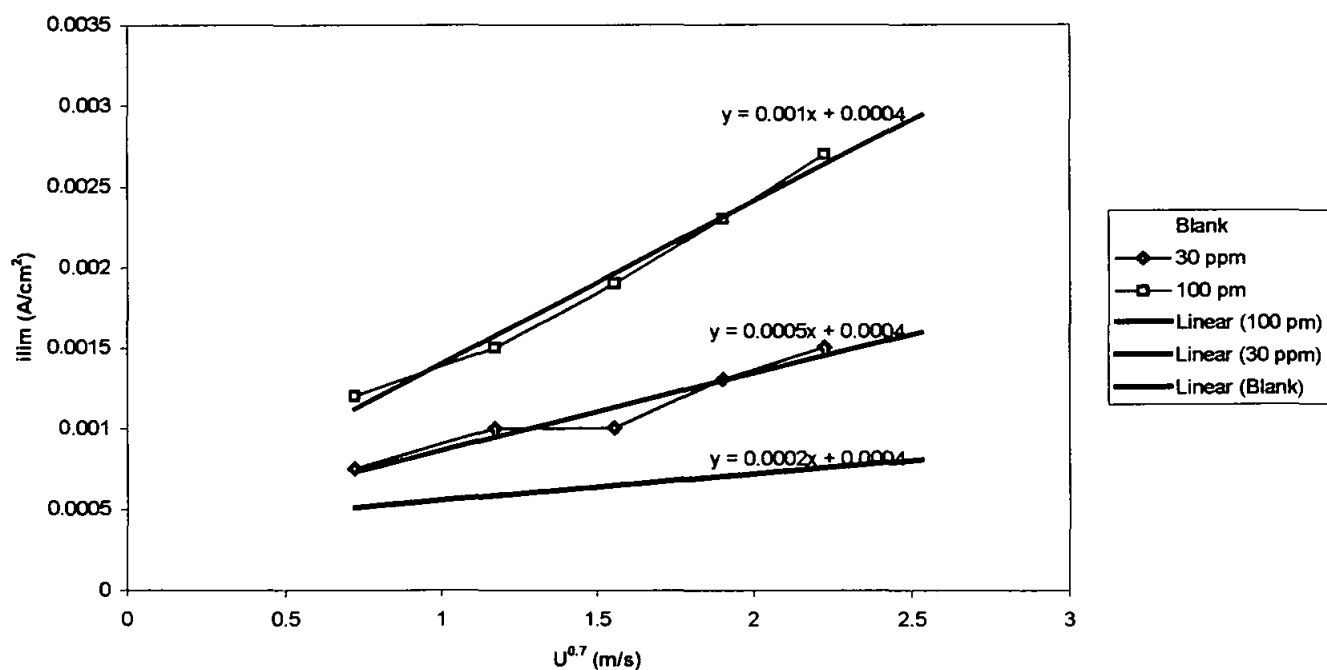

Figure 6.33: Limiting current densities (ilim) as a function of the peripheral velocity (U) to the power of 0.7, 50°C, pH 5.5

The plots based on Eisenberg's correlation in Figures 6.32 and 6.33 reveal that the intercepts are not zero and that indicates a flow independent contribution to the measured cathodic limiting current density. This could be either due to the slow hydration of carbonic acid or chemical reaction of HAc.

Since the reaction constant for HAc is fast, in the order of 10^6 s^{-1}, the flow-independent limiting current observed is not due to the slow chemical reaction of HAc dissociation. This suggests it is due to the slow hydration of carbonic acid as observed in pure CO_2 corrosion. The limiting current due the slow hydration of carbonic acid can be calculated from the following expression:

$$i_{lim_{(H_2CO_3)}} = F \, C_{b_{H_2CO_3}} \sqrt{(D_{H_2CO_3} k_{-1})}$$

The intercept value is approximately 0.0001 A/cm^2 at 22°C and 0.0004 A/cm^2 at 50°C and correlates well with the calculated values as shown in Table 6.1 below.

Table 6.1: Intercept values at 22°C and 50°C of the chemical reaction limiting current-calculated versus experimental values.

Test Condition	Limiting Current Density at Intercept (A/cm^2)	
	22°C	50°C
Blank (Calculation)	0.00012	0.00039
Blank (Experiment)	0.00008	0.0004
30 ppm HAc	0.0001	0.0004
100 ppm HAc	0.0002	0.0004

Since HAc does not contribute to the chemical reaction limiting current, we can suggest that the distinct limiting current regions observed with 30 –100 ppm at 22°C and 30-200 ppm at 50°C is due to mass transfer or diffusion of acetic acid species and other species present in the solution.

6.4.1.2 Flow-dependent Limiting Current Density

The mass transfer limiting current density arising from the presence of acetic acid can be calculated from the following expression.

$ilim = F\,k_m[HAc]_b$

where k_m is the HAc mass transfer coefficient in m/s and $[HAc]_b$ is the bulk concentration of HAc.

The mass transfer coefficient, k_m, is obtained from the expression for the rotating cylinder correlation (Eisenberg 1954):

$$Sh = \frac{k_m d}{D} = 0.0791 \times Re^{0.7} \times Sc^{0.356} = 0.079 \times \left(\frac{ud}{\nu}\right)^{0.7} \times \left(\frac{\nu}{D}\right)^{0.7}$$

where d is the diameter of the electrode in m, D is the diffusion coefficient in m²/s, Re is the Reynolds number and Sc is the Schmidt number.

The temperature dependence of the diffusion coefficient is given by:

$$D = D_{ref}\left(\frac{T}{T_{ref}}\right)\left(\frac{\mu_{ref}}{\mu}\right)$$

where D_{ref} is the diffusion coefficient at a reference temperature T_{ref}, μ is the viscosity in kg/(m s) and μ_{ref} is the viscosity at a reference temperature. At 20°C, the μ_{ref} of water is 1.002×10^{-3} kg/(m s) and the D_{ref} of hydrogen ion is 9.31×10^{-9} m²/s [82].

The density of water in kg/m³ is found from:

$\rho = 1152.3 - 0.5116\,T$, where T is temperature in K;

and the water viscosity is given by

$$\mu = \mu_{ref} 10 \ \{\frac{1.3272(20-t)-0.001053(t-20)^2}{t+105}\} \ , t \text{ is temperature in } °C.$$

Similarly, the limiting current densities due to the diffusion of H^+ ions and H_2CO_3 molecules can be calculated by the expression proposed by Eisenberg et al.

6.4.1.2.1 Limiting Current due to Hydrogen Ion (H^+) and Carbonic Acid (H_2CO_3) Species

Based on the experimental results of blank solutions at both 22°C and 50°C, the contribution of limiting current due to reduction of hydrogen ions (H^+) and carbonic acid (H_2CO_3) species is determined by subtracting the chemical reaction limiting current component at each rotation rate. The experimental data and calculated values are compared as shown in the Figures 6.34 and 6.35.
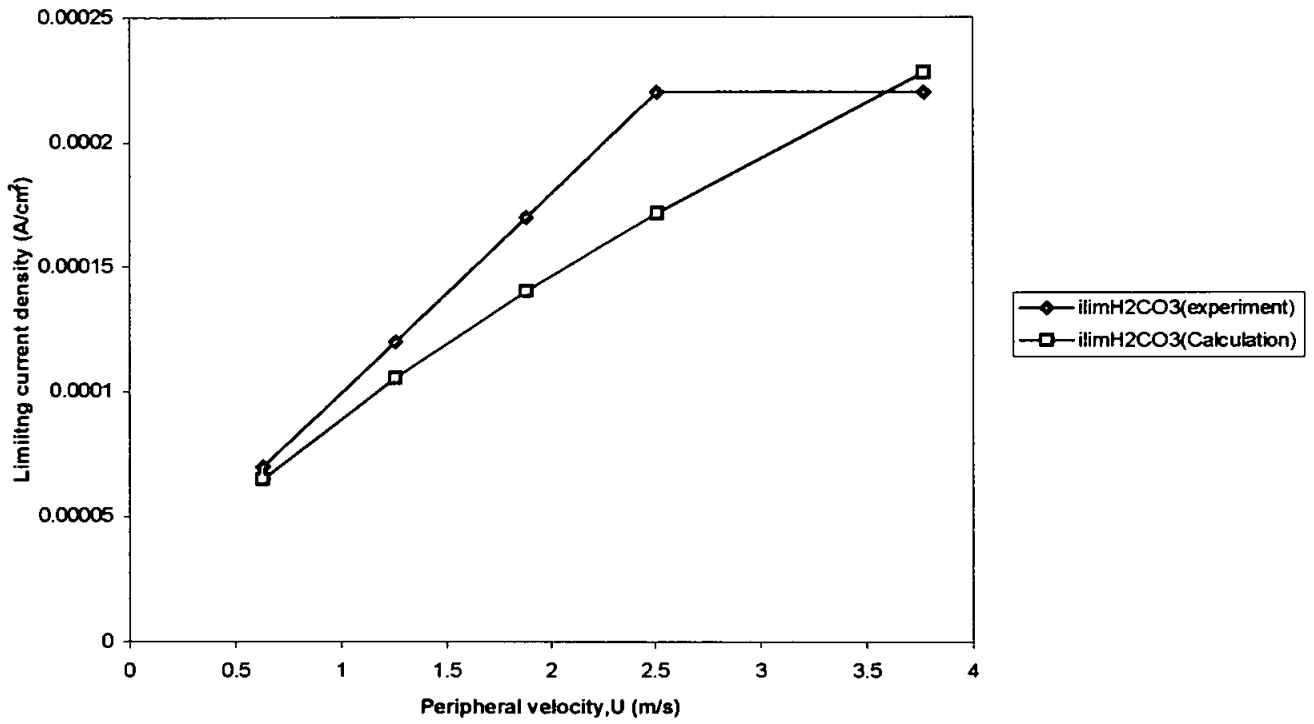
Figure 6.34 : Comparison of the limiting current due to H^+ and H_2CO_3 species at $22°C$.
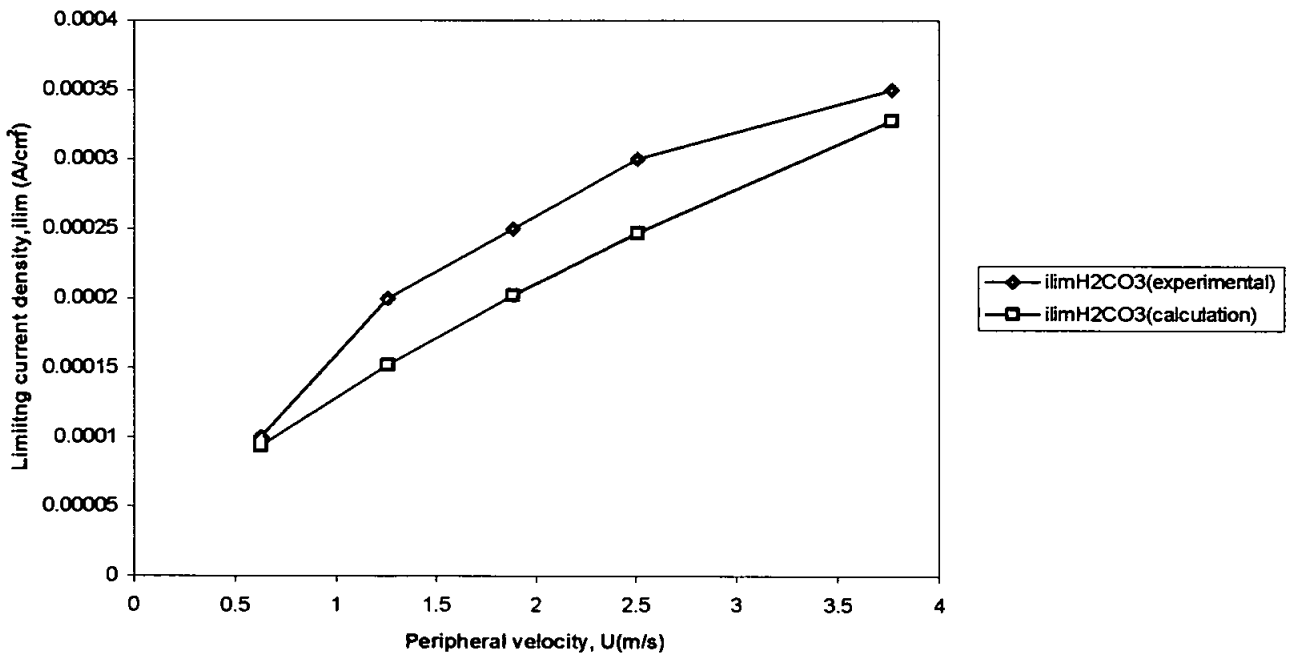

Figure 6.35 : Comparison of the limiting current due to H^+ and H_2CO_3 species at $50°C$.

6.4.1.2.2 Limiting Current Density due to Acetic Acid

The limiting current density due to acetic acid (HAc) is calculated by subtracting the contribution of limiting current density from other species of the blank solution.

The calculated values and experimental data of the ilim due to HAc species are presented in the Figures 6.36- 6.39. Both the calculated and experimental limiting current increases with the peripheral velocity. At low concentration of 30 ppm, the experimental and calculated values correlate well at both 22°C and 50°C.
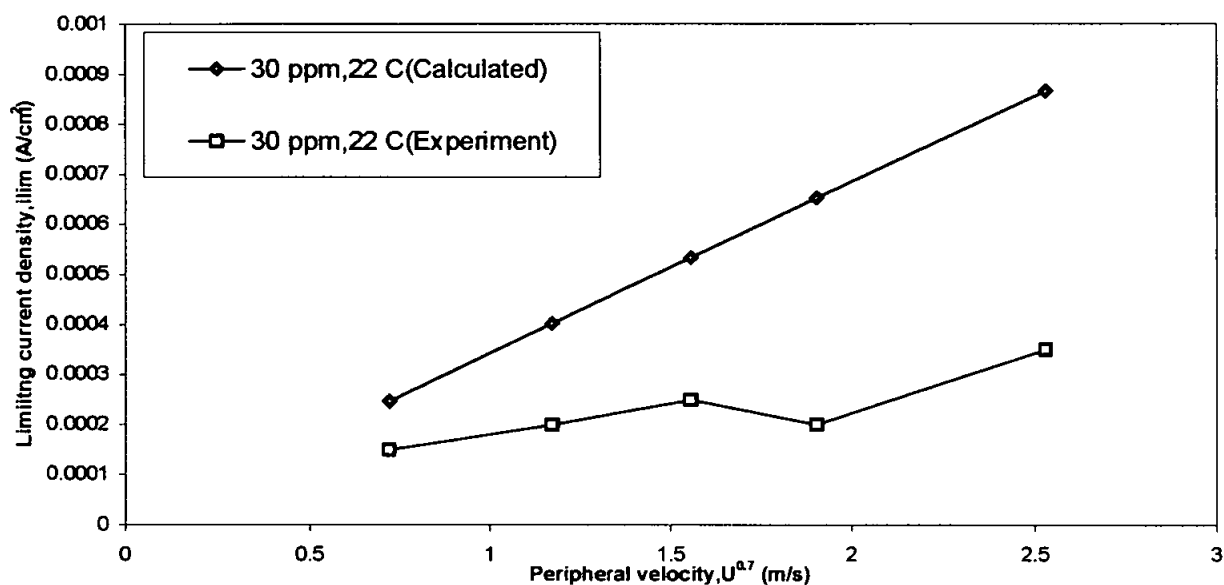
Figure 6.36: Calculated limiting current density due to HAc vs experimental ilim.
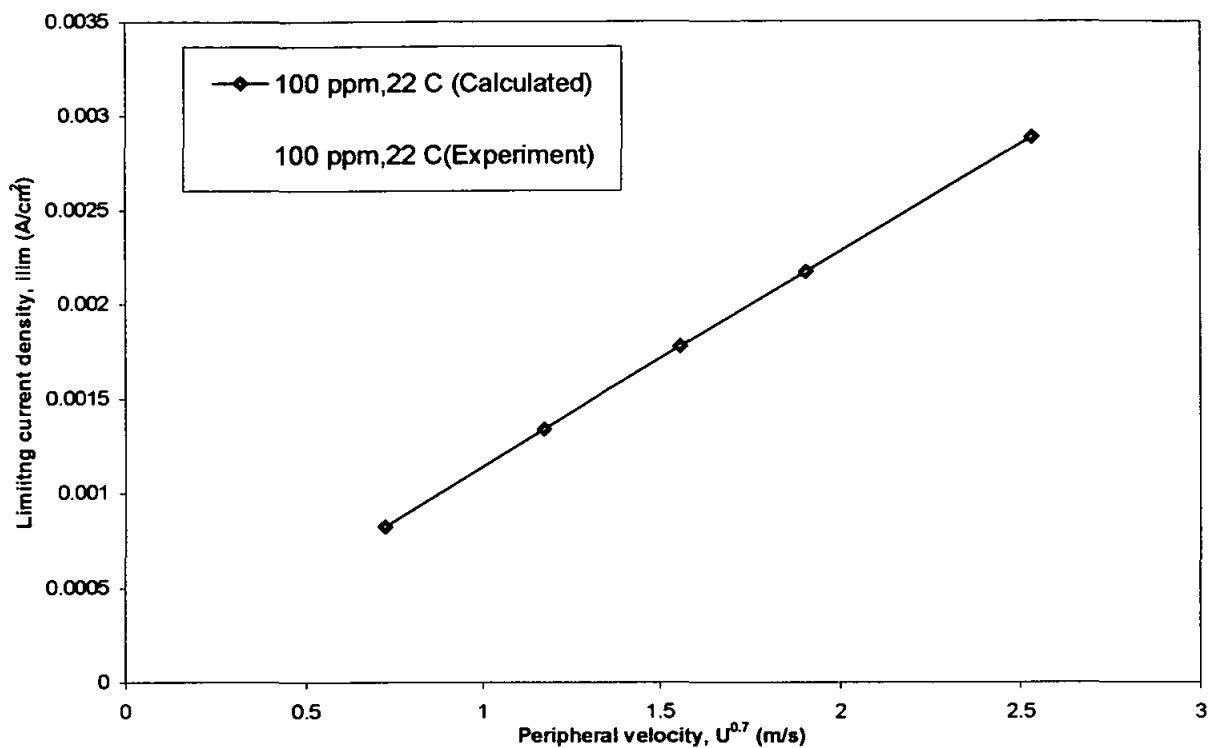
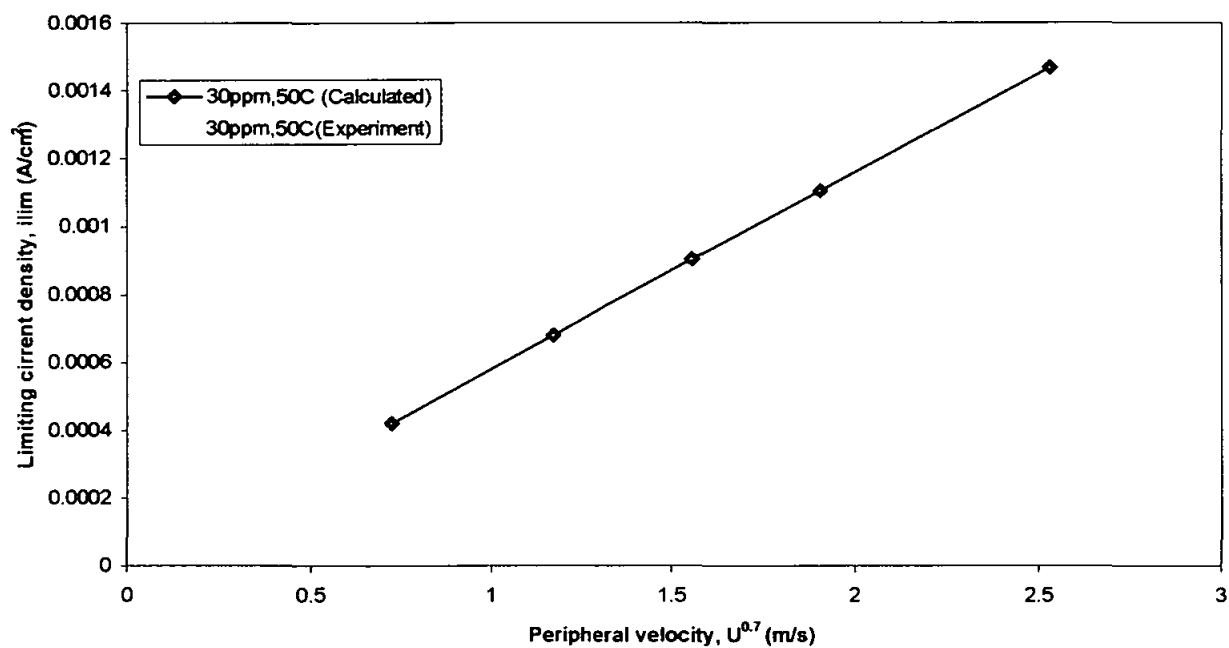Figure 6.37: Calculated limiting current density due to HAc vs experimental ilim.

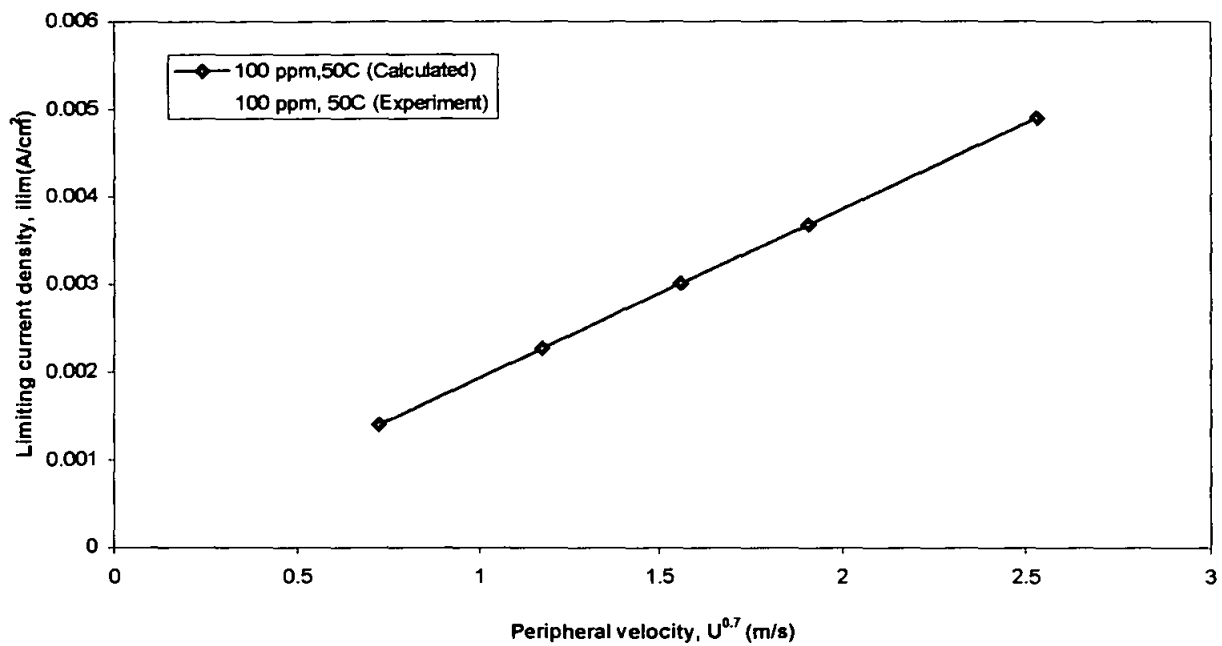Figure 6.38: Calculated limiting current density due to HAc vs experimental ilim.

Figure 6.39: Calculated limiting current density due to HAc vs experimental ilim.

The total ilim comes from the contribution of CO_2 corrosion and due to the presence of HAc species. However, we observe that the cathodic polarisation curve for the blank solution does not show a distinctive limiting current. Thus, it is envisaged that the reduction process consists of a mixed cathodic process. Hence, the ilim calculated is not representative and gives higher values of limiting current densities than the experimental results. This is evident from the comparison between the calculated total limiting current density and experimental values as presented in Figures 6.40-6.43 below.
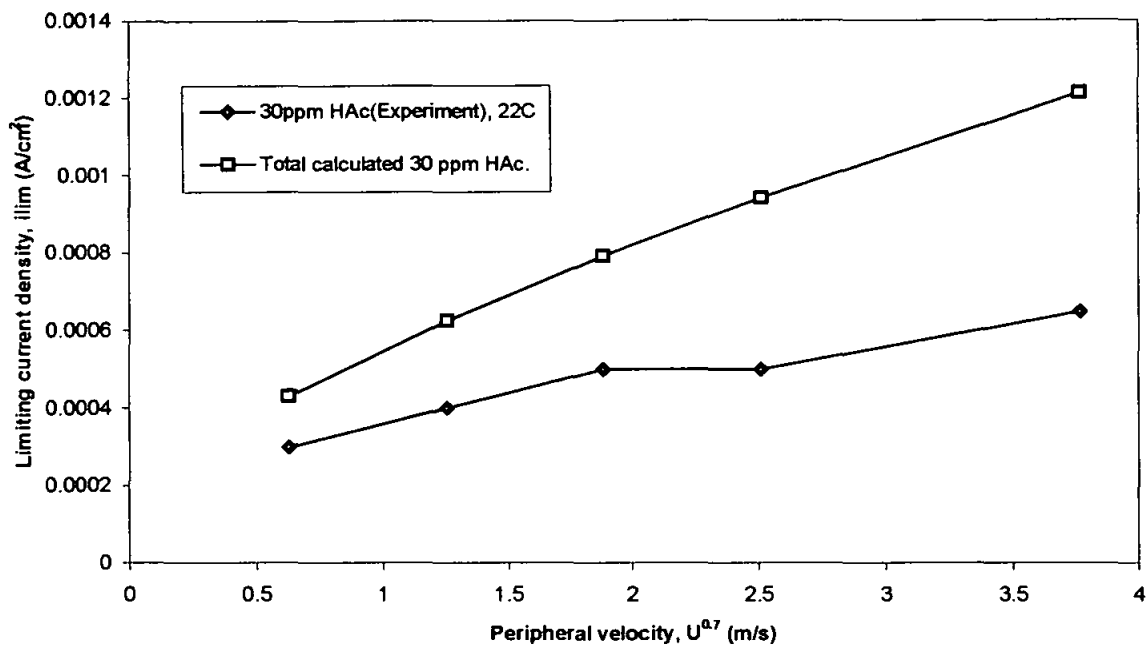
Figure 6.40: Comparing calculated total limiting current to experimental ilim.

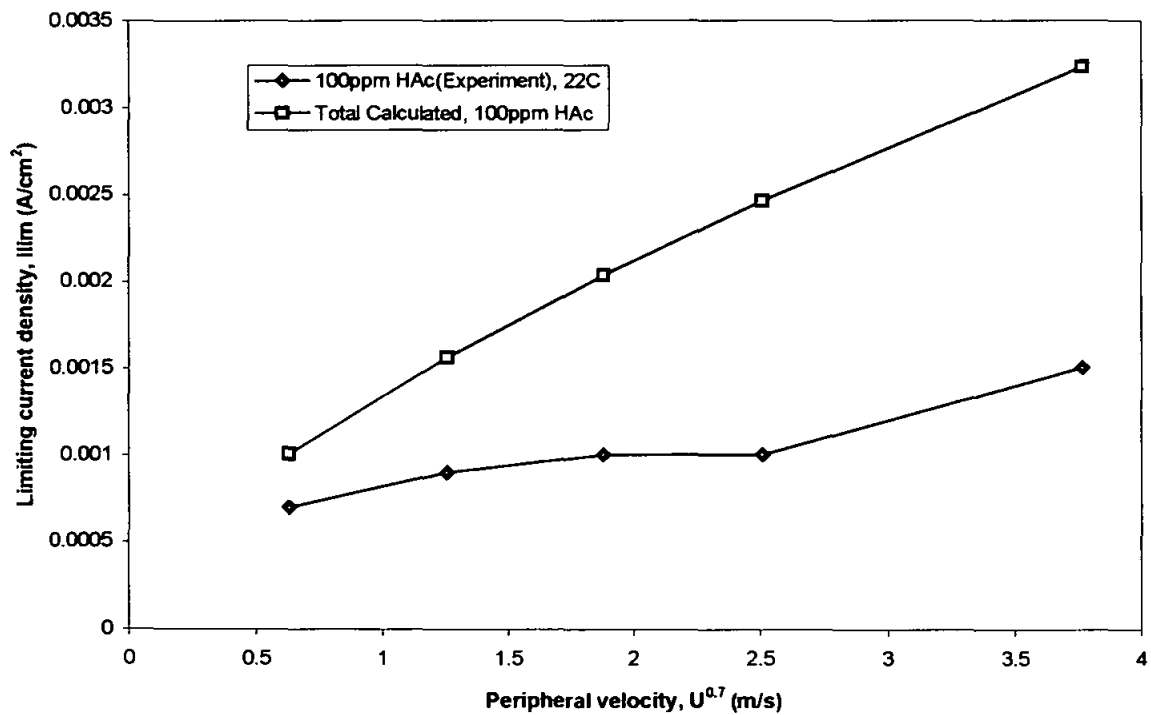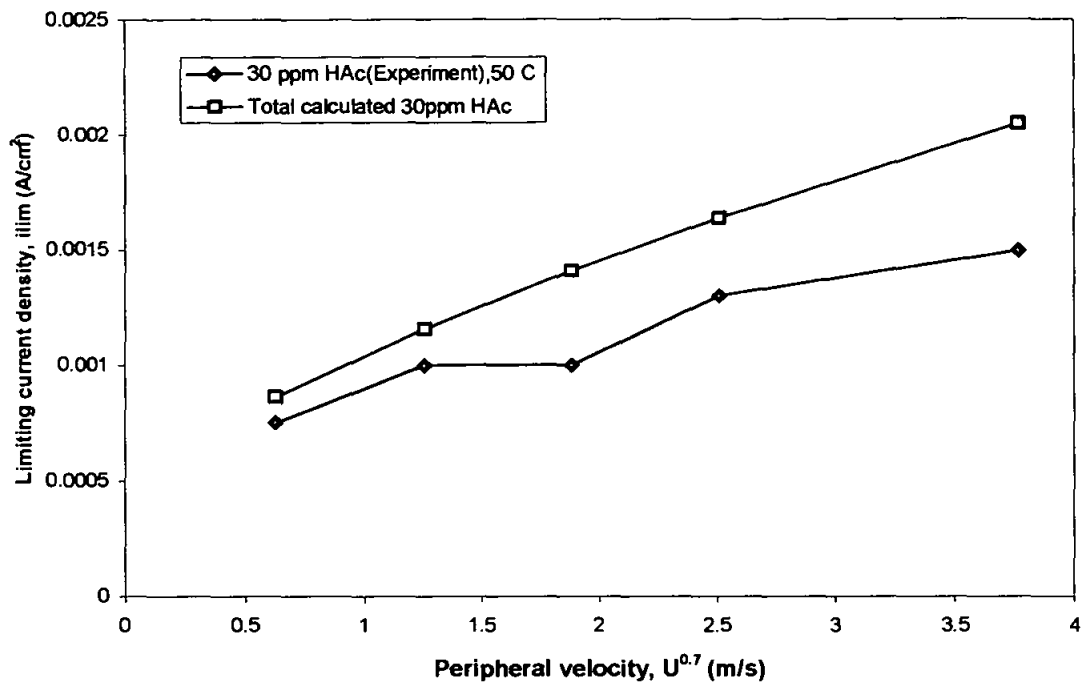Figure 6.41: Comparing calculated total limiting current to experimental ilim.

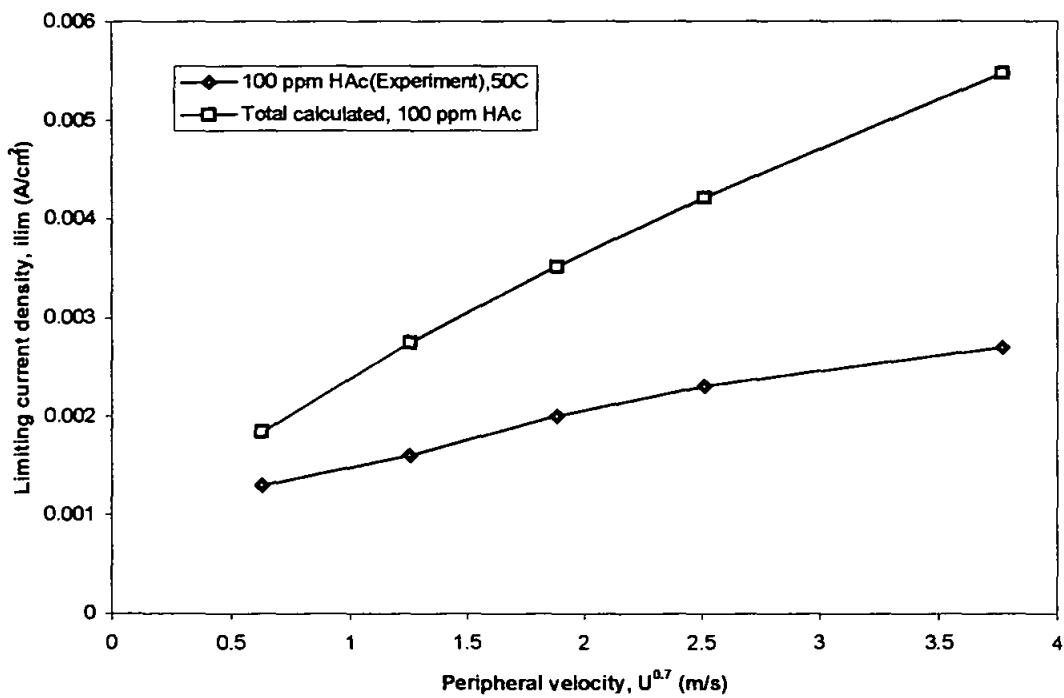Figure 6.42: Comparing calculated total limiting current to experimental ilim.

Figure 6.43: Comparing calculated total limiting current to experimental ilim.

6.1.4.2.3 The Effect of HAc Concentration on ilim

In both cases at 22°C and 50°C, the cathodic limiting current densities increase with the increase in HAc concentration. This increase can be attributed to the presence of more acetic acid species to be transported and reduced on the surface. The increase in ilim with concentration is shown in Table 6.2 below for both 22°C and 50°C.

Table 6.2: Experimental and calculated limiting current densities.

HAc Concentration	Limiting Current Density, ilim (A/cm^2)			
	22°C		50°C	
	Experimental	Calculation	Experimental	Calculation
30 ppm	0.0003	0.00025	0.0007	0.0008
100 ppm	0.00075	0.0004	0.0013	0.0014

6.4.2 Corrosion Rate

A substantial increase in corrosion rate is recorded with the presence of only minute concentrations of HAc. At 22°C, a significant increase of 100-180 % is registered with the presence of 30-100 ppm as compared to the system without HAc. The same phenomenon is observed at 50°C with the contribution of higher temperature. The increase in cathodic reaction in CO_2 corrosion is due to the acetic acid contribution to hydrogen ions through possibly dissociation and reduction. It is worth noting that the higher the concentration of acetic acid present, the higher is the concentration of hydrogen ions produced.

At higher temperature, the diffusion coefficient of acetic acid is higher which results in more species availability, approximately a twofold increase of corrosion rate with 30 ppm HAc at 50°C than at 22°C. At room temperature, the value of diffusion coefficient of HAc is 1.24×10^{-9} m^2/s whereas at 50°C the value is 2.45×10^{-9} m^2/s, which is 100% higher.

The threshold value acetic acid of approximately 400 ppm and 800 ppm is believed to be due to inhibitive effect of acetic acid at 22°C and 50°C respectively. The higher threshold at higher temperature relates to reducing efficiency of inhibition at higher temperature.

The comparison of the variation of the measured limiting current density (ilim) and corrosion current density(icorr) with the peripheral velocity is shown in Figures 6.44-6.49. As observed in previous data, ilim increases linearly with the velocity indicating the effect of diffusion in the reduction process. However, the corrosion current density (icorr) only varies a little with the velocity. In general we can conclude that the icorr values are practically lower than the ilim and independent of the peripheral velocity. Thus with the presence of the HAc species, the overall corrosion process taking place on the surface of the electrode is mainly controlled by a charge transfer process.
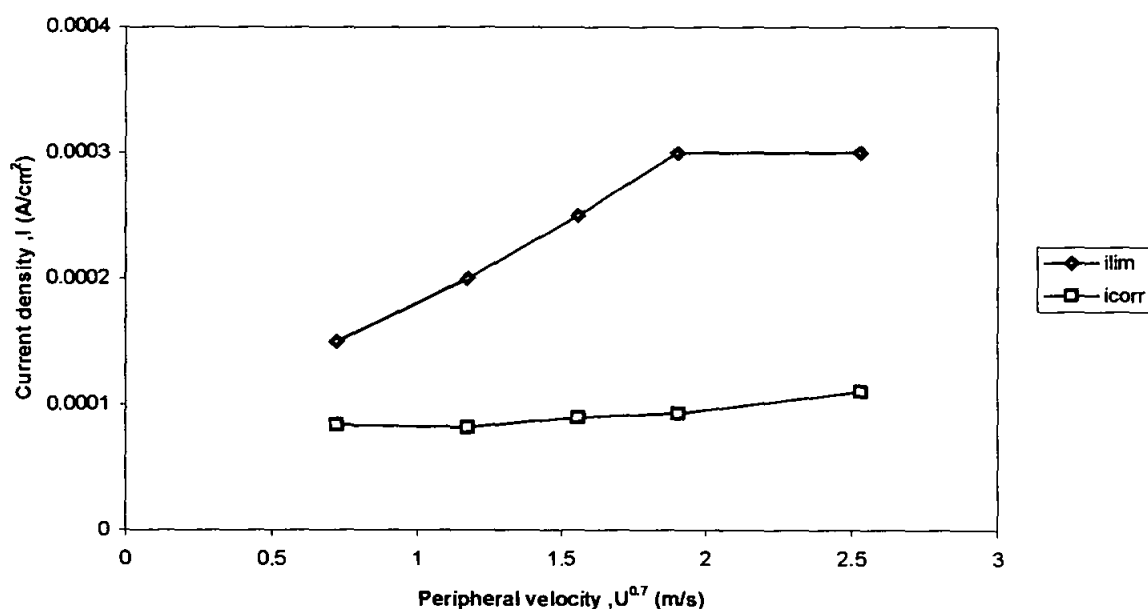
pH 5.5,Blank, 22 deg. C

Figure 6.44: Comparison of the measured limiting current density (ilim) with the corrosion current density (icorr) at different peripheral velocity.
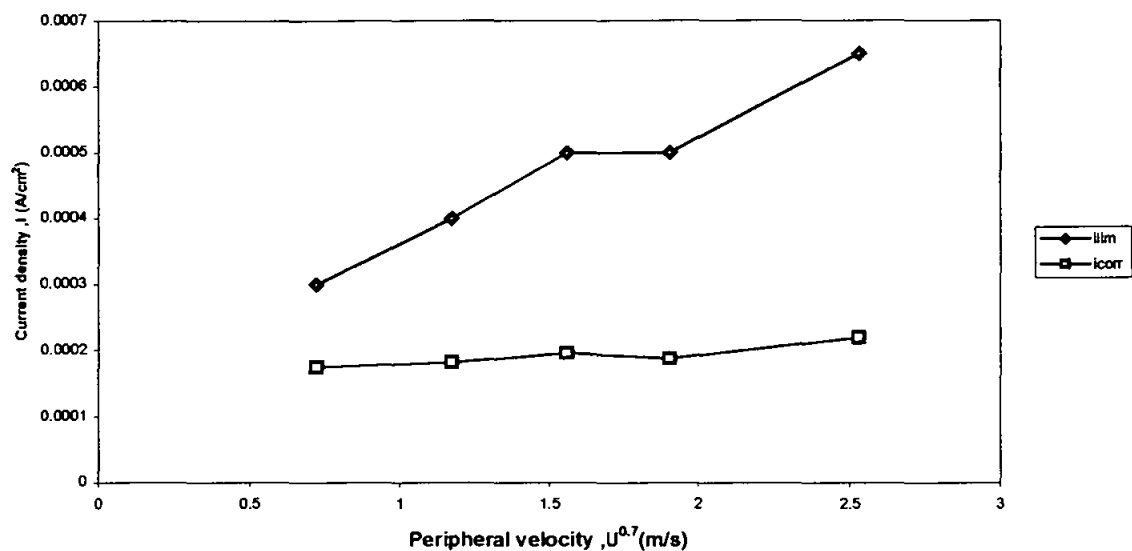
pH 5.5,Blank, 22 deg. C

Figure 6.45: Comparison of the measured limiting current density (ilim) with the corrosion current density (icorr) at different peripheral velocity.

pH 5.5,100 ppm,22 deg. C

Figure 6.46: Comparison of the measured limiting current density (ilim) with the corrosion current density (icorr) at different peripheral velocity.

pH5.5, Blank, 50 deg. C
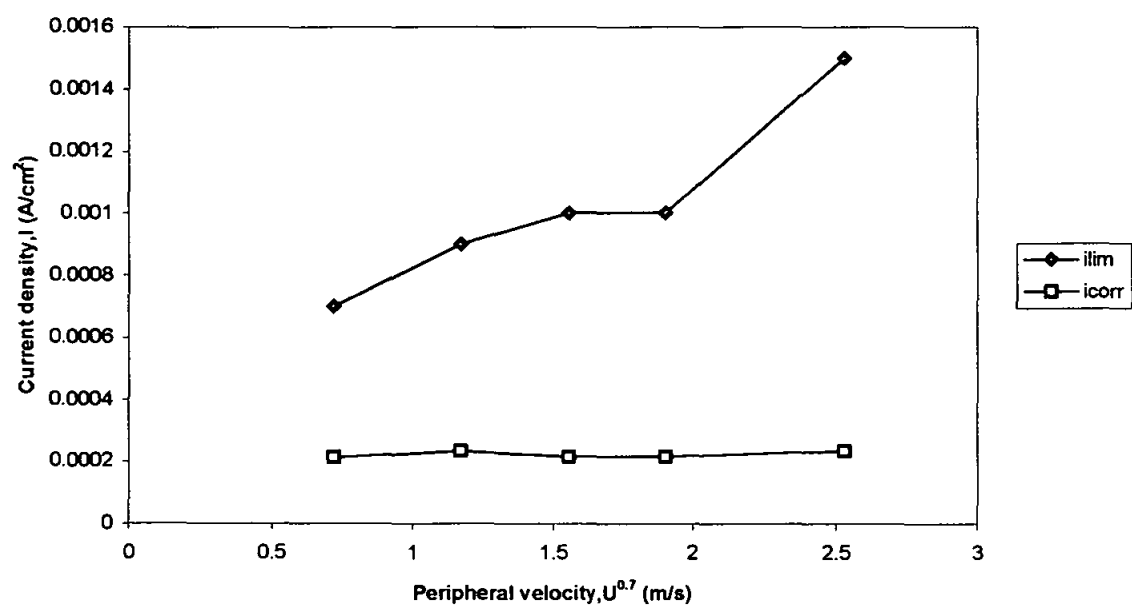

Figure 6.47: Comparison of the measured limiting current density (ilim) with the corrosion current density (icorr) at different peripheral velocity.

pH 5.5, 30 ppm, 50 deg. C
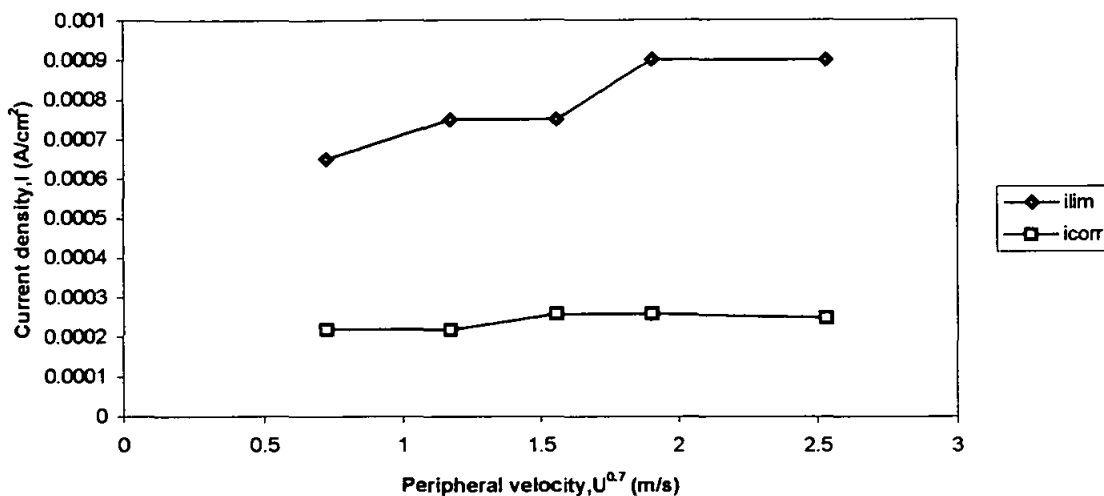

Figure 6.48: Comparison of the measured limiting current density (ilim) with the corrosion current density (icorr) at different peripheral velocity.

pH 5.5, 100 ppm, 50 deg. C
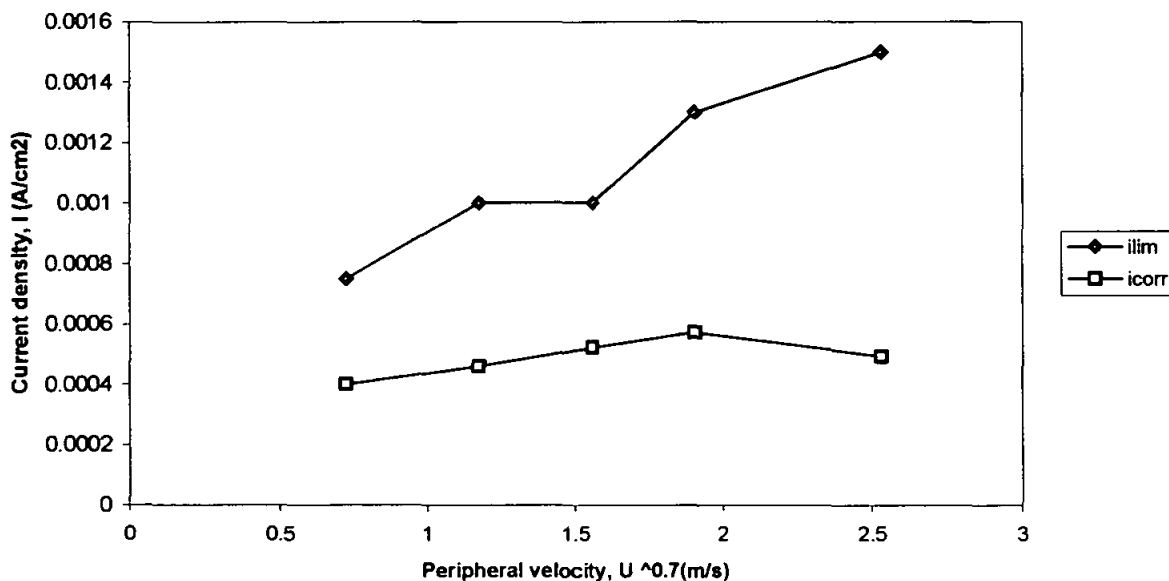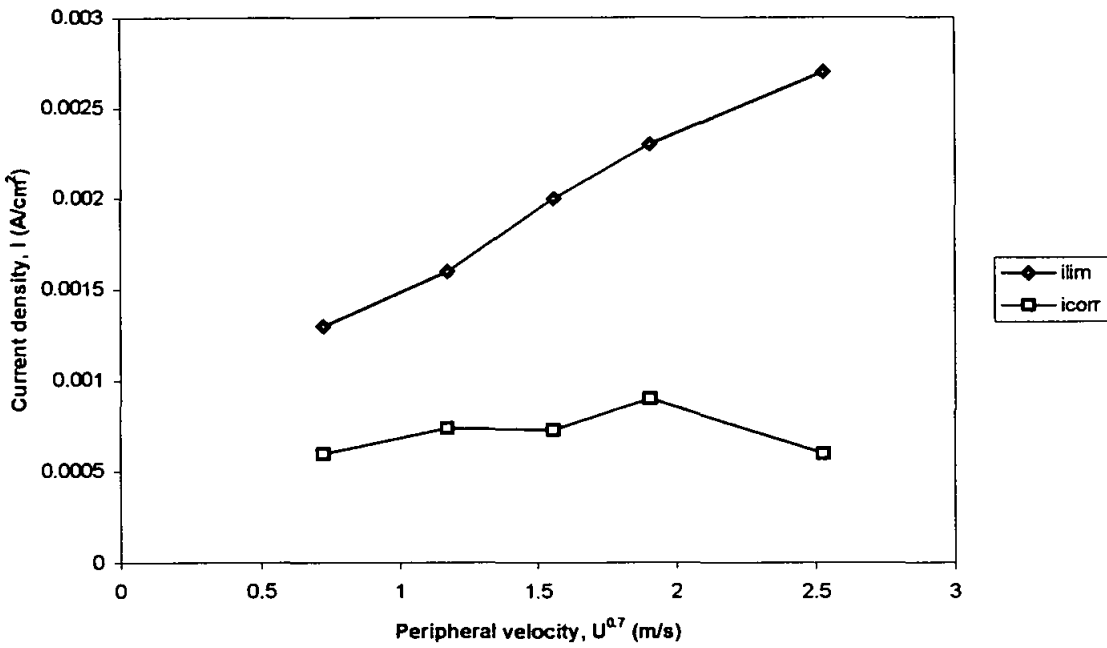

Figure 6.49: Comparison of the measured limiting current density (ilim) with the corrosion current density (icorr) at different peripheral velocity.

6.4.3 Comparison between Experimental Corrosion Rates and Predictive Models

The results from the RCE experiment are compared to the DWM 95, Cassandra 93/95 and NORSOK models. DWM 95 and Cassandra 93/95 take velocity as input whereas NORSOK takes wall shear stress as input. The comparisons are shown in Figure 6.50 and 6.51 below. At the test done at 22°C, the experimental results for blank solution register low corrosion rates. In general, Cassandra 93/95 correlates well with the experimental result.
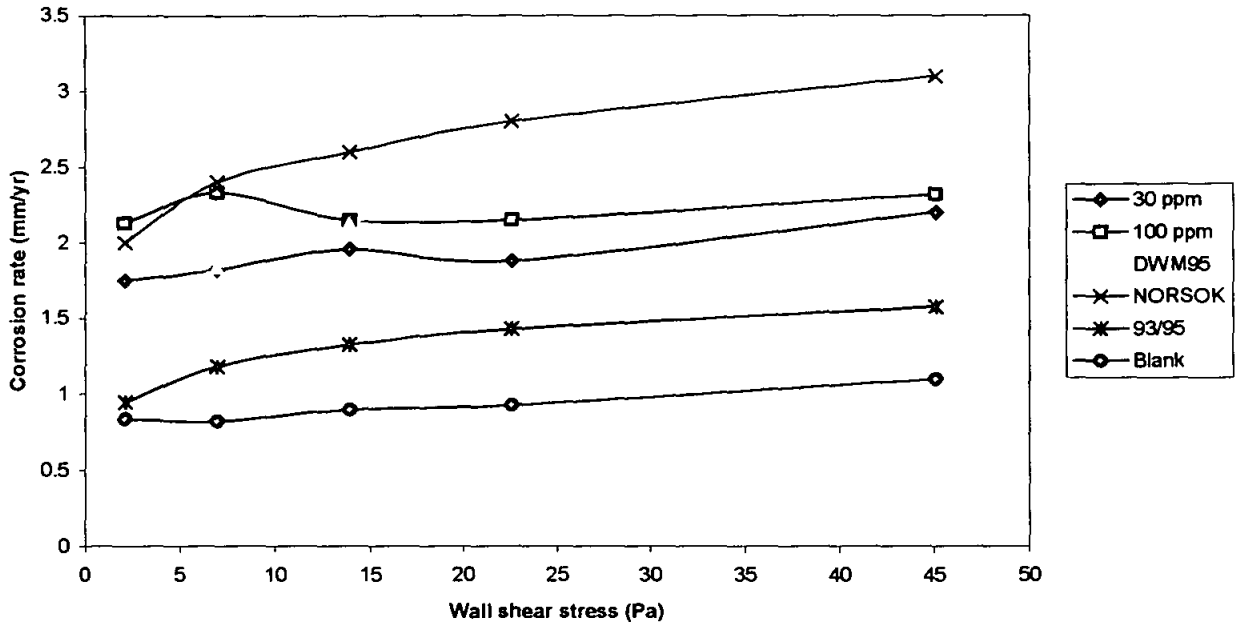
124

Figure 6.50: Comparison between experimental corrosion rates and predictive models at 22°C.
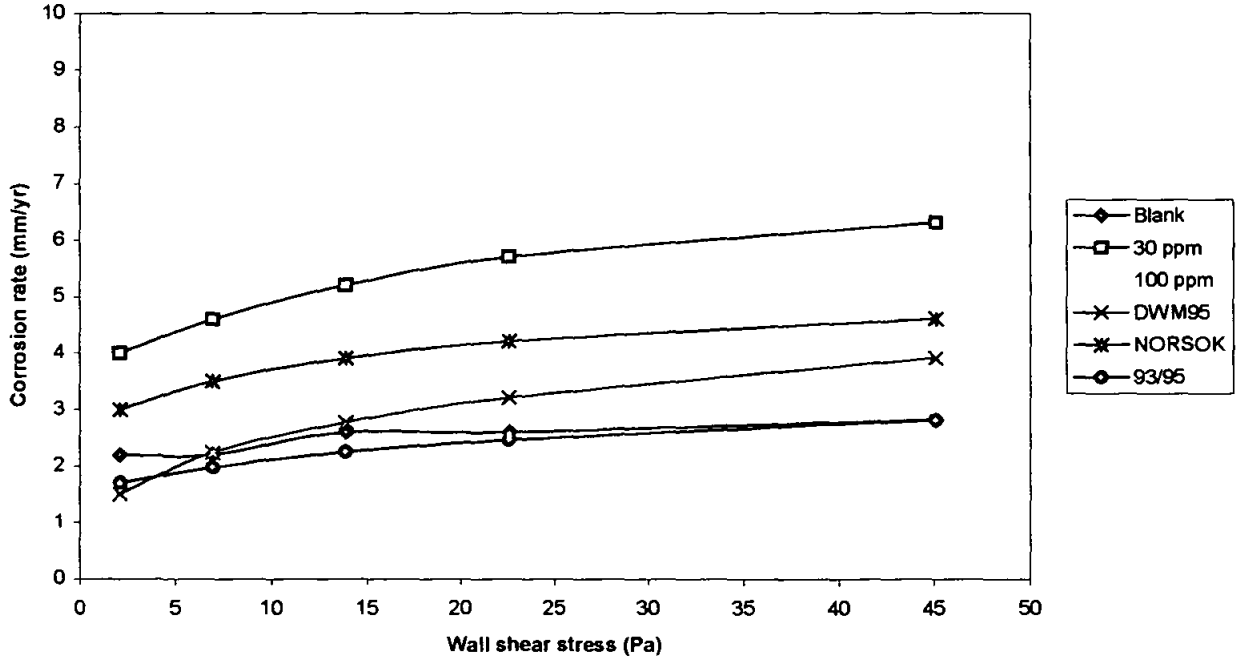

Figure 6.51: Comparison between experimental corrosion rates and predictive models at 50°C.

6.5 Conclusions: RCE

Acetic acid shows inhibitive property at higher concentration where the corrosion rate is reduced at 400 ppm and 800 ppm at 22°C and 50°C respectively.

Below the inhibitive level, the corrosion rate increases drastically with the presence of acetic acid. At 22°C, we see approximately 100-180% increase in corrosion rate with the increase in acetic acid concentration. At 50°C, 100-400% increase is registered.

The cathodic reaction is limiting current controlled with the presence of HAc but at high concentration it changes to mixed reaction of diffusion and charge –transfer control.

The flow independent contribution to the measured cathodic limiting current density is due to the slow hydration of carbonic acid and not due to the chemical reaction of HAc . The corrosion current density (icorr) is much lower than the mass limiting current transfer (ilim) which indicates the cathodic reduction is governed by activation control.

Cassandra 93/95 correlates well with the experimental results of the blank solution but does not accommodate the presence of acetic acid.

7.0 CO₂ PREDICTION WITH THE PRESENCE OF ACETIC ACID

A corrosion prediction equation is developed based on the experimental results of the static and RCE flow-simulated tests conducted at pH 5.5. The static tests represent the stagnant and low-flow conditions where as the RCE tests simulate turbulent-flow conditions. The prediction equation is then validated against the experimental data from the tests conducted at other test conditions.

7.1 Prediction Equation Based on Static Tests

The relationship between corrosion rate and acetic acid concentration is plotted at different temperatures below the Ts and shown in Figure 7.1 below.
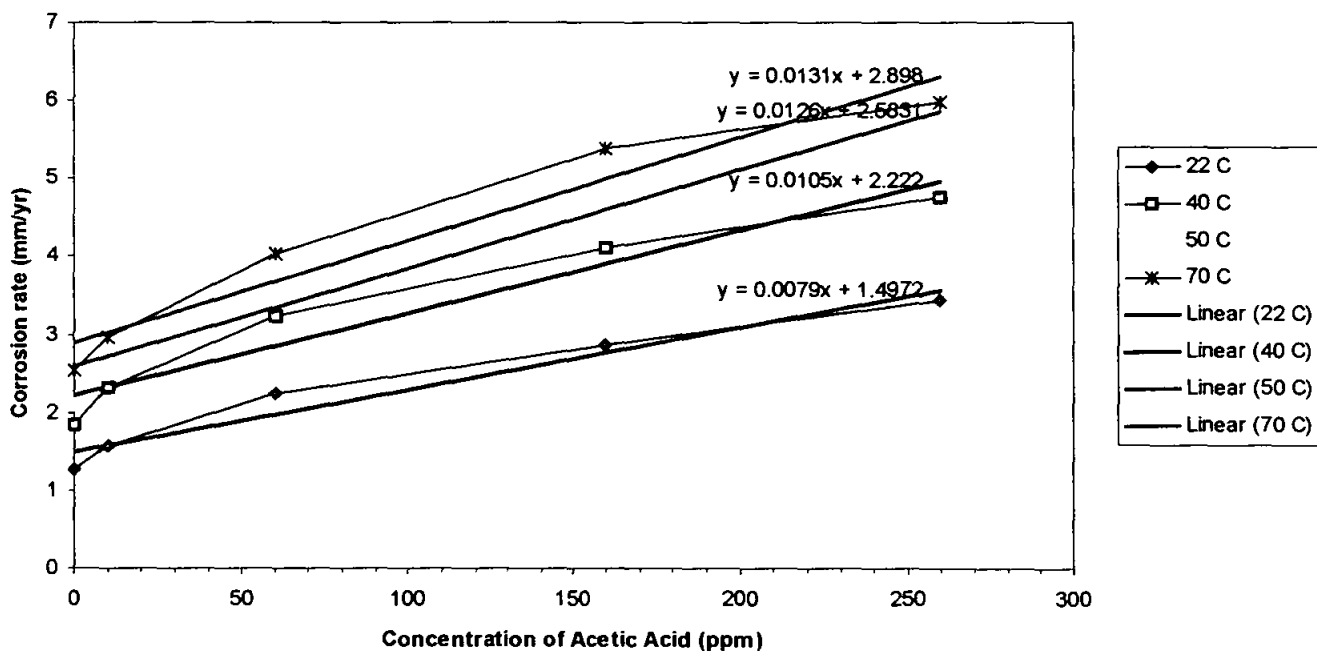

Figure 7.1: Prediction based on pH 5.5 static tests below Ts.

Corrosion rates vary almost linearly with the concentration of the added acetic acid. In general, this linear relationship can be represented by best-fit equations. The best-fit equations, as shown in the figure, reveal a good correlation and suggest a good linear

relationship between corrosion rate and the acetic acid concentration. This relationship can be expressed as:

Corrosion Rate (CR) = Corrosion rate of blank solution (CRb) + Constant x [HAc]

where, [HAc] = Concentration of acetic acid (ppm).

Thus, the corrosion rate of mild steel in CO_2-containing solution with the presence of acetic acid can be predicted by adding the contribution of the acetic acid to the blank corrosion rate.

The constant in the equation, which is the slope of curve, varies with temperature and could be approximated by plotting the slopes against temperatures as shown in Figure 7.2.

HAc Prediction
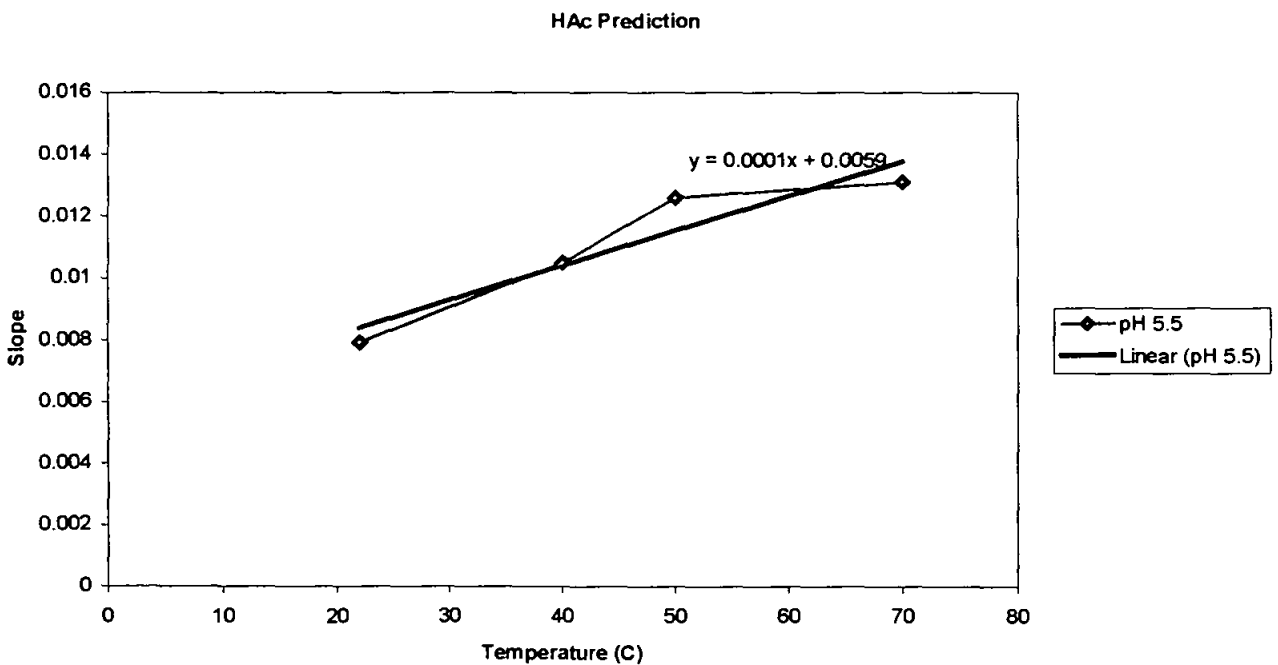
Figure 7.2: The variation of slopes with the temperatures.

Thus, by incorporating the temperature-dependent constant, the corrosion of mild steel in CO_2-containing solution with the presence of acetic acid can be predicted by the following expression

CR = CRb + (0.0001(T) + 0.006) x [HAc]

where, T = Temperature in $^{\circ}C$, [HAc] = Concentration of acetic acid (ppm).

The comparison of the predicted corrosion rates based on the above prediction equation and experimental results are shown in Figures 7.3 –7.6.
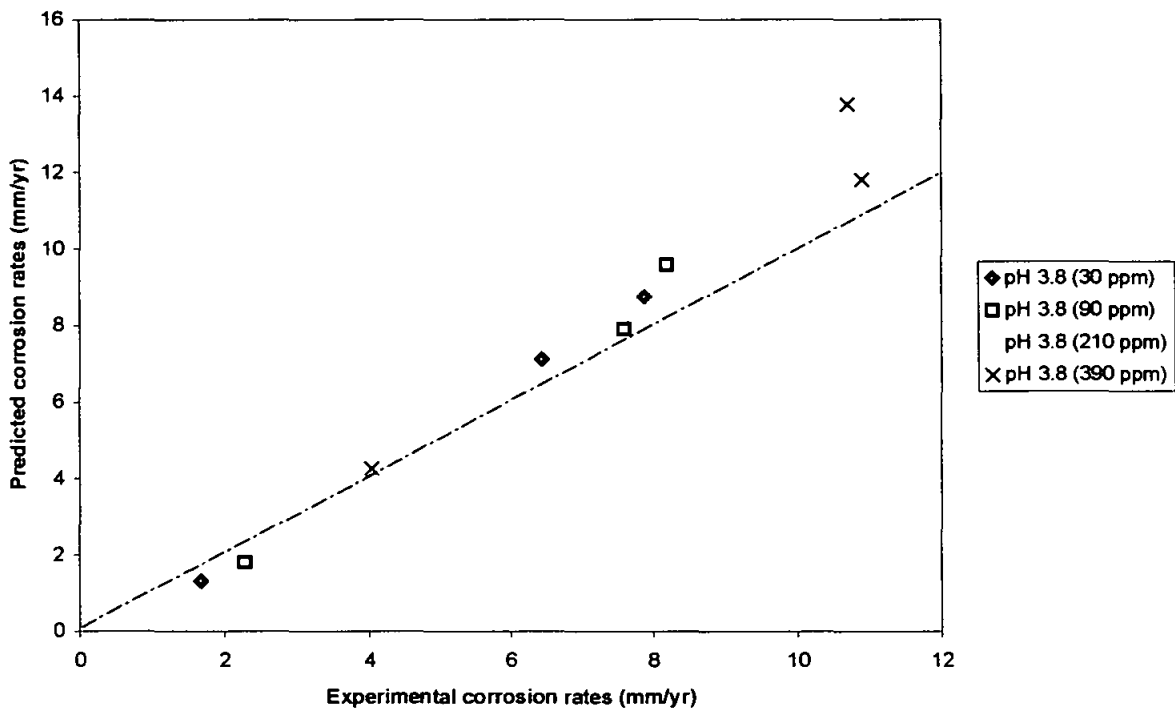
Figure 7.3: Comparison between experimental data and predicted corrosion rates at pH 3.8.

The predicted corrosion rates agree well with the experimental results at pH 3.8. At 22°C, the equation under-predicts the corrosion by 12 – 21 %. However, at higher HAc concentration than 210 ppm, the equation over predicts the corrosion rate by 5%. At other conditions, the equation predicts conservatively by 3-30%.
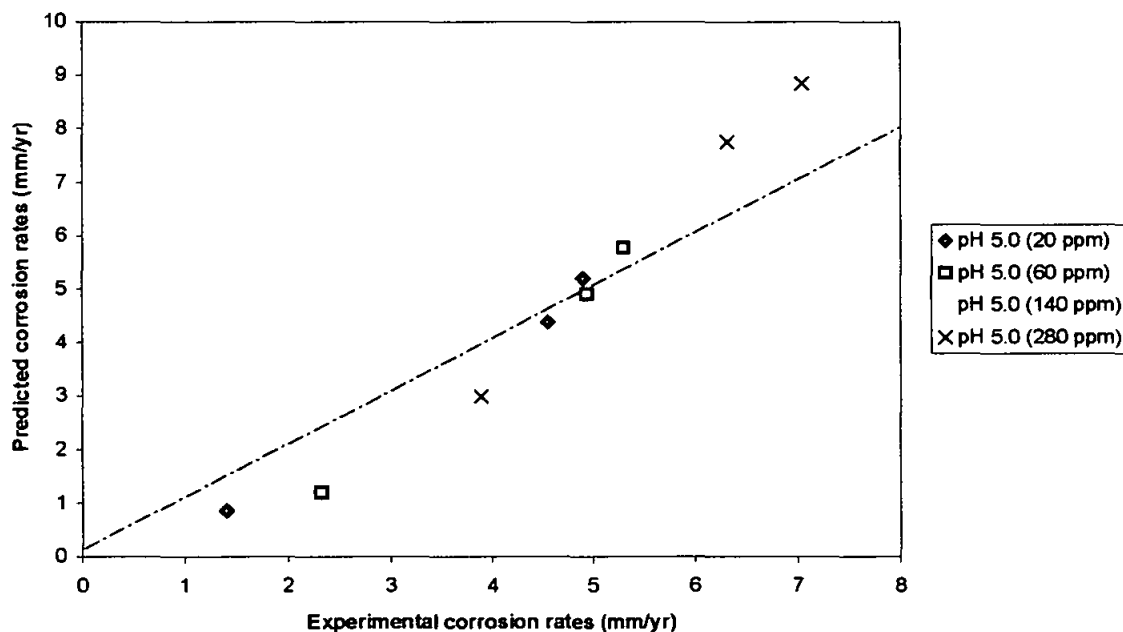
Figure 7.4: Comparison between experimental data and predicted corrosion rates at pH 5.0.

The validation at pH 5.0 shows that at 22°C, the equation under-predicts the corrosion by 23 – 48 %. However, at higher temperatures, the equation over predicts the corrosion rate by up to 25 %.

130
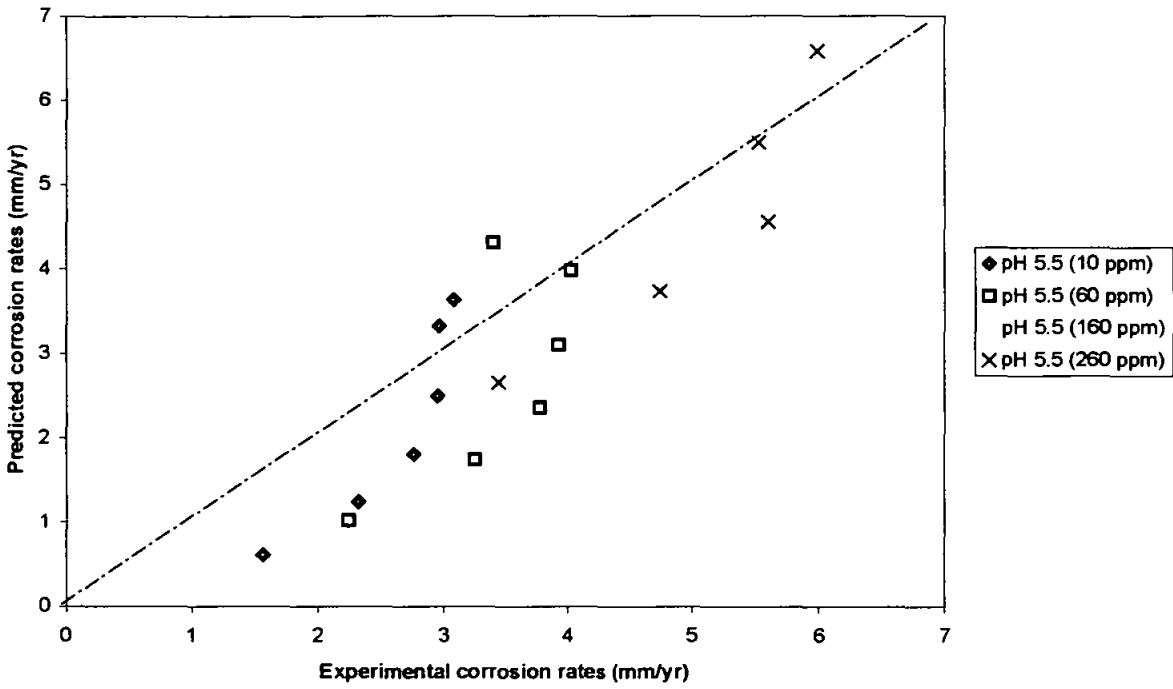
Figure 7.5: Comparison between experimental data and predicted corrosion rates at pH 5.5.

The validation at pH 5.5 shows that the equation under predicts between 15% and 60 % for the temperature range of 22°C to 60°C. However, at higher temperatures of 70°C to 75°C, the equation over predicts the corrosion rate by up to 30 %.
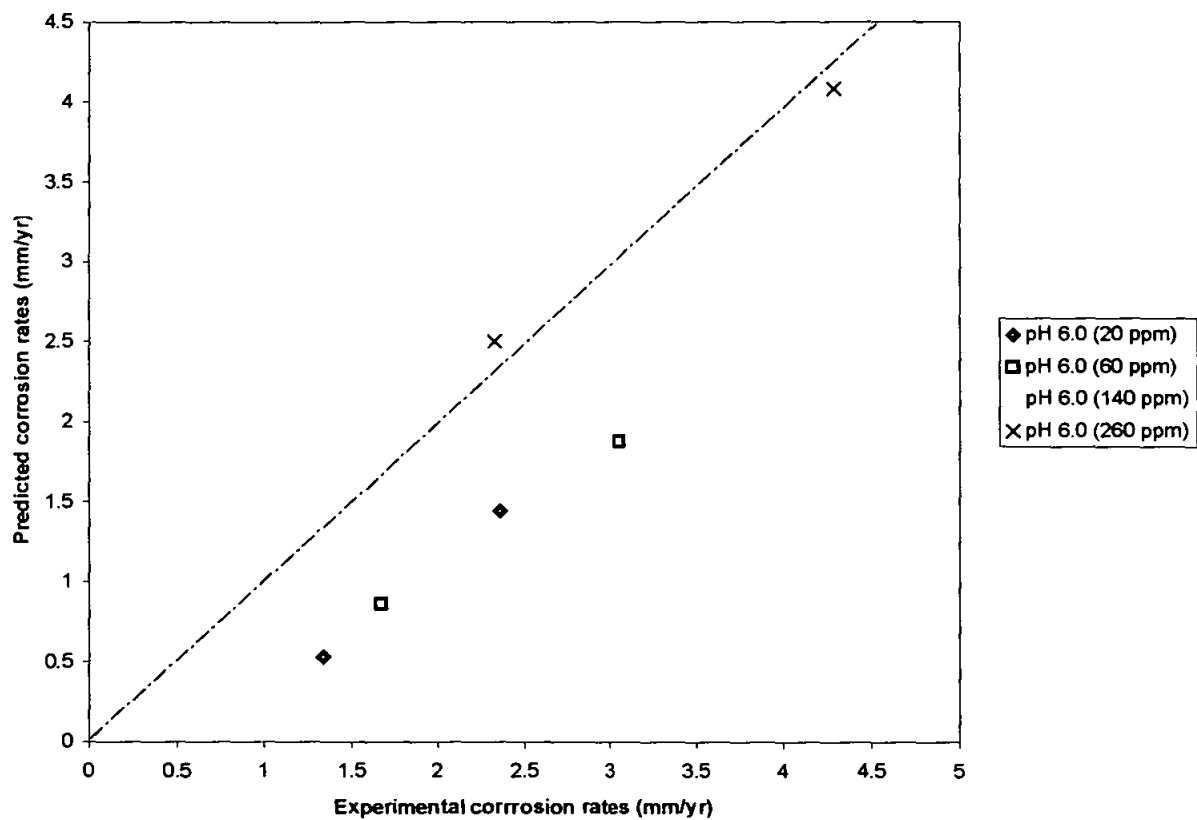
Figure 7.6: Comparison between experimental data and predicted corrosion rates at pH 6.0.

The equation under predicts between 7 and 55% of most condition at pH 6.0.

7.2 Prediction Based on RCE Tests

7.2.1 RCE Tests at 22°C.

The relationship between corrosion rate and acetic acid concentration is plotted at different rotation rates as shown in Figure 7.7 below. The linear relationship is only observed below the inhibitive threshold of HAc concentration and this is plotted as shown in Figure 7.8.
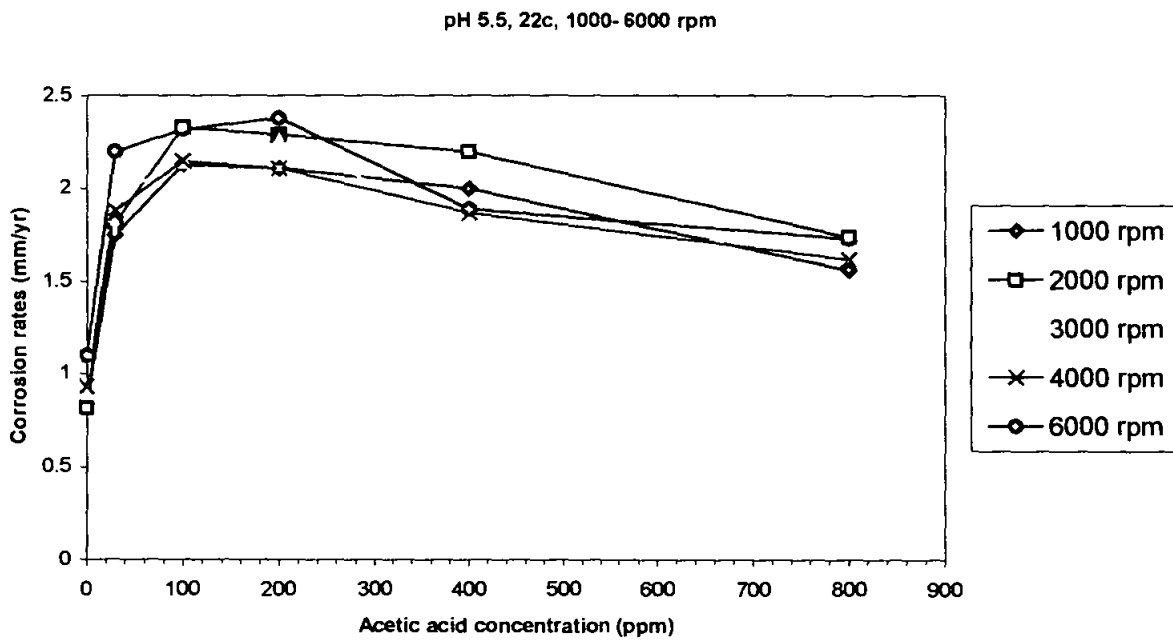
Figure 7.7: RCE tests at 22°C.
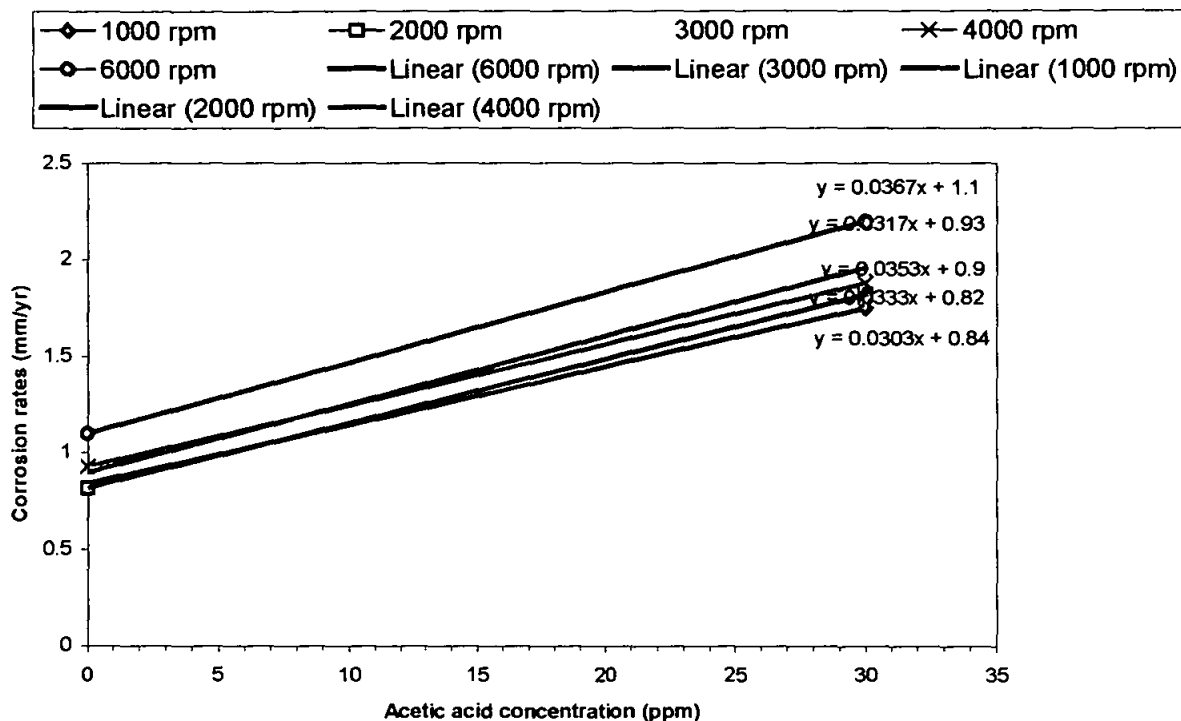
Figure 7.8: Prediction based on RCE at 22°C.

Similar to the prediction based on static tests, the RCE prediction relationship can be expressed as:

Corrosion Rate (CR) = Corrosion rate of blank solution (CRb) + Constant x [HAc]

where, [HAc] = Concentration of acetic acid (ppm).

The variation of the constant in the corrosion prediction equation at 22°C with rotation rates is plotted in Figure 7.9.
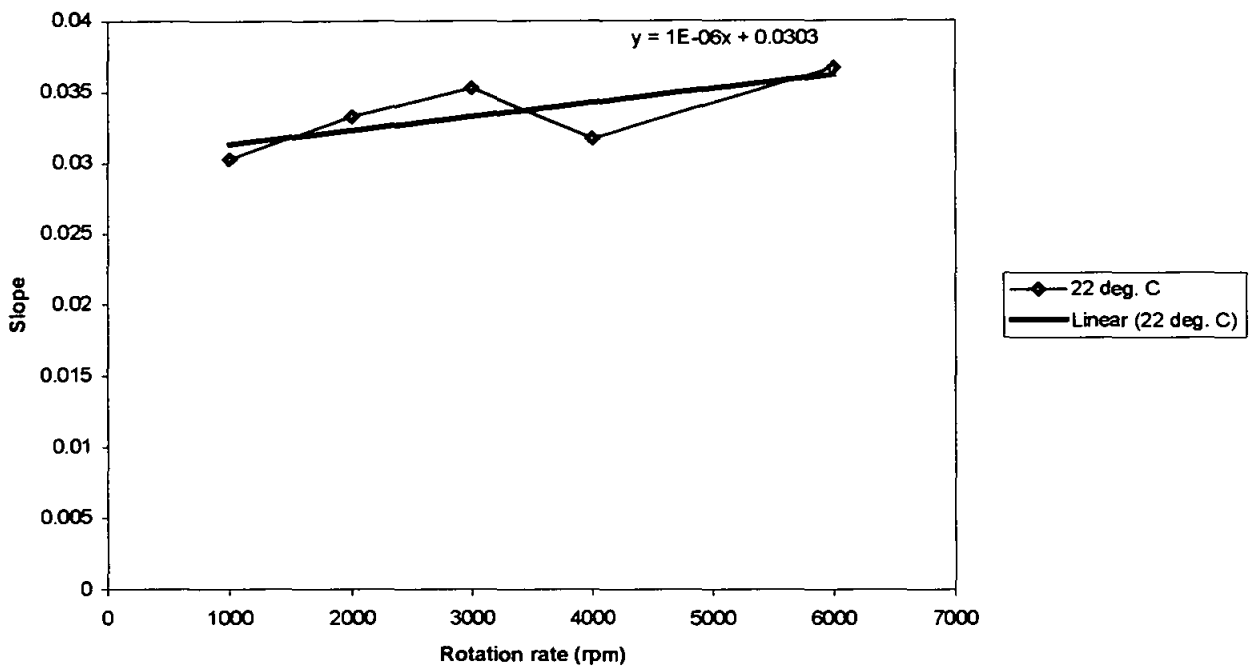
Figure 7.9: The variation of slopes with the rotation rate.

Thus, the corrosion rate prediction at 22°C can be expressed as:

CR = CRb + (0.000001(R) + 0.0303) x [HAc] ;

where CRb = Corrosion rate of blank solution, R = Rotation rate in rpm , [HAc] = Concentration of acetic acid (ppm)

7.2.2: RCE Tests at 50 C.

Similarly at 50°C, the relationship between corrosion rate and acetic acid concentration is plotted at different rotation rates as shown in Figure 7.10 below. The linear relationship is observed below 100 ppm, which is the inhibitive threshold of HAc concentration. This relationship is plotted in Figure 7.11.
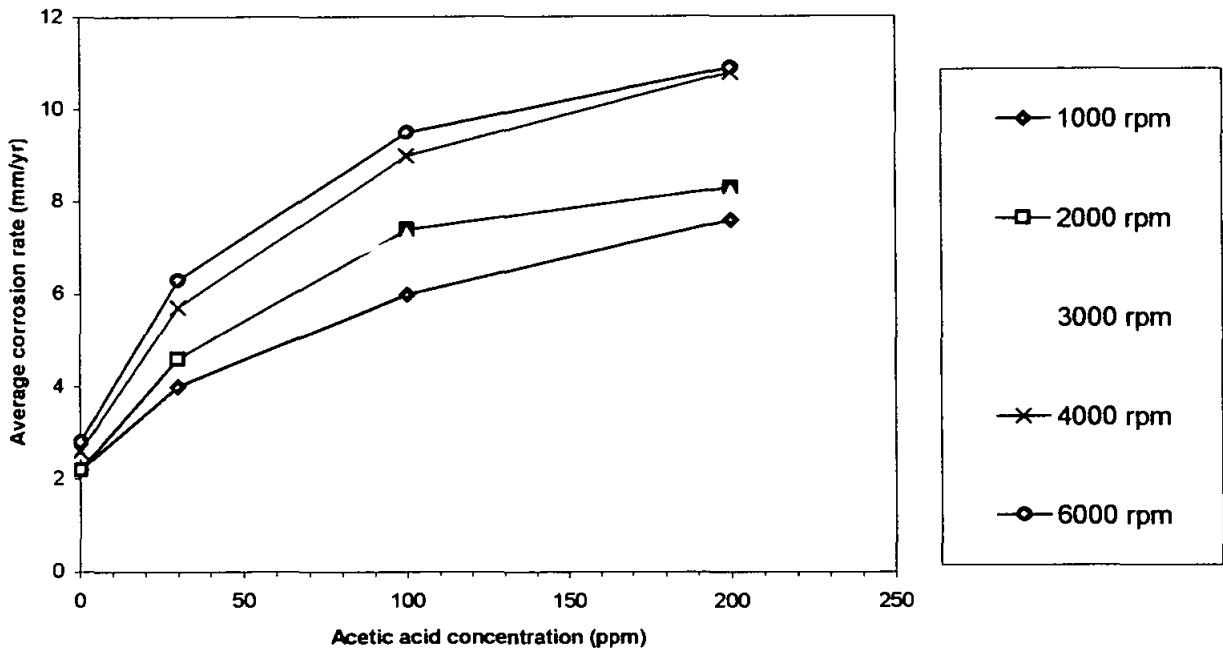
Figure 7.10: Relationship between corrosion rate and acetic acid concentration as plotted at different rotation rates at 50°C.
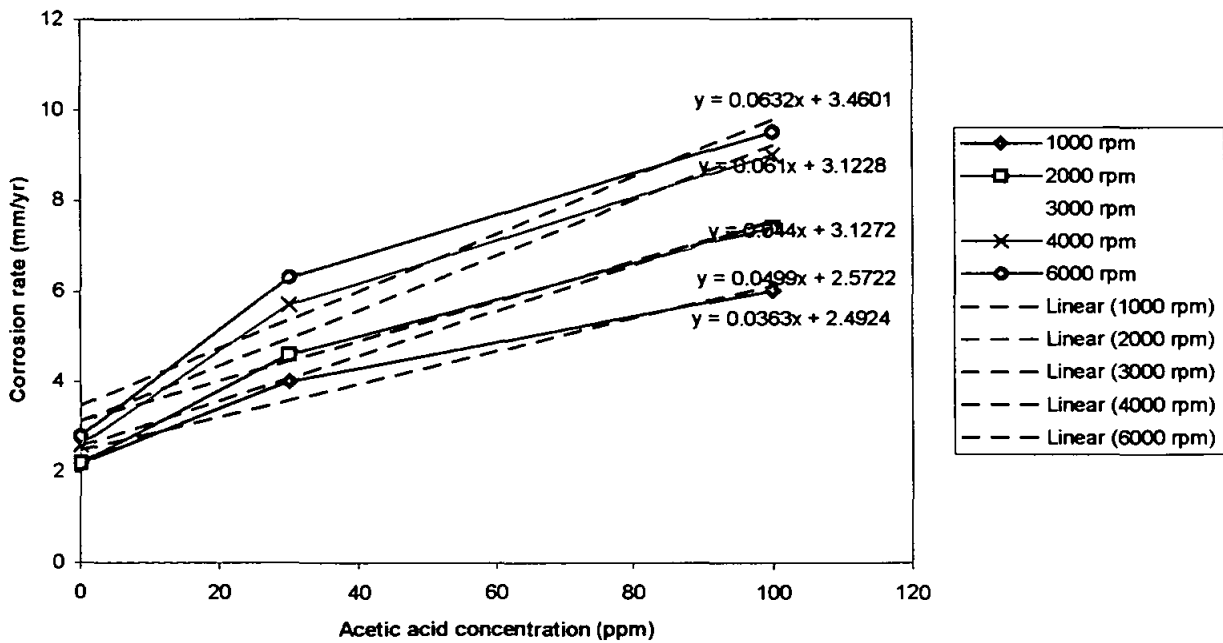
Figure 7.11: Best-fit equations for relationship between corrosion rate and acetic acid concentration at 50°C.

136

The change of the slope with the rotation rate is plotted below.
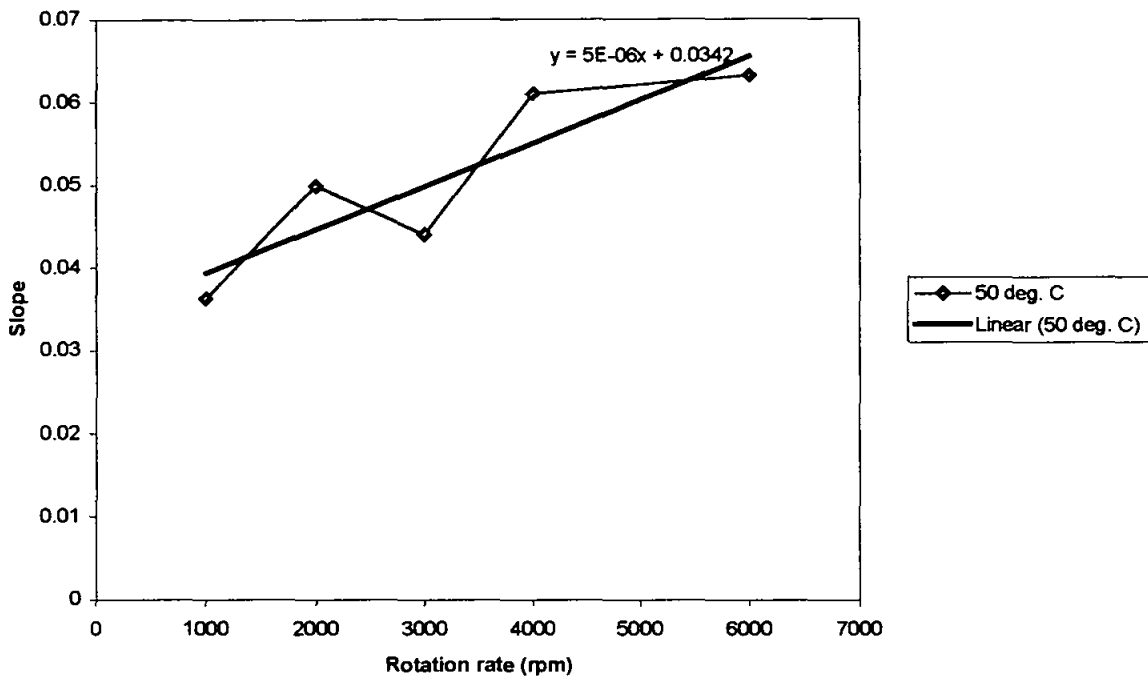
Figure 7.12: The variation of slopes with the rotation rate.

Thus, the corrosion rate prediction at 50°C can be expressed as:

CR = CRb + (0.000005(R) + 0.0342) x [Hac]

where R = Rotation rate in rpm , [HAc] = Concentration of acetic acid (ppm)

In order to include the effect of temperature in the prediction equation, the variation of the constants with the temperature of both expressions at 22°C and 50°C is plotted for each rotation rate and this is presented in Figure 7.13.
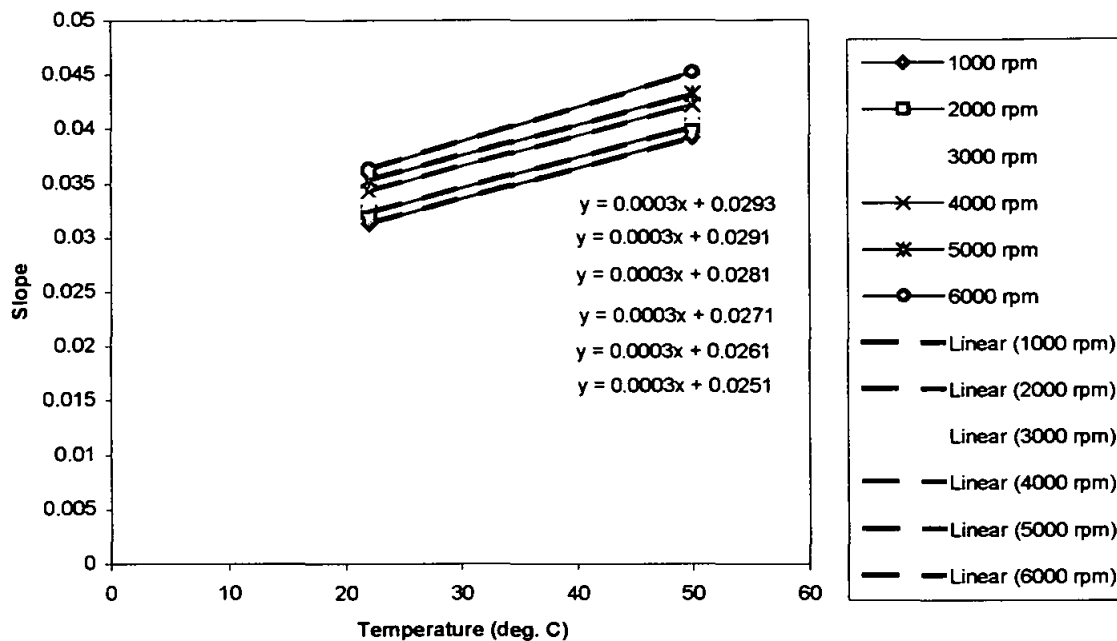
Figure 7.13: The variation of the constants with the temperature.

We observe that the corrosion rates are slightly affected by the increase in rotation rate at both temperatures. The prediction equation can be expressed as

CR = CRb + (0.0003(T) + 0.03) x [HAc] ;

where T = Temperature in °C, [HAc] = Concentration of acetic acid (ppm)

The comparison of the predicted corrosion rates based on the above prediction equation and experimental results are shown in Figures 7.14 –7.16.
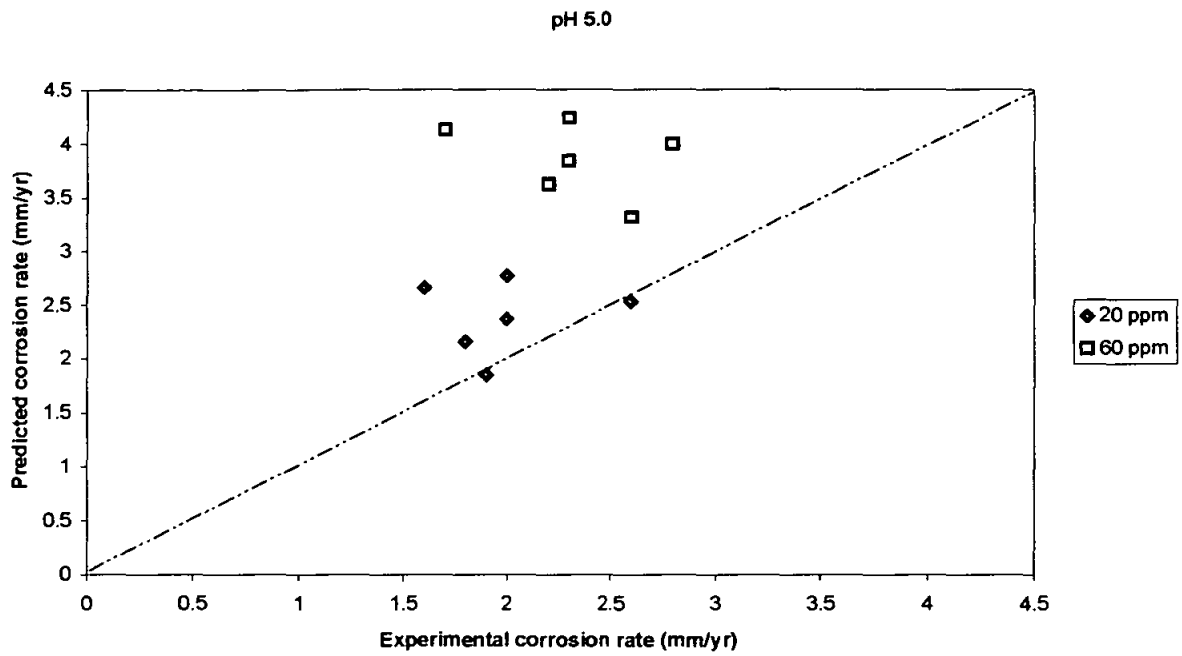
pH 5.0

Figure 7.14: Validation of the prediction equation at pH 5.0.

The prediction equation predicts conservatively for all cases at pH 5.0.
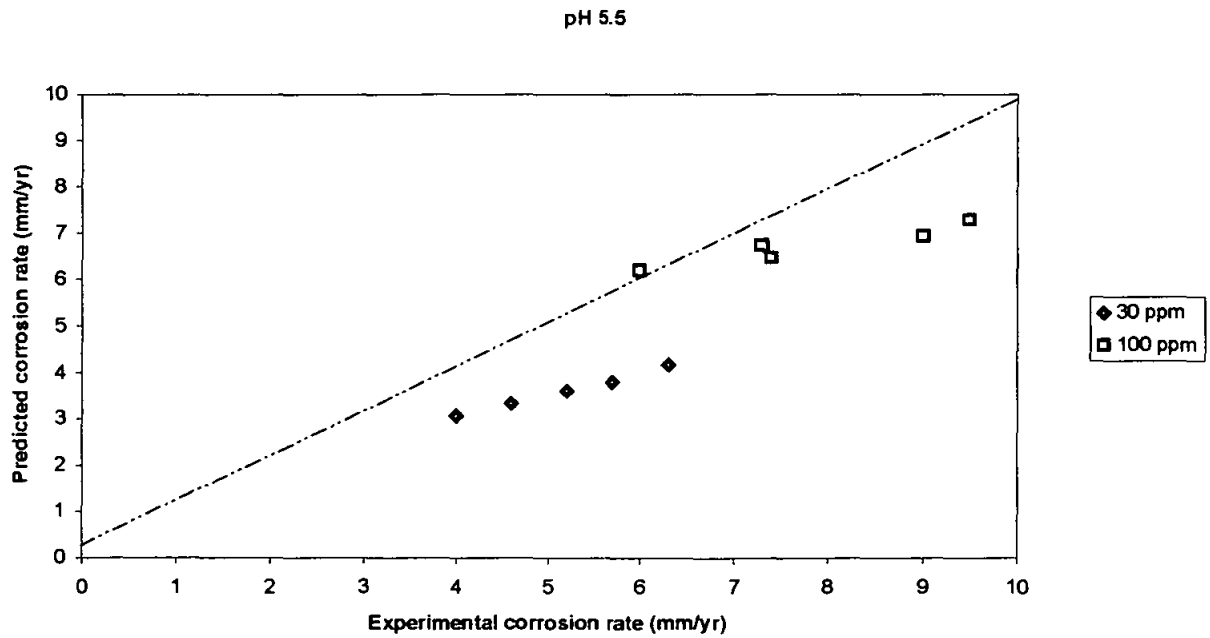
pH 5.5

Figure 7.15: Validation of the prediction equation at pH 5.5.

The prediction equation under predicts for most cases at pH 5.5.
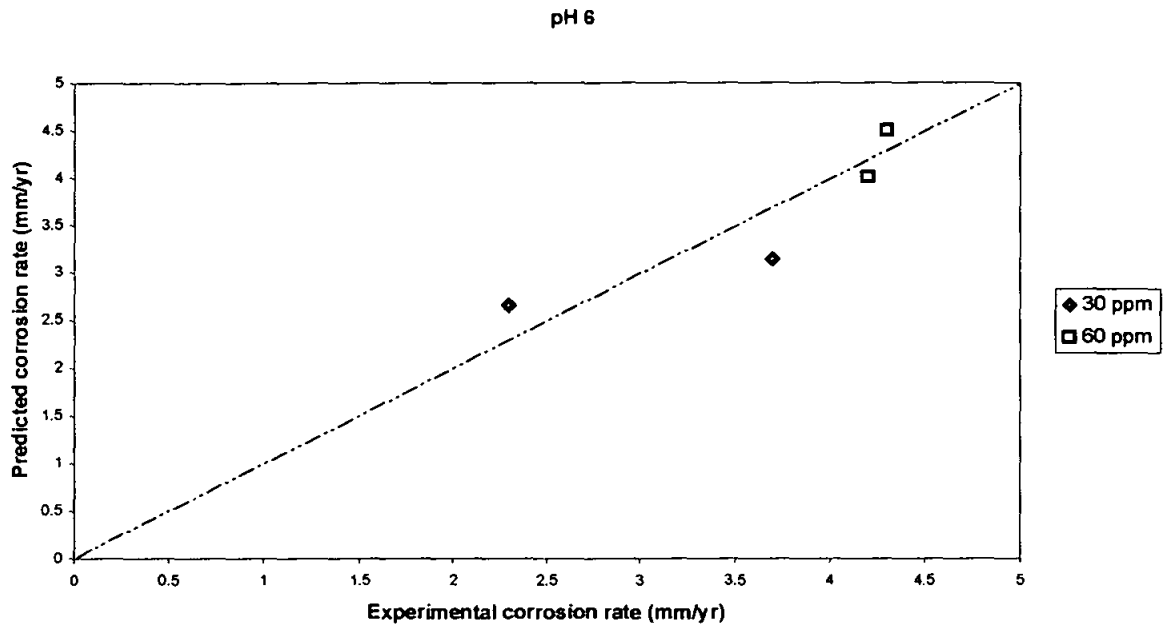
Figure 7.16: Validation of the prediction equation at pH 6.0.

The prediction equation predicts well for all cases at pH 6.0.

7.3: Conclusion

The corrosion rate of carbon steel in CO_2 corrosion with the presence of acetic acid can be predicted based on the static tests and RCE tests.

For static and low flow condition, the corrosion of mild steel in CO_2-containing solution with the presence of acetic acid can be predicted by the following expression

CR (mm/yr) = CRb + (0.0001(T) + 0.006) x [Hac]

where, CRb = Blank corrosion rate (mm/yr), T = Temperature in $^{\circ}C$, [HAc] = Concentration of acetic acid (ppm).

For turbulent condition, the prediction equation can be expressed as

CR (mm/yr) = CRb + (0.0003(T) + 0.03) x [HAc] ;

where, CRb = Blank corrosion rate (mm/yr), T = Temperature in $^\circ$C , [HAc] = Concentration of acetic acid (ppm).

8.0 CONCLUSIONS

Based on the static and RCE studies on the effect of acetic acid species on the corrosion of mild steel in the CO_2-saturated brine condition, the following conclusions are established.

8.1 Roles of Acetic Acid in CO_2 corrosion

The presence of acetic acid drastically increases the corrosion rate of mild steel in CO_2 corrosion below the scaling temperature and below the inhibitive threshold of acetic acid concentration. The increase in the corrosion rates are attributed to the following reasons:

1) Extra cathodic reaction.

This can be envisaged to be similar to that of the dissociation and reduction of carbonic acid in the CO_2 corrosion. The extra cathodic reactions with the presence of acetic acid are from extra source of hydrogen ions (H^+) from dissociation and direct reduction of acetic acid on the electrode surface. The sequence can be proposed as that of Crolet [18]:

a) Dissociation of acetic acid.

$$CH_3COOH \text{ (sol)} \rightarrow CH_3COOH \text{ (ads)} \rightarrow CH_3COO^- + H^+ \text{ (ads)}; \ H^+ \text{ (ads)} + e^- \rightarrow H$$
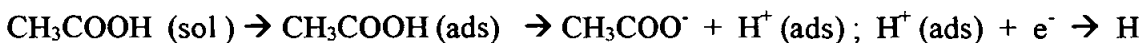
b) Direct reduction of undissociated acetic acid molecules.

$$CH_3COOH \text{ (sol)} \rightarrow CH_3COOH \text{ (ads)} + e^- \rightarrow CH_3COO^- + H$$
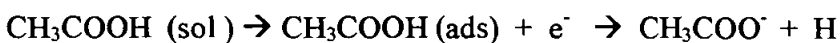
As highlighted by Garsany [37], the dissociation of acetic acid is fast, such that it is difficult to distinguish the above two reactions.

Thus, with the relatively large increase in the corrosion rate, we conclude that the cathodic reactions consist of both the dissociation and direct reduction of the acetic acid molecules.

2) Solubilising ferrous ion (Fe^{2+})

Below scaling temperature and without the presence of acetic acid, the film formed is not protective. The formation of iron carbonate ($FeCO_3$) can be represented by:

$$Fe^{2+} + HCO_3^- = FeCO_3 + H^+$$
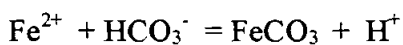
The formation of the protective $FeCO_3$ film depends on many factors, such as high temperature that accelerates the growth of the film, and high pH and Fe^{2+} concentration that reduce the solubility of iron carbonate.

Acetic acid solubilises the ferrous ion (Fe^{2+}) in the iron carbonate ($FeCO_3$) corrosion film promoting formation of iron acetate film, which is known to be soluble and hence not protective. We believe that below the scaling temperature, the thinning effect as proposed by Hedges [14] is not dominant as a film is not fully formed. This is evident in the invariant scaling temperature with or without acetic acid present in the system.

Beyond the scaling temperature, the thermodynamics and kinetics of protective film formation competes with the thinning effect from solubilising of ferrous iron by acetic acid and this results in delay in the formation of the protective film.

8.2 Prediction Equations

The corrosion rate of carbon steel in CO_2 corrosion with the presence of acetic acid can be predicted based on the static tests and RCE tests.

For static and low-flow condition, the corrosion rate (mm/yr) of mild steel in CO_2-containing solution with the presence of acetic acid can be predicted by the prediction equation,

CR (mm/yr) = CRb + (0.0001(T) + 0.006) x [HAc].

For turbulent-flow condition, the prediction equation is given by

CR (mm/yr) = CRb + (0.0003(T) + 0.03) x [HAc];

where, CRb = Corrosion rate of blank solution (mm/yr), T = Temperature ($^{\circ}$C) , [HAc] = Concentration of acetic acid (ppm).

9.0 FUTURE WORK

The formation of surface film is important in CO_2 corrosion of carbon steel and low alloy steels since this can influence the corrosion control methodology. The iron and carbonate ions concentrations and other environmental parameters such as pH, affect precipitation kinetics of $FeCO_3$ film. Once the film is nucleated, the subsequent formation and growth are dependent on temperature of the solution. Based on the open literature, the corrosion films formed in CO_2 –containing solution can be of different morphology and thickness consisting of iron carbide (Fe_3C) and iron carbonate ($FeCO_3$) films. The presence of acetic acid solubilises the ferrous ions that delays the formation of protective $FeCO_3$ films below the scaling temperature. Furthermore, the suggestion that acetic acid thins the $FeCO_3$ films above scaling temperature is also feasible. Thus, the interaction of iron acetate and iron carbonate films in the CO_2 corrosion requires further studies to explain the observations from the current study. The studies of the interaction of surface films can be conducted by the use of Scanning Electron Microscopy (SEM), AFS and other visual morphological methods. SEM and metallurgical microscopy can be used to examine surface morphology. X-ray Diffraction (XRD) and X-ray Photoelectron Spectroscopy (XPS) can be used to identify the structure and composition of the films.

Furthermore, as inhibition is commonly employed in corrosion control of CO_2 corrosion of carbon steel, further study is required to establish the effect of inhibitor on the CO_2 corrosion with the presence of acetic acid species. This is important in order to determine whether the inhibitor used for CO_2 corrosion is effective and quantify the dosage of inhibition with the presence of acetic acid.

10.0 REFERENCES

1. de Waard, C. and Milliams, D.E., Carbonic Acid Corrosion of Steel. Corrosion, 1975. 31(5): p. 131-135.

2. Wieckowski, A., Ghali, E., Szklarczyk, M. and Sobkowski, J., The Behaviour of Iron Electrode in CO_2-saturated Neutral Electrolyte -I. Electrochemical Study, J. Electrochimica Acta, Volume 28(11), p. 1619-1626, 1983.

3. Wieckowski, A., Ghali, E., Szklarczyk, M. and Sobkowski, J., The Behaviour of Iron Electrode in CO_2-saturated Neutral Electrolyte -II. Radiotracer Study and Corrosion Considerations, J. Electrochimica Acta, Volume 28(11), p. 1627-1633, 1983.

4. Eriksrud, E. and Sontvedt, T., Effect of Flow on CO_2 Corrosion Rates in Real and Synthetic Formation Waters, Advances in CO_2 Corrosion, Vol. 1, p.20,1984,NACE.

5. Ogundele, G.I., White W.E., Some Observations on Corrosion of Carbon Steel in Aqueous Environments Containing Carbon Dioxide, Corrosion, 42(2), p. 71-78, 1986.

6. Nesic, S and Postlethwaite, J., Modelling of CO_2 Corrosion Mechanisms, in K.R. Trethewey and P.R. Roberge(eds.), Modelling Aqueous Corrosion, p 317-335, 1994 Luwer Academics Publisher .

7. Videm, K. and Dugstad, A., Corrosion of Carbon Steel in an Aqueous CO_2 Environment. Part 1: Solution Effects, Material Performance, 1989. p.63-67.

8. Gray, L.G.S., Anderson, B.G., Danysh, M.J. and Tremaine,P.R., Mechanisms of Carbon Steel Corrosion in Brines Containing Dissolved CO_2 at pH 4, Corrosion/89, 1989: NACE International, Houston, Texas.

9. Gray, L.G.S., Anderson,B.G., Danysh, M.J. and Tremaine,P.R., Effect of pH and Temperature on the Mechanism of Carbon Steel Corrosion by Aqueous CO_2, Corrosion/90, 1990: NACE International, Houston, Texas.

10. de Waard, C., Lotz, U. and Milliams, D.E., Predictive Model for CO_2 Corrosion Engineering in Wet Natural Gas Pipelines, Corrosion, 1991. 47(12): p. 976-985.

11. de Waard, C. and Lotz, U., Prediction of CO_2 Corrosion of Carbon Steel, Corrosion/93. 1993: NACE International, Houston, Texas.

12. Nesic, S., et al., Electrochemical Properties of Iron Dissolution in the Presence of CO_2- Basics Revisited, Corrosion/96. 1996: NACE International, Houston, Texas.

13. Kermani, M.B. and Morshed, A. Carbon dioxide Corrosion in Oil and Gas Production - A compendium. Corrosion, 2003. 59(8): p. 659-683.

14. Hedges, B. and McVeigh, L., The Role of Acetate in CO_2 Corrosion: The Double Whammy, Corrosion/99. 1999: NACE International, Houston, Texas.

15. Joosten, M.W., Kolts, J., and Hembree, J.W., Organic Acid Corrosion in Oil and Gas Production, Corrosion/2002. 2002: NACE International, Houston, Texas.

16.   Kermani, M.B. and Smith, L. eds., A Working Party Report on CO_2 Corrosion Control in Oil and Gas Production: Design Considerations (EFC 23) 1997, The Institute of Materials.

17.   Crolet, J.L. and Bonis, M.R., pH Measurement in Aqueous CO_2 Solutions under High Pressure and Temperature, Corrosion, 1983. 39(2): p. 39-46.

18.   Crolet, J.L., Bonis,M.R., The Role of Acetates Ions in CO_2 Corrosion, Corrosion 83: 1983, NACE International, Houston, Texas.

19.   Edwards, J.D., Sydberger, T. and Mork, K.J. Realibility Based Design of CO2-Corrosion Control, Corrosion 96: 1996: NACE International, Houston, Texas.

20.   Rippon, I., Carbon Steel Pipeline Corrosion Engineering: Life Cycle Approach, Corrosion/2001, NACE International, Houston, Texas.

21.   Turgoose, S., Cottis, R.A., Lawson, K., "Modelling of Electrode Processes and Surface Chemistry in Carbon Dioxide Containing Solutions", in "Computer Modelling of Corrosion" Munn, R. S. (ed.), ASTM STP 1154, p. 67, 1992.

22.   Nesic, S., Postlethwaite, J. and Vrhovac, M., CO_2 Corrosion of Carbon Steel - from Mechanistic to Empirical Modelling, Corrosion Reviews, 1997. 15(1-2).

23.   Kern D.M., "The Hydration of Carbon Dioxide" in "CO_2 Corrosion in Oil and Gas Production - Selected Papers, Abstracts and References", Newton L.E., Hausler R.H. (eds), NACE T-1-3, NACE, USA, p. 75, 1984.

24.   Palmer, D.A., Van Eldik, R., Chem. Rev., 83, p. 651, 1983.

25. Bonis, M.R. and Crolet, J.L., Basics of the Prediction of the Risks of CO_2 Corrosion in Oil and Gas Wells. Corrosion/89. 1989: NACE International, Houston, Texas.

26. Schmitt, G., Rothman, B., EUROCORR 77, 6th European Congress on Metallic Corrosion, Soc. Chemical Industry, p. 321, 1977..

27. Schmitt, G., Rothman, B., Werkst. und Korrosion, 29, p. 237, 1978.

28. Mendoza-Flores, J., Turgoose, S., Corrosion 95, NACE, Paper 124, 1995.

29. Nesic, S., Postlethwaite, J. and Olsen, S., An Electrochemical Model for Prediction of CO_2 corrosion, Corrosion/95: 1995, NACE International, Houston, Texas.

30. Schmitt G, Rothmann B., "Studies on the Corrosion Mechanism of Unalloyed Steel in Oxygen-Free Carbon Dioxide Solutions, Part I. Kinetics of the Liberation of Hydrogen" in "CO_2 Corrosion in Oil and Gas Production - Selected Papers, Abstracts and References", Newton L.E., Hausler R.H. (eds), NACE T-1-3, p. 163, 1984.

31. Vetter, K.J., "Electrochemical Kinetics - Theoretical and Experimental Aspects", New York, Academic Press, p. 235, 1967.

32. Nesic, S., Pots, B.F.M., Postlethwaite, J., Thevenot, N., "Superposition of Diffusion and Chemical Reaction Limiting Currents - Application to CO_2 Corrosion", Journal of Corrosion Science and Engineering, Vol. 1, Paper 3. The Corrosion Information Server, The Corrosion & Protection Centre at UMIST, Manchester, UK, 1995.

33. Mendoza, F.J., "Kinetic Studies of CO_2 Corrosion Under Turbulent Flow", PhD Thesis, UMIST, Manchester, 1997.

34. Bockris, J.O.M., Drazic, D. and Despic, A.R. The Electrode Kinetics of the Deposition and Dissolution of Iron. Electrochimica Acta, 1961. 4: p. 325.

35. Videm, K., The Effect of Some Environmental Variables on the Aqueous CO_2 Corrosion of Carbon Steels, EFC Number 13, The Institute of Materials, 1994.

36. Videm, K., Kvarekvaal, J., Perez, T., and Fitzsimons, G., Surface Effects on the Electrochemistry of Iron and Carbon Steel Electrodes in Aqueous CO_2 Solutions. Corrosion/96, NACE International, Houston, Texas.

37. Garsany, Y. and Pletcher, D., The Role of Acetate in CO_2 Corrosion of Carbon Steel: Has the Chemistry been Forgotten? , Corrosion/2002: 2002, NACE International, Houston, Texas.

38. Kermani, M.B. and Smith, L. eds., A Working Party Report on Predicting CO_2 Corrosion in the Oil and Gas Industry (EFC 13). 1994, The Institute of Materials.

39. Ikeda, A., Mukai, S. and Ueda, M., Relationship between Environmental-Factors and Corrosion Product on CO_2 Corrosion. Transactions of the Iron and Steel Institute of Japan, 1984. 24(12): p. B401-B401.

40. Schmitt, G., Gudde, T. and Strobel-Effertz, E., Fracture Mechanical Properties of CO_2 Corrosion Product Scales and Their Relation to Localized Corrosion, Corrosion/96: 1996, NACE International, Houston, Texas.

41. van Hunnick, E.W.J., Pots, B.F.M. and Hendriksen, E.L.J.A, The Formation of Protective $FeCO_3$ Corrosion Products Layers in CO_2 Corrosion, Corrosion/96: 1996, NACE International, Houston, Texas.

42. Crolet, J.L., Thevenot, N. and Nesic, S., Role of Conductive Corrosion Products on the Protectiveness of Corrosion Layers. Corrosion/96:1996, NACE International, Houston, Texas.

43. Crolet, J.L., Thevenot, N. and Nesic, S., Role of Conductive Corrosion Products in the Protectiveness of Corrosion Layers, Corrosion, 1998. 54(3): p. 194-203.

44. Poulson, B., Electrochemical Measurements in Flowing Solutions, Corrosion Science, Volume 23, Number 4, p. 391-430, 1983.

45. Gabe, D.R., The Rotating Cylinder Electrode, Journal of Applied Electrochemistry, Volume 4, p. 91-108, 1974.

46. Gabe, D.R., Walsh, F.C., The Rotating Cylinder Electrode: A Review of Development, Journal of Applied Electrochemistry, 13, p. 3-21, 1983.

47. Efird, K.D., Wright, E.J., Boros, J.A., Hailey, T.G., Corrosion, 49, p. 992, 1993.

48. Eisenberg, M., Tobias, C.W., Wilke, C.R., Ionic Mass Transfer and Concentration Polarisation on Rotating Electrodes, J. Electrochem. Soc., 101, p. 306, 1954.

49. Silverman, D.C., Corrosion, 40, p. 220, 1984.

50. Turgoose, S., Dawson, J.L., Palmer, J.M., Rizk, T., Corrosion 95, NACE, Paper 112, 1995.

51.   Chiltorn, T.H. and Colburn, A.P., Ind.Engineering Chem.26, 1183,1934

52.   Berger, F.P. and Hau, K.F., Mass Transfer in Turbulent Pipe Flow Measured by the Electrochemical Method, J.Heat Mass Transfer, Vol. 20, p. 1185-1194, 1977.

53.   Silverman, D.C., Corrosion 90, NACE, Paper 13, 1990.

54.   Nyborg, R., Overview of CO_2 Corrosion Models for Wells and Pipelines. Corrosion/2002: 2002, NACE International, Houston, Texas.

55.   de Waard, C., Lotz, U. and Dugstad, A., Influence of Liquid Flow Velocity on CO_2 Corrosion, Corrosion/95:1995, NACE International, Houston, Texas.

56.   Webster, S., McMahon, A.J., BP Report No. 1993-220483, 1993.

57. CO_2 Corrosion Rate Calculation Model; NORSOK Standard No. M-506, http://www.nts.no/norsok (Oslo: Norwegian Technology Standards Institution, 1998).

58.   Crolet, J.L. and Bonis, M.R., An Optimized Procedure fro Corrosion Testing Under CO_2 and H_2S Gas Pressure, Material Performance, 1990: p. 81-87.

59.   Crolet, J.L. and Bonis, M.R., A Tentative Method for Predicting the Corrosivity of Wells in New CO_2 Fields, Material Performance, 1986. 25(3): p. 41-45.

60.   Gunaltun, Y.M., Combining Research and Field Data for Corrosion Rate Prediction, Corrosion/96: 1996, NACE International, Houston, Texas.

61.   Nesic, S., et al., A Mechanistic Model for CO_2 Corrosion with Protective Iron Carbonate Films, Corrosion/2001: 2001, NACE International, Houston, Texas.

62.   Nesic, S., Postlethwaite, J. and Olsen, S., An electrochemical model for Prediction of Corrosion of Mild Steel in Aqueous Carbon Dioxide Solutions, Corrosion, 1996. 52(4): p. 280-294.

63.   John, R.C., et al., Sweetcor:An Information System for the Analysis of Corrosion of Steels by Water and CO_2, Corrosion /98: 1998. NACE International, Houston, Texas.

64.   Rajappa, S., Zhang, R. and Gopal, M., Modelling the Diffusion Effects through the Iron Carbonate layer in the Carbon Dioxide Corrosion of Carbon Steel, Corrosion /98: 1998 , NACE International, Houston, Texas.

65.   Schmitt, G., Rothmann, B., "Studies on the Corrosion Mechanism of Unalloyed Steel in Oxygen-Free Carbon Dioxide Solutions, Part II. Kinetics of Iron Dissolution" in "CO_2 Corrosion in Oil and Gas Production - Selected Papers, Abstracts and References", Newton L.E., Hausler R.H. (eds), NACE T-1-3, NACE, USA, p. 163, 1984.

66.   www.gly.bris.ac.uk.

67.   Crolet, J.L., Thevenot, N. and Dugstad, A., Role of Free Acetic Acid on the CO_2 Corrosion of Steels, Corrosion/99: 1999, NACE International, Houston, Texas.

68. Parkhurst, D.L. and Appelo, C.A.J., "User's Guide to PHREEQC (Version 2), Water-Resources Report 994259, US Geological Survey, US Department of the Interior.

69. Garsany, Y., Pletcher, D. and Hedges, B., Speciation and Electrochemistry of Brines Containing Acetate Ion and CO_2, Electroanalytical Chemistry, 2002 (538-539): p. 285-297.

70. Ueda, M. and Takabe, H., Effect of Organic Acid on CO_2 Corrosion of Carbon and Cr Bearing Steels, Corrosion/98: 1998, NACE International, Houston, Texas.

71. Pots, B.F.M., et al., Improvement on de Waard-Milliams Corrosion Prediction and Applications to Corrosion Management, Corrosion/2002: 2002, NACE International, Houston, Texas.

72. Stern, M., Geary, A.L., Theoretical Analysis of the Shape of the Polarisation Curves, Journal Electrochemical Society, v. 104(10), January 1957,p 56-63.

73. Sun, Y., George, K. and Nesic, S., The Effect of Cl⁻ and Acetic Acid on Localized CO_2 Corrosion in Wet Gas Flow, CORROSION/2003, NACE International, Houston, Texas.

74. Plummer, L.N. and Busenberg, E., Geochimica et Cosmochimica Acta.46 (1982) 1011.

75. Patterson, C.S., Slocum, G.H., Busey, R.H., Mesmer, R.E., Carbonate Equilibria in Hydrothermal Systems: First Ionisation of Carbonic Acid in NaCl Media to 300°C, Geochimica et Cosmochimica Acta; v.46; 1982;p. 1653-1663.

76. Roberts, B.E., Tremaine, P.T., Vapour Liquid Equilibrium Calculations for Dilute Aqueous Solutions of CO_2, H_2S, NH_3 and NaOH to 300°C, Canada Journal of Chemical Engineering, v.63, April 1985, p. 314-319.

77. Ryzhenko, B.N., Determination of Dissociation Constants of Carbonic Acid and the Degree of Hydrolysis of the CO_3^{2-} and HCO_3^- Ions in Solutions of Alkali Carbonates at Elevated temperatures, Geochemistry, Geochemical Society, no.2, 1963, p 151-164.

78. Kharaka, Y.K., Solmineq, A Computer Program for Geochemical Modelling of Water-Rock Interactions, Alberta Research Council, Menlo Park, California, 1989.

79. Vetter, K.J., Electrochemical Kinetics - Theoretical and Experimental Aspects, Academic Press, New York, 1967, p.506.

80. Weast, R.C. and Astle, M.J. (eds.), CRC Handbook of Chemistry and Physics, 63rd ed. 1982, CRC Press Inc.

81. Hawaidi, I.A.M., MSc Thesis: Effect of acetate on CO2 Corrosion, Corrosion and Protection Centre, 2002, UMIST: Manchester, UK.

82. Atkins, P.W., Physical Chemistry, 5th Ed, Oxford University Press, UK, 1994.